



**THREE-DIMENSIONAL NUMERICAL INVESTIGATIONS  
OF TIDE AND WIND-INDUCED TRANSPORT  
PROCESSES IN BISCAYNE BAY**

**CIRCULATING COPY  
Sea Grant Depository**

**SUBRATA SENGUPTA  
SAMUEL S. LEE  
HARVEY P. MILLER**

**SEA GRANT TECHNICAL BULLETIN NO.39  
JULY, 1978**

PRICE: 4.00

This work is a result of research sponsored by the NOAA Office of Sea Grant, U.S. Department of Commerce, under Grant No. OI-7-158-44115. The U.S. Government is authorized to produce and distribute reprints for governmental purposes notwithstanding any copyright notation that might appear hereon.

Library of Congress Number: 78-63583

Information Services  
Sea Grant Program  
University of Miami  
P.O. Box 248106  
Coral Gables, Fla. 33124



THREE DIMENSIONAL NUMERICAL INVESTIGATIONS  
OF TIDE AND WIND INDUCED TRANSPORT  
PROCESSES IN BISCAYNE BAY

Subrata Sengupta, Samuel S. Lee and  
Harvey P. Miller  
Department of Mechanical Engineering  
University of Miami

July, 1978

## ACKNOWLEDGEMENT

The authors express their gratitude to the Office of Sea Grant, NOAA for funding the project which generated the information presented in this report. We are particularly indebted to Dr. E. H. Man of Sea Grant program in Miami for his encouragement and support of this work. We also wish to acknowledge the computational help provided by Dr. C. V. Carter,

## LIST OF SYMBOLS

A	Bottom bed deposition probability.
C	Concentration of suspended sediment particle or of dissolved chemical constituent.
$D_H$	Eddy mass diffusivity in horizontal direction.
$D_V$	Eddy mass diffusivity in vertical direction.
f	Coriolis parameter.
g	Acceleration due to gravity.
h	Depth relative to the mean water level.
H	Depth contour relative to the free-surface, $h + \eta$ .
I	Grid index in x-direction, or $\alpha$ -direction.
J	Grid index in y-direction, or $\beta$ -direction.
K	Grid index in z-direction, or $\sigma$ -direction.
$K_H$	Horizontal kinematic eddy viscosity.
$K_V$	Vertical kinematic eddy viscosity.
P	Pressure
$P_s$	Surface pressure.
t	Time
u	Velocity component in x-direction.
v	Velocity component in y-direction.
w	Velocity component in z-direction.
$W_s$	Suspended particle settling velocity.
x	Horizontal coordinate.
y	Horizontal coordinate.
z	Vertical position relative to the mean water level.
Z	Vertical position relative to the free-surface, $z + \eta$ .

## GREEK SYMBOLS

$\alpha$	Horizontal coordinate in stretched system, x.
$\beta$	Horizontal coordinate in stretched system, y.
$\sigma$	Vertical coordinate in stretched system, Z/H.
$\Omega$	Transformed (or equivalent) vertical velocity.
$\rho$	Density.
$\eta$	Free-surface elevation above mean water level.
$\tau_{zx}$	Surface shear stress in x-direction.
$\tau_{zy}$	Surface shear stress in y-direction.

## SUBSCRIPTS AND SUPERSCRIPTS

H	Horizontal quantity.
i	Initial quantity.
n	One time level back.
n+1	Current time level.
n-1	Two time levels back.
o	Quantity at inlet (ocean-exchange area).
s	Quantity at free-surface.
v	Vertical quantity.
w	Quantity at lateral boundary.
w+1	Quantity at interior point one grid step from lateral boundary.

TABLE OF CONTENTS

	Pages
i Acknowledgement	I
ii List of Symbols	II
1. Introduction	6
2. Physical Models	8
2.1. Sediment Transport	8
2.2. Conservative Dissolved Chemical Transport	9
3. Mathematical Model	10
3.1. Simplifying Assumptions and Approximations	10
3.1.1. The Boussinesq Approximation	10
3.1.2. The Hydrostatic Approximation	11
3.1.3. Constant Eddy Transport Coefficients	11
3.1.4. Variation of Surface Wind Stresses	12
3.1.5. Velocity Slip Conditions	12
3.1.6. Higher Order Terms	13
3.2. Governing Equations for Hydrodynamic Models	13
3.2.1. Hydrodynamic Model Equations for Sediment Transport in (x,y,z) Coordinate System	14
3.2.2. Hydrodynamic Model Equations for Dissolved Chemical Transport in (x,y,z) Coordinate System	15
3.2.3. Hydrodynamic Model Equations for Sediment Transport in ( $\alpha,\beta,\sigma$ ) Coordinate System	16
3.2.4. Hydrodynamic Model Equations for Dissolved Chemical Transport in ( $\alpha,\beta,\sigma$ ) Coordinate System	20

3.3.	Boundary Conditions for Hydrodynamic Models	21
3.3.1.	Boundary Conditions for Hydrodynamic Model for Sediment Transport	22
3.3.2.	Boundary Conditions for Hydrodynamic Model for Dissolved Chemical Transport	23
3.4.	Initial Conditions for Hydrodynamic Models	24
3.5.	Concentration Equation in Cartesian Coordinate System (x,y,z)	24
3.6.	Concentration Equation in ( $\alpha,\beta,\sigma$ ) Coordinate System	25
3.7.	Boundary Conditions for Concentration Equation	26
3.7.1.	Boundary Conditions for Sediment Transport	26
3.7.2.	Boundary Conditions for Dissolved Chemical Transport	30
3.8.	Initial Conditions for Concentration Equation	31
3.8.1.	Initial Conditions for Sediment Transport	
3.8.2.	Initial Conditions for Dissolved Chemical Transport	
4.	Numerical Method of Solution	38
4.1.	General	38
4.2.	Finite Difference Representation of Concentration Equation	38
4.3.	Finite Difference Representation of Boundary Conditions	40
4.3.1.	Boundary Conditions for Sediment Transport	41



4.3.2.	Boundary Conditions for Dissolved Chemical Transport	41
4.4.	Top and Bottom Boundary Finite Difference Equations from Conservation of Mass Considerations	42
4.5.	Initial Conditions in Finite Difference Form	49
4.5.1.	Initial Conditions for Sediment Transport	49
4.5.2.	Initial Conditions for Dissolved Chemical Transport	49
4.6.	Second Upwind Differencing of Horizontal Convection Terms	49
4.7.	Total System Mass Algorithm	52
4.7.1.	Mass in Domain of Bay	52
4.7.2.	Settled Out Mass Algorithm	53
4.7.3.	Total System Mass Without Flushing	54
4.7.4.	Computation of Percent of Tidal Flushing	54
5.	Coupling of Velocity Field and Surface Height Variations to Concentration Equation	56
5.1.	Staggered Grid System for Computing Velocity Field and Surface Heights for Storage on Magnetic Tape for Dissolved Chemical Transport	56
5.2.	Numerical Solutions of the Hydrodynamic Model Used for Coupling to the Dissolved Chemical Transport Equation	57

5.3.	Calibration of Hydrodynamic Model Used for Dissolved Chemical Transport Studies	58
5.4.	Interpolation of Staggered Grid Variables for Obtaining Solutions of the Dissolved Chemical Transport Equation	59
5.5.	Numerical Solutions of Hydrodynamic Model Used for Coupling to the Sediment Transport Equation	60
6.	Results for Sediment Transport	76
6.1.	Grid System for Studying Intracoastal Waterway Channel in South Biscayne Bay	76
6.2.	Computer Runs for Different Values of Settling Velocity and Bottom Deposition Rate for an Instantaneous Line Source	76
7.	Results for Dissolved Constituent Transport	78
7.1.	Grid System for Studying Dissolved Chemical Transport	78
7.2.	Definition of Flushing	79
7.3.	Flushing Rates for Dissolved Chemical Transport	80
7.4.	Model Dye Release Site Studies	82
8.	Discussion and Conclusions	108
8.1.	Sediment Transport	108
8.2.	Dissolved Chemical Transport	110
8.3.	Conclusions	111
9.	References	114
10.	Appendices	117

(a)	Settling Velocity in a Turbulent Flow Field	117
(b)	Fluid and Particle Eddy Transport Coefficients	118
(c)	Wind Stresses and Coriolis Parameter in Rotated Grid System	119
(d)	Convective and Diffusive Terms in $(\alpha, \beta, \sigma)$ Coordinate System	122
(e)	Velocity Calibration	128

## 1. Introduction

Biscayne Bay in South Florida is a shallow estuary bordering the city of Miami. It is open through a shoal area and some creeks to the Atlantic Ocean. It has a number of basins connected by shallow constricted openings and causeways. South Biscayne Bay is of interest for this study. It extends from Rickenbacker Causeway in the north to Card Sound in the southern end. The tide and wind driven circulation in this domain is of interest to environmentalists for assessing the impact of anthropogenic disturbances.

Systematic observational studies on estuaries began with Stommel and Farmer (1952) who compiled data on 20 estuaries of great diversity. Some studies were conducted by Ketchum (1955). Numerical investigations have been conducted by Reid et al (1958), Leendertse (1973) and Blumberg (1977, a,b). A review of mixing and dispersion processes in estuaries is provided by Fischer (1976).

The objective of the present study is to calibrate two three-dimensional numerical free surface models such that they can be used in the predictive mode for transport analysis. While simplified two-dimensional studies were made by Verma et al (1969) and Lee and Rooth (1972) three-dimensional models which provide considerably greater details are imperative for specific engineering decisions.

Sengupta et al (1976) and Lee and Sengupta (1977) have presented initial investigations in Biscayne Bay using

rigid-lid and free-surface three dimensional models. Sengupta et al (1977) have presented a calibration effort for a three-dimensional free-surface model using infra-red data for surface temperatures. Carter (1977) developed a free surface model for Lake Okeechobee. This model differs from Sengupta et al (1977) in using a Richardson Lattice and ignoring horizontal diffusion term. All these models use finite difference techniques with forward time central space schemes. DuFort Frankel schemes on diffusion terms are used.

The present study uses the free-surface model of Sengupta (1977) et al to develop velocity fields which are used for simplified simulation of sediment transport near the intracoastal water way. The second phase of the study uses Carter's (1977) model to simulate velocity fields for dye diffusion and flushing studies for the bay. Verification using dye release experiments and velocity measurements have been attempted.

The models have performed well in predicting velocity, temperature and surface heights. Qualitative agreement with dye release experiments have been obtained. The models should be further verified including salinity effects.

## 2. Physical Model

### 2.1. Sediment Transport

Gemmel (1971), Allen (1970) and Camp (1946) summarize the various physical processes governing sediment transport in the fluid, and the modes of sedimentation deposit on the bed of a water basin. Sheng (1975) has investigated contaminant dispersion in the near-shore of large lakes using a three-dimensional, time-dependent numerical model. His approach is that of applying a predictive dispersion model which is solved by the method of finite differences. Sheng's governing equations and attendant method of solution has been quite useful for our formulation, however, Sheng doesn't take account of free surface variations in space and time. Instead, he invokes a "rigid-lid" approximation.

The effects of ideal particle settling, hindered particle settling, flocculation, and bed scour, or viscous turbulent entrainment of sediment particles is discussed in detail by Raudkivi (1975), Allen (1970) and Camp (1946). Empirical relationships have been obtained for hindered particle settling, flocculation and entrainment. However, current research investigations by Sheng (1975), Apman and Rumer (1970), Hjelmfelt and Lenau (1970), Jobson (1970), Jobson and Sayre (1970), and Mei (1969) have not accounted for entrainment (or bed scour) in their dispersion models, and have only included particle settling effects in terms of "ideal" gravitational settling, thus ignoring hindered

settling and flocculation.

Appendix A presents in detail the method of calculation of settling velocity,  $W_s$ , in a turbulent flow field and Appendix B presents and discusses the eddy transport coefficients for the fluid and for the suspended sediment particles.

The momentum transfer, in our investigation, is related to the particulate mass transfer through the dimensionless turbulent Schmidt number  $=K_v/D_v=1$ . Jobson's (1970) experimental investigation indicated an average turbulent Schmidt number of 1.03. Note that the momentum equation affects the concentration equation, but not vice versa, since the effect of suspended particles on the dynamics of the flow can be neglected for sufficiently small Richardson number. Barenblatt (1953, 1955).

## 2.2 Conservative Dissolved Chemical Transport

As in the first case of sediment transport, we set the turbulent Schmidt number  $=K_v/D_v=1$  for coupling the hydrodynamic model equations to the concentration equations. For conservative dissolved chemical transport, we ignore any possible chemical reactions taking place, and we set the particle settling, velocity,  $W_s$ , to zero. Again we use the eddy transport concept as will be presented in detail in Appendix B.

### 3. Mathematical Model

This section will present the details of the formulation of the mathematical model, in both the Cartesian coordinate system  $(x,y,z)$ , and in the vertically stretched coordinate system  $(\alpha,\beta,\sigma)$ . Inclusion of the free surface and actual bottom topography will be discussed, and the full set of initial and boundary conditions, to complete the formulation of the mathematical model, will be presented for both cases of sediment transport and conservative, dissolved chemical transport. The assumption and simplifying approximations invoked in our investigation will be given in the next subsection, 3.1, and mention will be made of the approximations used by other researchers in numerical studies in sediment and chemical transport. Lastly in this section, we will summarize the initial and boundary conditions used by other researchers, and give the complete set used in our model studies. First, however, we will describe the hydrodynamic models used which are coupled (through convection) to the concentration equation for both cases of sediment transport and dissolved chemical transport.

#### 3.1 Simplifying Assumptions and Approximations

The following simplifying assumptions and approximations have been invoked in the mathematical model presented herein, this was done in the interest of saving computational time without losing significant accuracy.

##### 3.1.1 The Boussinesq Approximation

This approximation was used for the first case of sediment transport, for the second case of dissolved chemical transport the hydrodynamic model used is for



constant density. That is, as already noted in the Introduction, Section 1, two different hydrodynamical models were used separately to obtain results for sediment transport and chemical transport. Thus, for the first case of variable density, the effect of density variations on the inertial and diffusion terms in the governing momentum conservation equations is neglected. Density variation is retained only in the buoyancy term.

### 3.1.2. The Hydrostatic Approximation

The hydrostatic approximation involves neglecting the vertical convection and diffusion terms in the vertical momentum equation. This approximation implies that the vertical fluid acceleration,  $\frac{Dw}{Dt}$  is negligible.

### 3.1.3. Constant Eddy Transport Coefficients

Turbulence modeling is very complex and has an extensive body of literature of its own. Turbulent closure has been obtained in this model by using constant eddy transport coefficients, although the horizontal eddy transport coefficient is orders of magnitude larger than the vertical eddy transport coefficient, being due to the much larger horizontal scale length,  $L$ , in comparison with the vertical scale length  $H$ . Note, however, that the hydrodynamic model used for the first case of sediment transport used a depth dependent vertical eddy transport coefficient, as follows:

$$K_v = 0.0018 (\text{DEPTH})^{4/3} \dots\dots\dots(3-1)$$

This was done to increase the numerical time step  $\Delta t$ , as

will be discussed in Section 4. However, the hydrodynamic model used for the second case of dissolved chemical transport used a constant value for  $K_v$ , since it was learned that introducing a depth-dependent value for  $K_v$  in this second model produced time steps inordinately small during low water in the South Biscayne Bay.

#### 3.1.4. Variation of Surface Wind Stresses

The variation of the wind produced surface shear stresses with respect to  $x$  and  $y$ ,  $\frac{\partial \tau_{zx}}{\partial x}$  and  $\frac{\partial \tau_{zy}}{\partial y}$ , are considered negligible for the horizontal length scales of the bay. This microscale approximation was also used by Dean and Verma (1969) in their numerical/hydrodynamic model of the South Biscayne Bay.

#### 3.1.5. Velocity Slip Conditions

The hydrodynamic model used for sediment transport uses an unstaggered numerical grid system, and, thus, required two velocity boundary conditions to be specified at solid lateral boundaries. No normal velocity and tangential slip velocity were specified (that is, zero shear stress). The assumption of slip conditions is necessary for the free-surface model to allow for surface height variations at the solid boundaries, Freeman et al (1972), Lee et al (1977). Numerically it has been seen that lateral boundary layers are smaller than the relatively large grid spacing used, specifically for the South Biscayne Bay, for

which the grid spacing  $\Delta x = \Delta y = 1.6$  kilometers in the horizontal mesh. Estimates by Sengupta and Lick (1974) have indicated that the sidewall boundary layers are thin for similar situations, and do not extend as far as the nearest interior node. Freeman et al (1972) used velocity slip boundary conditions in their free surface model formulation.

#### 3.1.6. Higher Order Terms

Higher order terms resulting from the transformation of the governing equations from  $(x, y, z)$  to  $(\alpha, \beta, \sigma)$  have been neglected. These terms are presented in Appendix D. As will be seen in Appendix D these terms are neglected, justifiably, since the magnitude of the horizontal diffusion terms are several orders of magnitude smaller than the vertical diffusion terms, and these higher order terms only appear in the transformed horizontal diffusion terms. Furthermore, these terms may be neglected for gradual variations in bottom topography - this is surely the case for the South Biscayne Bay, which is a relatively shallow water body. Sheng (1975) also neglected these terms in his numerical investigations of Lake Erie.

#### 3.2. Governing Equations for Hydrodynamic Models

The governing hydrodynamic equations for the separate cases of sediment transport and dissolved chemical transport will be given in this subsection. Note, both numerical studies use the identical concentration equation as given in subsection 3.3, but the hydrodynamic equations are somewhat different.

### 3.2.1. Hydrodynamic Model Equations for Sediment Transport in (x,y,z) Coordinate System

The Cartesian coordinate system is used with the z-coordinate in the downward vertical direction as shown in Fig.3-1, that is, a so-called "left-handed" coordinate system. The following system of non-linear, coupled, partial differential equations in Cartesian coordinates describe the three-dimensional, time-dependent hydrodynamics.

#### Continuity Equation

$$\frac{\partial u}{\partial x} + \frac{\partial v}{\partial y} + \frac{\partial w}{\partial z} = 0 \quad (3-2)$$

#### Momentum Equations

$$\begin{aligned} \frac{\partial u}{\partial t} + u \frac{\partial u}{\partial x} + v \frac{\partial u}{\partial y} + w \frac{\partial u}{\partial z} \\ = - \frac{1}{\rho} \frac{\partial p}{\partial x} + fv + K_H \frac{\partial^2 u}{\partial x^2} \\ + K_H \frac{\partial^2 u}{\partial y^2} + K_V \frac{\partial^2 u}{\partial z^2} \end{aligned} \quad (3-3)$$

$$\begin{aligned} \frac{\partial v}{\partial t} + u \frac{\partial v}{\partial x} + v \frac{\partial v}{\partial y} + w \frac{\partial v}{\partial z} \\ = - \frac{1}{\rho} \frac{\partial p}{\partial y} - fu + K_H \frac{\partial^2 v}{\partial x^2} \\ + K_H \frac{\partial^2 v}{\partial y^2} + K_V \frac{\partial^2 v}{\partial z^2} \end{aligned} \quad (3-4)$$

### Hydrostatic Equation

$$\frac{\partial P}{\partial z} = - \rho g \quad (3-5)$$

The symbols in equations (3-2) through (3-5) are defined in the list of symbols.

Note, that the nonlinear inertia terms and horizontal diffusion terms, as well as Coriolis acceleration, have been retained in the hydrodynamic model equations for the first case of sediment transport.

#### 3.2.2. Hydrodynamic Model Equations for Dissolved Chemical Transport in (x,y,z) Coordinate System

The Cartesian coordinate system is used now with the z-coordinate in the upward vertical direction as shown in Fig.3-2, this is the conventional x,y,z coordinate system. Carter (1977) has gone through an order of magnitude analysis and deduced, for the South Biscayne Bay, that the horizontal diffusion terms are small and, thus, have been neglected. Hence, the hydrodynamic models equations in the Cartesian coordinate system, with the convective terms (nonlinear inertia terms) written in conservative form are as follows.

#### Continuity Equation

$$\frac{\partial u}{\partial x} + \frac{\partial v}{\partial y} + \frac{\partial w}{\partial z} = 0 \quad (3-6)$$

### Momentum Equations

$$\begin{aligned} \frac{\partial u}{\partial t} + \frac{\partial uu}{\partial x} + \frac{\partial vu}{\partial y} + \frac{\partial wu}{\partial z} \\ - g \frac{\partial \eta}{\partial x} + fv + K_v \frac{\partial^2 u}{\partial z^2} \end{aligned} \quad (3-7)$$

$$\begin{aligned} \frac{\partial v}{\partial t} + \frac{\partial uv}{\partial x} + \frac{\partial vv}{\partial y} + \frac{\partial wv}{\partial z} \\ = -g \frac{\partial \eta}{\partial y} - fu + K_v \frac{\partial^2 v}{\partial z^2} \end{aligned} \quad (3-8)$$

Where the hydrostatic equation has been used to eliminate P from the horizontal momentum equations, that is:

$$\frac{\partial P}{\partial x} = \rho g \frac{\partial \eta}{\partial x} \quad (3-9)$$

and,

$$\frac{\partial P}{\partial y} = \rho g \frac{\partial \eta}{\partial y} \quad (3-10)$$

Where the hydrostatic pressure equation (refer to Fig.3-2) is,

$$P = P_0 + \rho g (-z + \eta) \quad (3-11)$$

#### 3.2.3. Hydrodynamic Model Equations for Sediment Transport in $(\alpha, \beta, \sigma)$ Coordinate System.

One major difficulty in the treatment of the free-surface model is at the free surface boundary. The boundary

conditions can be specified, but the position of the free surface is irregular and time-dependent, thus making it very difficult to apply any grid system at this "moving" boundary for numerical solution. The approach used in the model formulation is to follow a vertical stretching transformation suggested by Phillips (1957) and used successfully in studies by Freeman et al (1972) and Lee et al (1977). Using this transformation, the free surface becomes a fixed flat surface and the variable depth bottom becomes a flat bottom boundary. Thus, constant vertical grid size can be used throughout the domain without losing resolution in shallow parts, and, also, without requiring excessive computer storage by requiring unnecessarily fine spacing in deeper regions.

The transformation of the vertical coordinate for the free surface model is obtained by letting

$$\begin{aligned}\alpha &= x \\ \beta &= y\end{aligned}\tag{3-12}$$

and,

$$\sigma = \frac{Z(x,y,z,t)}{H(x,y,t)} = \frac{z + \eta(x,y,t)}{H(x,y,t)}\tag{3-13}$$

Fig.3-3 shows the  $(\alpha, \beta, \sigma)$  coordinate system. Note, that the values of  $\sigma$  range monotonically from zero at the free surface to unity at the bottom boundary. By substituting transformations (3-12) and (3-13) into equations (3-2) through (3-5) the free surface hydrodynamic model equations (for this case of sediment transport) in the  $(\alpha, \beta, \sigma)$  coordinate

system are expressed in what follows. The details of this coordinate system transformation are given in Appendix D.

### Continuity Equation

$$\frac{\partial H}{\partial t} + \frac{\partial(Hu)}{\partial \alpha} + \frac{\partial(Hv)}{\partial \beta} + H \frac{\partial \Omega}{\partial \sigma} = 0 \quad (3-14)$$

### Momentum Equations

$$\begin{aligned} & \frac{\partial(Hu)}{\partial t} + \frac{\partial(Huu)}{\partial \alpha} + \frac{\partial(Huv)}{\partial \beta} \\ & + H \frac{\partial(u\Omega)}{\partial \sigma} = H \left\{ -\frac{1}{\rho} \left( \frac{\partial P}{\partial \alpha} \right) + \right. \\ & g \left( \sigma \frac{\partial H}{\partial \alpha} - \frac{\partial \eta}{\partial \alpha} \right) + fv \left. \right\} + \\ & K_H \left\{ \frac{\partial}{\partial \alpha} \left( H \frac{\partial u}{\partial \alpha} \right) + \frac{\partial}{\partial \beta} \left( H \frac{\partial u}{\partial \beta} \right) \right\} \\ & + \frac{1}{\rho} \left\{ \frac{\partial}{H \partial \sigma} \left( \rho K_V \frac{\partial u}{\partial \sigma} \right) \right\} \end{aligned} \quad (3-15)$$

$$\begin{aligned} & \frac{\partial(Hv)}{\partial t} + \frac{\partial(Huv)}{\partial \alpha} + \frac{\partial(Hvv)}{\partial \beta} \\ & + H \frac{\partial(v\Omega)}{\partial \sigma} = H \left\{ -\frac{1}{\rho} \left( \frac{\partial P}{\partial \beta} \right) + g \left( \sigma \frac{\partial H}{\partial \beta} \right. \right. \\ & \left. \left. - \frac{\partial \eta}{\partial \beta} \right) - fu \right\} + K_H \left\{ \frac{\partial}{\partial \alpha} \left( H \frac{\partial v}{\partial \alpha} \right) + \right. \\ & \left. \frac{\partial}{\partial \beta} \left( H \frac{\partial v}{\partial \beta} \right) \right\} + \frac{1}{\rho} \left\{ \frac{\partial}{H \partial \sigma} \left( \rho K_V \frac{\partial v}{\partial \sigma} \right) \right\} \end{aligned} \quad (3-16)$$



### Hydrostatic Equation

$$P(\alpha) = P(\alpha=0) + gH \int_{\alpha=0}^{\alpha} \rho(\sigma) \alpha \sigma. \quad (3-17)$$

Now, instead of using equation (3-14), following the work by Freeman et al (1972), two integrated forms of the continuity equations are used as follows.

### Surface Height Equation

$$\frac{\partial H}{\partial t} = - \int_{\alpha=0}^1 \left[ \frac{\partial(Hu)}{\partial \alpha} + \frac{\partial(Hv)}{\partial \beta} \right] \partial \sigma \quad (3-18)$$

Equivalent Vertical Velocity ( $\alpha, \beta, \sigma$ )

$$\begin{aligned} \Omega = & - \frac{1}{H} \int_{\sigma=0}^{\sigma} \left[ \frac{\partial(Hu)}{\partial \alpha} + \frac{\partial(Hv)}{\partial \beta} \right] \partial \sigma \\ & + \frac{\sigma}{H} \int_{\sigma=0}^1 \left[ \frac{\partial(Hu)}{\partial \alpha} + \frac{\partial(Hv)}{\partial \beta} \right] \partial \sigma \end{aligned} \quad (3-19)$$

$$\text{Where } \Omega = \frac{\partial \sigma}{\partial t}$$

The actual vertical velocity  $w (= \frac{dz}{dt})$  is then computed from the following kinematic relationship:

$$w = H \Omega + \sigma \frac{\partial h}{\partial t} + (\sigma-1) \frac{\partial \eta}{\partial t} \quad (3-20)$$

$$\text{Where } \frac{d}{dt} = \frac{\partial}{\partial t} + u \frac{\partial}{\partial \alpha} + v \frac{\partial}{\partial \beta}$$

Hence we are left with 5 equations to compute H, u, v,  $\Omega$  and P.

### 3.2.4. Hydrodynamic Model Equations for Dissolved Chemical Transport in $(\alpha, \beta, \sigma)$ Coordinate System

Carter (1977) incorporates the sigma-coordinate method by defining a new vertical coordinate  $\sigma$  as:

$$\sigma = \frac{z - \eta(x, y, t)}{H(x, y, t)}$$

Where  $\sigma$  varies monotonically from zero at the free surface to -1 at the bottom boundary. The hydrodynamic model equations are in  $(\alpha, \beta, \sigma)$  as follows:

#### Continuity Equation

$$\frac{\partial (Hu)}{\partial \alpha} + \frac{\partial (Hv)}{\partial \beta} + H \frac{\partial \Omega}{\partial \sigma} + \frac{\partial \eta}{\partial t} = 0 \quad (3-21)$$

Since  $\frac{\partial h}{\partial t} = 0$  and  $H = \eta + h$

#### Momentum Equations

$$\begin{aligned} & \frac{1}{H} \frac{\partial (Hu)}{\partial t} + \frac{1}{H} \left\{ \frac{\partial (Huu)}{\partial \alpha} + \frac{\partial (Hvu)}{\partial \beta} \right. \\ & + H \frac{\partial (u\Omega)}{\partial \sigma} + \left. (1 + \sigma) \frac{\partial u}{\partial \sigma} \frac{\partial \eta}{\partial t} \right\} = f_v - g \frac{\partial \eta}{\partial \alpha} \\ & + \frac{K_v}{H^2} \frac{\partial^2 u}{\partial \sigma^2} \end{aligned} \quad (3-22)$$

$$\begin{aligned} & \frac{1}{H} \frac{\partial (Hv)}{\partial t} + \frac{1}{H} \left\{ \frac{\partial (Huv)}{\partial \alpha} + \frac{\partial (Hvv)}{\partial \beta} \right. \\ & + H \frac{\partial (v\Omega)}{\partial \sigma} + \left. (1 + \sigma) \frac{\partial v}{\partial \sigma} \frac{\partial \eta}{\partial t} \right\} \end{aligned}$$

$$= -fu - g \frac{\partial \eta}{\partial \beta} + \frac{Kv}{H^2} \frac{\partial^2 v}{\partial \alpha^2} \quad (3-23)$$

The underlined terms have been retained by Carter (1977), but by dimensional analysis were considered negligible by Lee et al (1977) with regard to equations (3-15) and (3-16). Secondly, the above equations are only truly valid for constant density, whereas Lee et al (1977) derived their model equations for the more general case of variable density. Again, notice that horizontal diffusion terms have been neglected in equations (3-22) and (3-23), which is perfectly valid for South Biscayne Bay. Now, the continuity equation (3-21) is not used, but instead the two vertically integrated forms are used, that is:

$$\frac{\partial \eta}{\partial t} = - \int_{\sigma=-1}^0 \left\{ \frac{\partial(Hu)}{\partial \alpha} + \frac{\partial(Hv)}{\partial \beta} \right\} d\sigma \quad (3-24)$$

and,

$$\Omega = \frac{\sigma}{H} \frac{\partial \eta}{\partial t} + \frac{1}{H} \int_{\sigma}^0 \left\{ \frac{\partial(Hu)}{\partial \alpha} + \frac{\partial(Hv)}{\partial \beta} \right\} d\sigma \quad (3-25)$$

Equation (3-20) is again used to compute the actual vertical velocity, w.

Thus we have 4 equations to compute  $\eta, u, v$  and  $\Omega$ . P has been replaced directly by the hydrostatic approximation in the horizontal momentum equations.

### 3.3. Boundary Conditions for Hydrodynamic Models

The nature of the system of governing equations requires initial and boundary conditions to be specified. The boundary conditions for both hydrodynamic models will now be presented. The initial conditions will be presented in section 3.4.

3.3.1. Boundary Conditions for Hydrodynamic Model for Sediment Transport

The free surface, far-field hydrodynamic model has been applied to the South Biscayne Bay by Lee et al (1977). The boundary conditions are in summary:

At the surface,  $\sigma = 0$

$$\Omega = 0$$

$$\frac{\partial u}{\partial \sigma} = - \left( \frac{H}{\rho K_V} \right) \tau_{zx}$$

$$\frac{\partial v}{\partial \sigma} = - \left( \frac{H}{\rho K_V} \right) \tau_{zy}$$

At the bottom,  $\sigma = 1$

$$\Omega = 0$$

$$u = 0$$

$$v = 0$$

At the inlet

$$\Omega \neq 0$$

$$u = 0$$

$$\frac{\partial v}{\partial y} = 0$$

At lateral solid boundaries

On x - boundaries

$$\Omega \neq 0$$

$$u = 0$$

$$\frac{\partial v}{\partial x} = 0$$

On y-boundaries

$$\Omega \neq 0$$

$$\frac{\partial u}{\partial y} = 0$$

$$v = 0$$

At the outlet

$$\Omega \neq 0$$

$$u = 0$$

$$\frac{\partial v}{\partial y} = 0$$

\*  $n = n_0(\tau)$ , forcing function.

\* Note: A continuous sinusoidal function  $n_0(\tau) = A_1 + A_2 \sin(\omega\tau + \phi)$  was specified at the inlet to represent the tide level variation. The data was taken from Schneider (1969).

### 3.3.2. Boundary Conditions for Hydrodynamic Model for Dissolved Chemical Transport

Following the work of Carter (1977) the hydrodynamic boundary conditions for the second case of dissolved chemical transport will now be presented.

Normal velocities  $u, v, w$  are maintained at zero on all solid boundaries. Tangential velocities are maintained at zero on the bottom (the no-slip condition). As will be discussed in Chapter 5, a Richardson lattice is used for the grid arrangement in the horizontal plane. With this type of grid, the horizontal velocity components  $u$  and  $v$  appear on solid boundaries only as normal velocities. Thus, in summary:

At the surface,  $\sigma = 0$

$$\Omega = 0$$

$$\frac{\partial u}{\partial \sigma} = - \left( \frac{H}{\rho K_V} \right) \tau_{zx}$$

$$\frac{\partial v}{\partial \sigma} = - \left( \frac{H}{\rho K_V} \right) \tau_{zy}$$

At the bottom,  $\sigma = 1$

$$\Omega = 0$$

$$u = 0$$

$$v = 0$$

At the inlet

$$\Omega = \frac{\sigma}{H} \frac{\partial n}{\partial t}$$

$$u = 0$$

$$\frac{\partial v}{\partial y} = 0$$

$$n = n_0(\tau)$$

At lateral solid boundaries

On X - boundaries

$$\Omega \neq 0$$

$$u = 0$$

$v$  unspecified

On y - boundaries

$$\Omega \neq 0$$

$u$  unspecified

$$v = 0$$

At the outlet

$$\Omega \neq 0$$

$$u = 0$$

$$\frac{\partial v}{\partial y} = 0$$

### 3.4. Initial Conditions for Hydrodynamic Models

The initial conditions are specified by zero velocity everywhere in the domain ( $u=v=w=0$ ), since it is quite difficult to obtain ground truth current measurements for the entire domain for the kind of grid size resolution that would be required. Although an initial free surface,  $\eta=\eta(x,y,t=0)$  can be specified from existing tide data bases, compatibility between surface height and the velocities requires starting the computations with a flat surface,  $\eta(x,y,t=0)=0$ , initially.

### 3.5. Concentration Equation in Cartesian Coordinate System (x,y,z)

This subsection presents the concentration equation in general form for both sediment transport and dissolved chemical transport. All new symbols are given at the beginning of this report in the nomenclature section. Thus, the concentration equation in turbulent flow can be expressed in terms of turbulent eddy transport coefficients as in  $(x,y,z)$ :

$$\begin{aligned} \frac{\partial c}{\partial t} + u \frac{\partial c}{\partial x} + v \frac{\partial c}{\partial y} + w \frac{\partial c}{\partial z} = D_H \frac{\partial^2 c}{\partial x^2} \\ + D_H \frac{\partial^2 c}{\partial y^2} + D_V \frac{\partial^2 c}{\partial z^2} \end{aligned} \quad (3-26)$$

We assume, as did other researchers, that molecular diffusion is unimportant by comparison with turbulent diffusion, and, hence, can be neglected. Sheng (1975), Lam (1975). The dispersion of suspended sediment particles in turbulent flow can be considered as follows. Following Sheng's argument, for small concentration and small particles, and if the fluid particle accelerations are small in comparison with the gravitational acceleration, it may be assumed that the horizontal velocities of the fluid and the sediment particle are the same, whereas

the vertical velocities differ by an amount  $W_s$  defined as the "settling velocity" of the suspended sediment particle relative to the ambient fluid.

$$W = W_f + W_s \quad (3-27)$$

Where  $W_f$  is the vertical velocity of the fluid. Then for convenience letting  $W = W + W_s$ , equation (3-26) becomes for sediment transport:

$$\begin{aligned} \frac{\partial c}{\partial t} + u \frac{\partial c}{\partial x} + v \frac{\partial c}{\partial y} + (W + W_s) \frac{\partial c}{\partial z} \\ = D_H \frac{\partial^2 c}{\partial x^2} + D_H \frac{\partial^2 c}{\partial y^2} + D_V \frac{\partial^2 c}{\partial z^2} \end{aligned} \quad (3-28)$$

Note, that equation (3-28) also applies for dissolved chemical transport (or for neutrally buoyant particles) by setting  $W_s=0$ .

Appendix A discusses settling velocity in much more detail.

3.6. Concentration Equation in  $(\alpha, \beta, \sigma)$  Coordinate System, ignoring settling velocity, is:

$$\begin{aligned} \frac{\partial(Hc)}{\partial t} + \frac{\partial(Huc)}{\partial \alpha} + \frac{\partial(Hvc)}{\partial \beta} + H \frac{\partial(\Omega c)}{\partial \sigma} \\ = D_H \left\{ \frac{\partial}{\partial \alpha} \left( H \frac{\partial c}{\partial \alpha} \right) \right\} + D_H \left\{ \frac{\partial}{\partial \beta} \left( H \frac{\partial c}{\partial \beta} \right) \right\} \\ + \frac{D_V}{H} \frac{\partial^2 c}{\partial \sigma^2} \end{aligned} \quad (3-29)$$

It is quite important to note that the work of Sheng (1975), Apmann et al (1970), Jobson (1970) and others does not account for free surface variations in space and time; and only Sheng takes account of bottom topography. In fact Sheng and Lick (1976) reported further that their investigations used a "rigid-lid" condition at the surface,

thus not allowing the surface to move at all.

Following Tchen (1947) and Lumley (1957) the sediment particle is assumed to be so small that its motion relative to the ambient fluid follows Stoke's law of resistance. The eddy diffusion coefficient for the particle is the same as that of the fluid. Sayre (1962) concluded that small sediment particles (diameter less than 0.1 mm) with a settling velocity in the Stoke's range, very nearly follow the turbulent fluctuations, and, consequently, have a diffusion coefficient nearly equal to that of the fluid. Thus, equation (3-29) becomes, for a finite settling velocity  $W_s$ , for suspended sediment particles:

$$\begin{aligned} & \frac{\partial(Hc)}{\partial t} + \frac{\partial(Huc)}{\partial \alpha} + \frac{\partial(Hv\phi)}{\partial \beta} + H \frac{\partial(\Omega + \frac{W_s}{H})c}{\partial \sigma} \\ & D_H \left\{ \frac{\partial}{\partial \alpha} \left( H \frac{\partial c}{\partial \alpha} \right) \right\} + D_H \left\{ -\frac{\partial}{\partial \beta} \left( H \frac{\partial c}{\partial \beta} \right) \right\} \\ & + \frac{D_v}{H} \frac{\partial^2 c}{\partial \sigma^2} \end{aligned} \quad (3-30)$$

Where, this equation is valid for dissolved chemical transport by merely setting  $W_s=0$ .

### 3.7. Boundary Conditions for Concentration Equation

The nature of equation (3-30) is such that boundary conditions and initial conditions are required to complete the mathematical model. Thus, this section will present the full set of boundary conditions for both sediment transport and dissolved chemical transport. Then the next section of this chapter will give the initial conditions for both these numerical concentration studies.

#### 3.7.1. Boundary Conditions for Sediment Transport

The boundary conditions we've used for sediment transport



in the South Biscayne Bay are zero convective and diffusive mass flux across the lateral boundaries (Sheng (1975) also used this boundary condition), zero flux across the free surface, and deposition of sediment particles at the bottom surface. Following Sheng, a boundary condition sufficiently general to describe practically all situations encountered in sediment transport can be written as (Monin and Yaglom (1971):

$$-W_s c + Dv \frac{\partial c}{\partial z} = \beta c - E \quad (3-31)$$

Where the first term represents the flux to the bottom boundary due to gravitational settling. The second term represents the flux to the boundary due to vertical turbulent diffusion. The first term on the right hand side of equation (3-31) depends on the "porosity" or "stickiness" of the boundary.  $\beta = 0$  corresponds to perfect reflection and  $\beta \rightarrow \infty$  corresponds to perfect absorption. For  $0 < \beta < \infty$  partial reflection and absorption is permitted. Finally E corresponds to viscous entrainment. At the free surface no layer of contaminant (or sediment particles) is present, and, hence, equation (3-31) reduces to:

$$-W_s c + Dv \frac{\partial c}{\partial z} = 0 \quad (3-32)$$

Table 3-1 presents the free surface and bottom surface boundary conditions used by other researchers.

TABLE 3-1

RESEARCHER(S)	TOP BOUNDARY	BOTTOM BOUNDARY
Sheng (1975)	$-W_{sc} + Dv \frac{\partial c}{\partial z} = 0$	$-W_{sc} + Dv \frac{\partial c}{\partial z} = \beta c$
Apmann et al (1970)	$-W_{sc} + Dv \frac{\partial c}{\partial z} = 0$	$c = \text{Const.}$
Hjelmfelt et al (1970)	$-W_{sc} + Dv \frac{\partial c}{\partial z} = 0$	$c = \text{Const.}$
Jobson (1970)	$-W_{sc} + Dv \frac{\partial c}{\partial z} = 0$	$Dv \frac{\partial c}{\partial z} = W_{sc} (1-A)$
Jobson et al (1970)	$-W_{sc} + Dv \frac{\partial c}{\partial z} = 0$	$Dv \frac{\partial c}{\partial z} = W_{sc} (1-A)$
Mei (1969)	$-W_{sc} + Dv \frac{\partial c}{\partial z}$	$c = \text{Const.}$

Where A = probability of sediment particles leaving suspension and depositing on the bottom bed; it represents the rate of mass transfer from suspension to the bed. Now, the values used by these researchers for A and  $\beta$ , respectively, are presented in Table 3-2.

TABLE 3-2

RESEARCHER	$\beta$	A
Sheng (1975)	$\beta = 0$ and $\beta \rightarrow \infty$	Not applicable
Jobson (1970)	Not applicable	$A = 0.3$ and $A = 1.0$

Note,  $\beta = 0$  corresponds to perfect reflection and  $\beta \rightarrow \infty$  corresponds to perfect absorption,  $C = 0$ . In our investigation we've used the form of the bottom boundary condition as used by Jobson (1970):

$$Dv \frac{\partial C}{\partial z} = Wsc (1-A) \quad (3-33)$$

In our numerical studies we've used two different values for A, that is,  $A = 0.3$  and  $A = 0.9$ . Therefore, the boundary conditions we've used for sediment transport in the  $(x,y,z)$  coordinate system are in summary:

#### Lateral Boundaries

$$\frac{\partial C}{\partial x} = 0 \quad \text{at } y\text{-boundaries} \quad (3-34)$$

$$\frac{\partial C}{\partial y} = 0 \quad \text{at } x\text{-boundaries} \quad (3-35)$$

#### Free Surface

$$-Wsc + Dv \frac{\partial C}{\partial z} = 0 \quad (3-36)$$

#### Bottom Surface

$$Dv \frac{\partial C}{\partial z} = Wsc (1-A) \quad (3-37)$$

Noting, that these boundary conditions were expressed in the  $(\alpha, \beta, \sigma)$  coordinate system for our numerical sediment transport studies by making the following transformations:

$$\frac{\partial}{\partial x} \approx \frac{\partial}{\partial \alpha} \quad \text{for } \frac{\partial H}{\partial \alpha} \quad \text{and } \frac{\partial \eta}{\partial \alpha} \text{ small}$$

$$\frac{\partial}{\partial y} \approx \frac{\partial}{\partial \beta} \quad \text{for } \frac{\partial H}{\partial \beta} \quad \text{and } \frac{\partial \eta}{\partial \beta} \text{ small}$$

and,

$$\frac{\partial C}{\partial z} = \frac{1}{H} \frac{\partial C}{\partial \sigma}$$

### 3.7.2. Boundary Conditions for Dissolved Chemical Transport.

The boundary conditions we've used for dissolved chemical transport in the South Biscayne Bay are zero flux lateral solid boundaries, zero flux across the free surface, and zero flux across the bottom boundary. Tidal flushing at the ocean-exchange area is treated as follows following Lo et al (1976):

$$\frac{\partial c}{\partial y} = 0 \quad \text{during outflow from the bay } (V > 0)$$

$$c = 0 \quad \text{during inflow to the bay } (V < 0)$$

Therefore, the boundary conditions we've used for dissolved chemical transport in the (x, y, z) coordinate system are in summary:

#### Lateral Boundaries

$$\frac{\partial c}{\partial y, x} = 0 \quad \text{at } x, y\text{-boundaries} \quad (3-38)$$

#### Free Surface

$$-Wsc + Dv \frac{\partial c}{\partial z} = 0 \quad (3-39)$$

#### Bottom Surface

$$-Wsc + Dv \frac{\partial c}{\partial z} = 0 \quad (3-40)$$

#### Ocean-Exchange Area

$$\frac{\partial c}{\partial y} = 0 \quad \text{for } v > 0 \quad (3-41)$$

$$c = 0 \quad \text{for } v < 0$$

Again, these boundary conditions were expressed in the ( $\alpha, \beta, \rho$ ) coordinate system for our numerical dissolved chemical studies by making the following transformations:

$$\frac{\partial}{\partial y} = \frac{\partial}{\partial \beta} \quad \text{for } \frac{\partial H}{\partial \beta} \quad \text{and} \quad \frac{\partial \eta}{\partial \beta} \quad \text{small}$$

And,

$$\frac{\partial c}{\partial z} = \frac{1}{H} \frac{\partial c}{\partial \sigma}$$

### 3. 8. Initial Conditions for Concentration Equation

The initial conditions for both sediment transport and dissolved chemical transport will now be presented.

#### 3. 8. 1. Initial Conditions for Sediment Transport

The numerical study of sediment transport consisted of specifying an instantaneous line source of unit concentration along the intracoastal waterway channel in the South Biscayne Bay. Fig. 3-4 shows the location of the intracoastal waterway channel in the <sup>\*\*</sup> grid system used for these studies. Therefore, the initial condition is:

$$C(\alpha, \beta, \sigma) = 0 \quad \text{for } \alpha, \beta, \sigma \text{ not along channel}$$

$$C(\alpha, \beta, \sigma) = 1 \quad \text{for } \alpha, \beta, \sigma \text{ along channel.}$$

#### 3. 8. 2. Initial Conditions for Dissolved Chemical Transport

The numerical studies of dissolved chemical transport consisted of specifying first, an instantaneous uniform unit concentration distribution initially, that is,  $C = 1$  for all  $\alpha, \beta, \sigma$ ; and, specifying instantaneous vertical line sources at various points to simulate dye release sites. Neumann and Pierson (1966) state that specifying line sources at a point is perfectly legitimate for shallow water bodies.

Therefore, the initial conditions in summary are:

$$C(\alpha, \beta, \sigma) = 1 \quad \text{everywhere in the domain for an instantaneous uniform unit concentration distribution.}$$

And,

$$C(\alpha, \beta, \sigma) = 1 \quad \text{at dye-release sites}$$

$$C(\alpha, \beta, \sigma) = 0 \quad \text{elsewhere in domain}$$

<sup>\*\*</sup> Note: This grid system was used such that the channel is aligned with the x-axis as shown in Fig. 3-4

Fig. 3-5 shows the map of South Biscayne Bay indicating the dye-release sites at Snapper Creek Canal, Black Creek, and Mowry Creek; and Fig.3-6 shows the numerical grid system indicating the nodes at which these dye release sites were initially specified. Note, however, that the grid used in these studies is different from that used for the sediment transport studies, which was rotated approximately  $20^{\circ}$  clockwise with respect to due North. This was necessary in order to align the intracoastal waterway channel with the x-axis (or  $\alpha$ -axis) in the grid system.

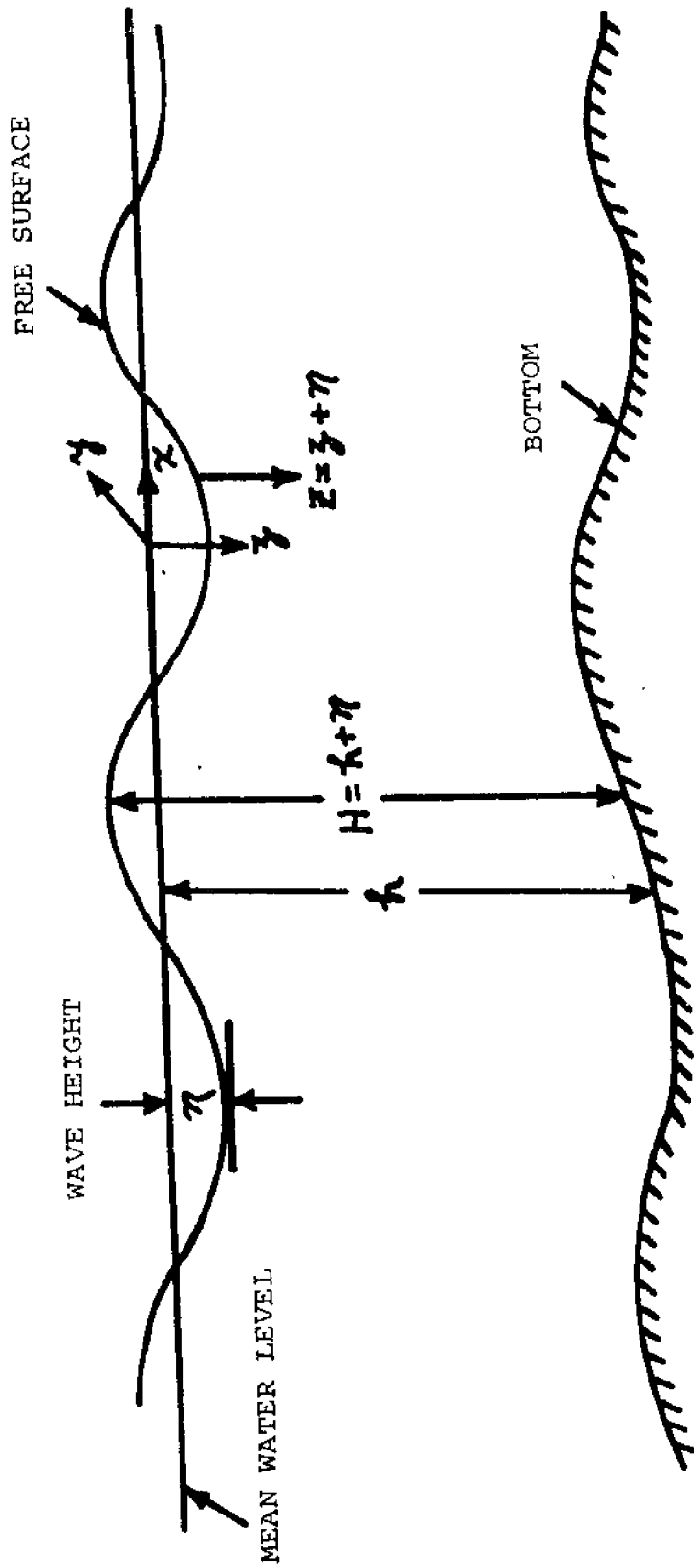


Fig. 3-1 The xyz Coordinate System for the Free-Surface Model for Sediment Transport.

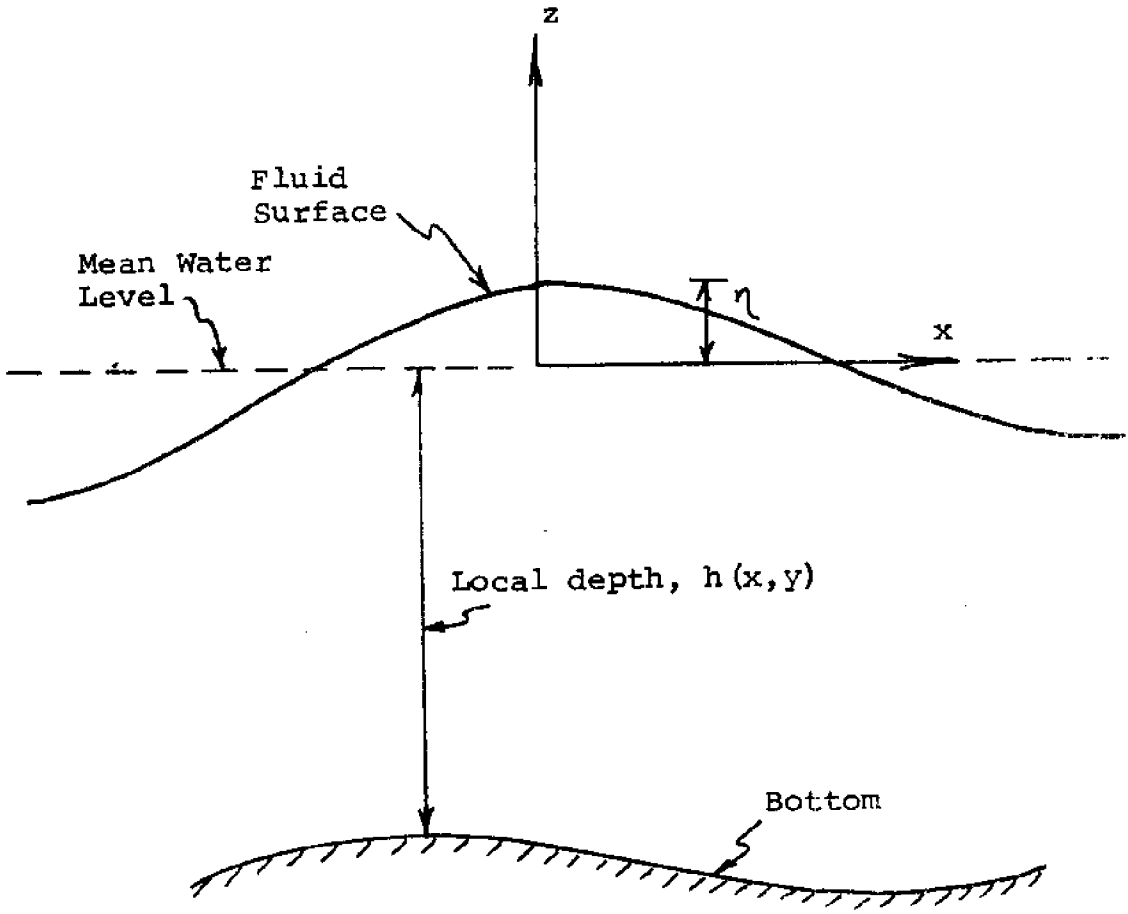


Fig. 3-2 The xyz Coordinate System for the Free-Surface Model for Dissolved Chemical Transport.



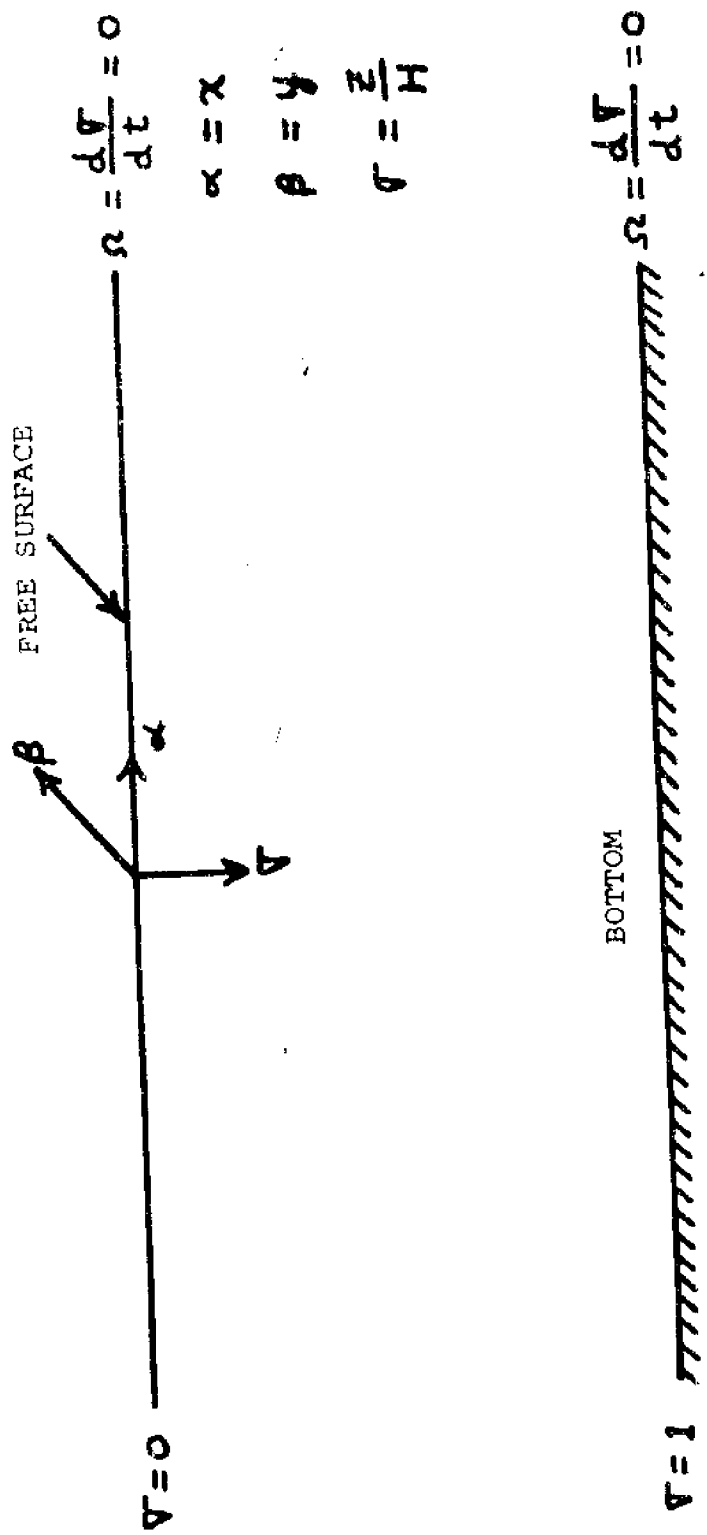


FIG: 3-3 The  $\alpha\beta\sigma$  Coordinate System for the Free-Surface Model

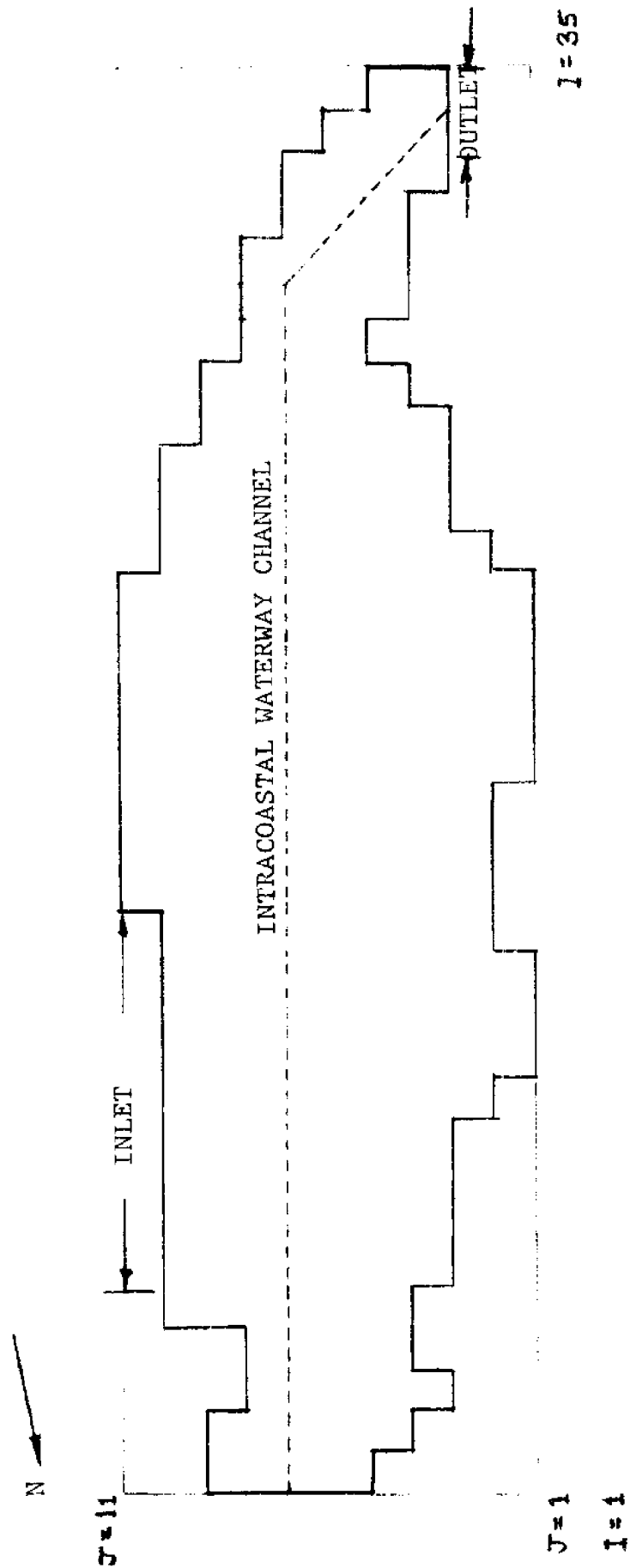
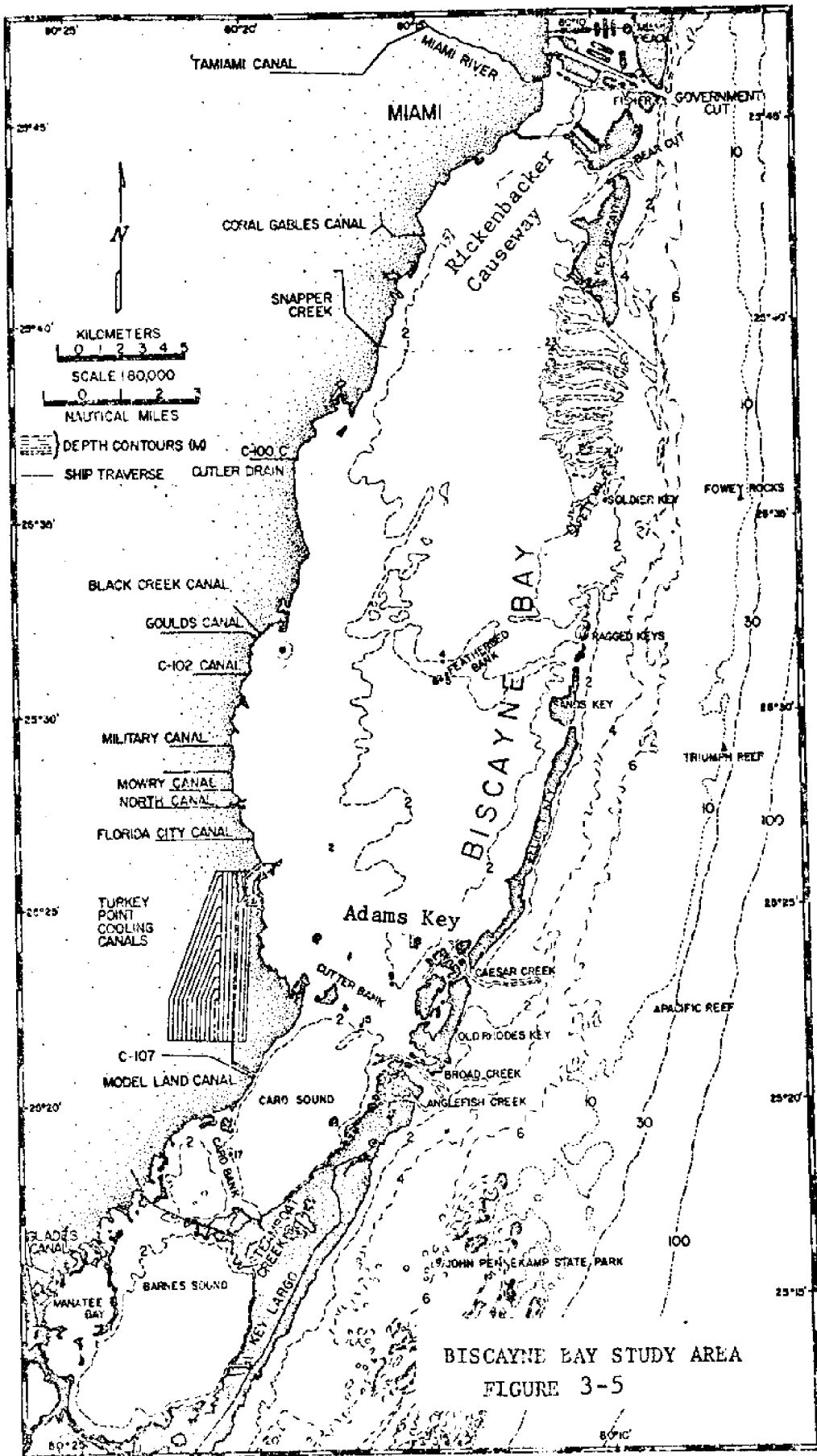


Fig. 3-4 Horizontal Grid System for Biscayne Bay used in Sediment Transport.



BISCAYNE BAY STUDY AREA  
FIGURE 3-5

#### 4. Numerical Method of Solution

##### 4.1. General

It is obvious that closed form analytical solution of the hydrodynamic equations and the concentration equation is impossible to get. The set of equations consists of coupled, time-dependent, three-dimensional, nonlinear partial differential equations. Therefore, the finite difference method is used to obtain numerical solutions. Note, however, that the numerical method of solving the hydrodynamic equations for both cases of sediment transport and dissolved chemical transport will be presented in Chapter 5, as well as the manner in which the resultant surface height and velocity field are coupled to the numerical model of the concentration equation. This chapter will only deal with the numerical model used for solving the concentration equation itself. The explicit finite difference method is used for numerical solution of the concentration equation, and the details will now be discussed.

##### 4.2. Finite Difference Representation of Concentration Equation

This section presents the numerical scheme for solving the three-dimensional, time-dependent concentration equation. The general form of the equation, including settling velocity,  $W_s$ , will be presented, realizing of course that the equation also applies to dissolved chemical transport by simply setting  $W_s = 0$ .

A forward-time, central-space (so-called FTCS method) explicit finite difference scheme is used with

DuFort-Frankel differencing performed on the vertical diffusion term. This scheme is referred to as a "modified DuFort-Frankel scheme", since the standard scheme is central-time, central-space, Roache (1972). This FTCS scheme was used by Sengupta and Lick (1974) to ensure against "time splitting", and was later incorporated by Sheng (1975) for contaminant and dispersion studies: Thus equation (3-30) becomes:

$$\begin{aligned}
 & \frac{(H_{I,J}^{n+1} C_{I,J,K}^{n+1} - H_{I,J}^n C_{I,J,K}^n)}{\Delta t} \\
 &= \frac{-(H_{I+1,J}^n U_{I+1,J,K}^n C_{I+1,J,K}^n - H_{I-1,J}^n U_{I-1,J,K}^n C_{I-1,J,K}^n)}{2 \Delta \alpha} \\
 & - \frac{(H_{I,J+1}^n V_{I,J+1,K}^n C_{I,J+1,K}^n - H_{I,J-1}^n V_{I,J-1,K}^n C_{I,J-1,K}^n)}{2 \Delta \beta} \\
 & - \frac{H_{I,J}^n \{ \Omega_{I,J,K+1}^n C_{I,J,K+1}^n + (W_s/H_{I,J}^n) C_{I,J,K+1}^n \}}{2 \Delta \sigma} \\
 & + \frac{H_{I,J}^n \{ \Omega_{I,J,K-1}^n C_{I,J,K-1}^n + (W_s/H_{I,J}^n) C_{I,J,K-1}^n \}}{2 \Delta \sigma} \\
 & + D_H \left\{ \frac{H_{I+1,J}^n - H_{I-1,J}^n}{2 \Delta \alpha} \right\} \left\{ \frac{C_{I+1,J,K}^n - C_{I-1,J,K}^n}{2 \Delta \alpha} \right\} \\
 & + D_H H_{I,J}^n \left\{ \frac{C_{I+1,J,K}^n + C_{I-1,J,K}^n - 2C_{I,J,K}^n}{(\Delta \alpha)^2} \right\}
 \end{aligned}$$

$$\begin{aligned}
& + D_H \left\{ \frac{H_{I,J+1}^n - H_{I,J-1}^n}{2 \Delta \beta} \right\} \left\{ \frac{C_{I,J+1,K}^n - C_{I,J-1,K}^n}{2 \Delta \beta} \right\} \\
& + D_H H_{I,J}^n \left\{ \frac{C_{I,J+1,K}^n + C_{I,J-1,K}^n - 2C_{I,J,K}^n}{(\Delta \beta)^2} \right\} \\
& + \left( \frac{Dv}{H_{I,J}^n} \right) \left\{ \frac{C_{I,J,K+1}^n + C_{I,J,K-1}^n - C_{I,J,K}^{n+1} - C_{I,J,K}^{n-1}}{(\Delta \sigma)^2} \right\}
\end{aligned} \tag{4-1}$$

$$\text{Where } Dv_{I,J} = 0.0018 (H_{I,J})^{4/3} \tag{4-2}$$

Note:  $Dv = \text{Const.}$  for dissolved chemical transport.

The last term in equation (4-1) corresponds to DuFort-Frankel differencing, and, as can be seen, is semi-implicit in time. It has been learned, however, that equation (4-1) is only used for values of the vertical grid index  $1 < K < 5$ , since for  $K = 1$  (top boundary) and  $K = 5$  (bottom boundary) the inclusion of the mass flux boundary conditions into equation (4-1) does not conserve mass. This will be further discussed in section 4.4. The next section 4.3 presents the boundary conditions in finite difference notation.

### 4.3. Finite Difference Representation of Boundary Conditions

This section presents the finite difference form of the boundary conditions for sediment transport and dissolved chemical transport.

#### 4.3.1. Boundary Conditions for Sediment Transport

Now the boundary conditions for sediment transport will be expressed in finite difference form. In summary these boundary conditions are:

##### Lateral Boundaries

$$C_w = C_{w+1} \quad (4-3)$$

That is, the concentration at the interior node adjacent to the lateral boundary is used to yield the value at the boundary. This is a numerical approximation to equation (3-34) and (3-35).

##### Free Surface

$$-W_s C_{I,J,K} + \left(\frac{Dv}{H}\right)_{I,J} \frac{\partial C}{\partial \sigma} \Big|_{I,J,K} = 0 \quad (4-4)$$

Where  $K = 1$ ,

##### Bottom Surface

$$\left(\frac{Dv}{H}\right)_{I,J} \frac{\partial C}{\partial \sigma} \Big|_{I,J,K} = W_s C_{I,J,K} (1 - A) \quad (4-5)$$

Where  $K = 5$ .

#### 4.3.2. Boundary Conditions for Dissolved Chemical Transport

The boundary conditions for dissolved chemical transport will now be expressed in finite difference form. In summary these boundary conditions are:

##### Lateral Boundary

$$C_w = C_{w+1} \quad (4-6)$$

##### Free Surface

$$-W_s C_{I,J,K} + \left(\frac{Dv}{H}\right)_{I,J} \frac{\partial C}{\partial \sigma} \Big|_{I,J,K} = 0 \quad (4-7)$$

Where  $K = 1$ ,

Bottom Surface

$$-W_s C_{I,J,K} + \left(\frac{Dv}{H}\right)_{I,J} \frac{\partial C}{\partial \sigma} \Big|_{I,J,K} = 0 \quad (4-8)$$

At  $K = 5$ ,

Ocean-Exchange Area

$$\left. \begin{array}{l} C_w = C_{w+1} \quad \text{for } V > 0 \quad (\text{outflow}) \\ C_w = 0 \quad \text{for } V < 0 \quad (\text{inflow}) \end{array} \right\} (4-9)$$

#### 4.4. Top and Bottom Boundary Finite Difference Equations from Conservation of Mass Considerations

In this section the top and bottom boundary finite difference equations will be derived from a conservation of mass control volume formulation, Sheng (1975). We have learned that merely substituting the aforementioned boundary conditions into equation (4-1) does not conserve mass, and, hence, we've derived two additional finite difference equations for the top and bottom boundaries, respectively. Then, upon substitution of the top and bottom boundary conditions into these equations mass is conserved. Note, that we will use the general form of the concentration equation (3-30) and the boundary conditions for sediment transport in these derivations. The resulting finite difference equations are valid for dissolved chemical transport by setting  $W_s = 0$  and  $A = 0$ .

The full concentration equation (3-30) can be expressed as:



$$\begin{aligned}
& \frac{\partial(Hc)}{\partial t} + \frac{\partial(Huc)}{\partial \alpha} + \frac{\partial(Hvc)}{\partial \beta} + H \frac{\partial(\Omega'c)}{\partial \sigma} \\
& = D_H \left\{ \frac{\partial}{\partial \alpha} \left( H \frac{\partial c}{\partial \alpha} \right) \right\} + D_H \left\{ \frac{\partial}{\partial \beta} \left( H \frac{\partial c}{\partial \beta} \right) \right\} \\
& + \left( \frac{Dv}{H} \right) \frac{\partial^2 c}{\partial \sigma^2}
\end{aligned} \tag{4-10}$$

$$\text{Where } \Omega' = \Omega + Ws/H \tag{4-11}$$

So that,

$$\begin{aligned}
& \frac{\partial(Hc)}{\partial t} = - \frac{\partial(Huc)}{\partial \alpha} - \frac{\partial(Hvc)}{\partial \beta} - H \frac{\partial(\Omega'c)}{\partial \sigma} \\
& + D_H \left\{ \frac{\partial}{\partial \alpha} \left( H \frac{\partial c}{\partial \alpha} \right) \right\} + D_H \left\{ \frac{\partial}{\partial \beta} \left( H \frac{\partial c}{\partial \beta} \right) \right\} \\
& + \left( \frac{Dv}{H} \right) \frac{\partial^2 c}{\partial \sigma^2}
\end{aligned} \tag{4-12}$$

Now, equation (4-12) is integrated over the volume of a half-cell either at the top surface or at the bottom surface, and integration over  $\Delta t$  is also performed. Fig.4-1 illustrates the top half-cell, and Fig.4-2 illustrates the bottom half-cell. The volume of these half-cells =  $\frac{H}{2} \Delta \alpha \Delta \beta \Delta \sigma$ . Upon integrating equation (4-12) over  $\frac{H}{2} \Delta \alpha \Delta \beta \Delta \sigma$  and over  $\Delta t$  we obtain at the top boundary:

$$\begin{aligned}
& \Delta t \int_0^{I+\frac{1}{2}} \int_{I-\frac{1}{2}}^{J+\frac{1}{2}} \int_{J-\frac{1}{2}}^{K+\frac{1}{2}} \frac{\partial(Hc)}{\partial t} \cdot \frac{H}{2} d\alpha d\beta d\sigma dt \\
& = \int_{\alpha} \int_{\beta} \int_{\sigma} (H^{n+1} c^{n+1} - H^n c^n) \frac{H}{2} d\alpha d\beta d\sigma
\end{aligned}$$

$$\begin{aligned}
&= - \Delta t \int_{\beta} \int_{\sigma} \{ (Huc)_{I+\frac{1}{2}} - (Huc)_{I-\frac{1}{2}} \} \cdot \frac{H}{2}^* d\beta d\sigma \\
&- \Delta t \int_{\alpha} \int_{\sigma} \{ (Hvc)_{J+\frac{1}{2}} - (Hvc)_{J-\frac{1}{2}} \} \cdot \frac{H}{2} d\alpha d\sigma \\
&- \Delta t \int_{\alpha} \int_{\beta} \{ (H\Omega' C)_{K+\frac{1}{2}} - (H\Omega' C)_{K} \} \cdot \frac{H}{2} d\alpha d\beta \\
&+ \Delta t \int_{\beta} \int_{\sigma} (D_H H \frac{\partial c}{\partial \alpha})_{I-\frac{1}{2}}^{I+\frac{1}{2}} \cdot \frac{H}{2} d\beta d\sigma \\
&+ \Delta t \int_{\alpha} \int_{\sigma} (D_H H \frac{\partial c}{\partial \beta})_{J-\frac{1}{2}}^{J+\frac{1}{2}} \cdot \frac{H}{2} d\alpha d\sigma \\
&+ \Delta t \int_{\alpha} \int_{\beta} (\frac{Dv}{H}) (\frac{\partial c}{\partial \sigma})_K^{K+\frac{1}{2}} \cdot \frac{H}{2} d\alpha d\beta \quad (4-13)
\end{aligned}$$

Now, define volume average of first term (unsteady term):

$$** \quad H_{I,J} C_{I,J,K} \equiv \left\{ \frac{1}{\Delta\alpha\Delta\beta\Delta\sigma} \frac{H_{I,J}}{2} \right\} \int_{I-\frac{1}{2}}^{I+\frac{1}{2}} \int_{J-\frac{1}{2}}^{J+\frac{1}{2}} \int_K^{K+\frac{1}{2}} (HC) \cdot H d\alpha d\beta d\sigma$$

Thus, equation (4-13) yields for the first term,

\* Note: H is assumed relatively constant over  $\Delta t$  and over  $\Delta\alpha, \Delta\beta,$

\*\* Note: This application of the mean value theorem yields a volume averaged concentration somewhere in the half-cell. It is assumed it is at (I,J,K).

$$(H_{I,J}^{n+1} C_{I,J,K}^{n+1} - H_{I,J}^n \cdot C_{I,J,K}^n) \Delta\alpha\Delta\beta\Delta\sigma \frac{H_{I,J}}{2}$$

Then, surface averages are defined for the convective and diffusive fluxes crossing the cell boundaries as follows:

$$- \Delta t \int_{\beta} \int_{\sigma} \{ (Huc)_{I+\frac{1}{2}} - (Huc)_{I-\frac{1}{2}} \} H_{I,J} d\beta d\sigma \equiv$$

$$- \Delta t \{ (Huc)_{I+\frac{1}{2}} - (Huc)_{I-\frac{1}{2}} \} \underbrace{\frac{H\Delta\beta\Delta\sigma}{2}}_{\text{Surface Area}}$$

$$- \Delta t \int_{\alpha} \int_{\sigma} \{ (Hvc)_{J+\frac{1}{2}} - (Hvc)_{J-\frac{1}{2}} \} \cdot Hd\alpha d\sigma \equiv$$

$$- \Delta t \{ (Hvc)_{J+\frac{1}{2}} - (Hvc)_{J-\frac{1}{2}} \} \cdot \frac{H}{2} \Delta\alpha\Delta\sigma$$

$$- \Delta t \int_{\alpha} \int_{\beta} \{ (H\Omega' C)_{K+\frac{1}{2}} - (H\Omega' C)_K \} \cdot Hd\alpha d\beta \equiv$$

$$- \Delta t \{ (H\Omega' C)_{K+\frac{1}{2}} - (H\Omega' C)_K \} \cdot H\Delta\alpha\Delta\beta$$

$$\Delta t \int_{\beta} \int_{\sigma} (D_H H \frac{\partial c}{\partial \beta})_{I-\frac{1}{2}}^{I+\frac{1}{2}} \cdot Hd\beta d\sigma \equiv D_H \Delta t (H \frac{\partial c}{\partial \alpha})_{I-\frac{1}{2}}^{I+\frac{1}{2}} \cdot \frac{H}{2} \Delta\beta\Delta\sigma$$

$$\Delta t \int_{\alpha} \int_{\sigma} (D_H H \frac{\partial c}{\partial \beta})_{J-\frac{1}{2}}^{J+\frac{1}{2}} \cdot Hd\alpha d\sigma \equiv D_H \Delta t (H \frac{\partial c}{\partial \beta})_{J-\frac{1}{2}}^{J+\frac{1}{2}} \cdot \frac{H}{2} \Delta\alpha\Delta\sigma$$

$$\Delta t \int_{\alpha} \int_{\beta} (\frac{Dv}{H}) (\frac{\partial c}{\partial \sigma})_K^{K+\frac{1}{2}} \cdot H \cdot d\alpha d\beta \equiv Dv \Delta t (\frac{\partial c}{\partial \sigma})_K^{K+\frac{1}{2}} \cdot \Delta\alpha\Delta\beta$$

Therefore, equation (4-13) becomes,

$$(H_{I,J}^{n+1} C_{I,J,K}^{n+1} - H_{I,J}^n C_{I,J,K}^n) \Delta\alpha\Delta\beta\Delta\sigma \frac{H}{2} = -\Delta t (Huc)_{I-\frac{1}{2}}^{I+\frac{1}{2}} \cdot$$

$$\frac{H}{2} \Delta\beta\Delta\sigma$$

$$-\Delta t (Hvc)_{J-\frac{1}{2}}^{J+\frac{1}{2}} \cdot \frac{H}{2} \Delta\alpha\Delta\sigma - \Delta t (H\Omega' C)_K^{K+\frac{1}{2}} \cdot H \Delta\alpha\Delta\beta$$

$$+ \Delta t \cdot D_H \left( H \frac{\partial c}{\partial \alpha} \right)_{I-\frac{1}{2}}^{I+\frac{1}{2}} \cdot \frac{H}{2} \Delta\beta\Delta\sigma + \Delta t \cdot D_H \left( H \frac{\partial c}{\partial \beta} \right)_{J-\frac{1}{2}}^{J+\frac{1}{2}}$$

$$\cdot \frac{H}{2} \Delta\alpha\Delta\sigma + \Delta t \cdot D_v \left( \frac{\partial c}{\partial \sigma} \right)_K^{K+\frac{1}{2}} \Delta\alpha\Delta\beta \quad (4-14)$$

Now, by dividing equation (4-19) by  $\Delta\alpha\Delta\beta\Delta\sigma \cdot \frac{H}{2}$  we obtain,

$$H_{I,J}^{n+1} C_{I,J,K}^{n+1} - H_{I,J}^n C_{I,J,K}^n = -\Delta t (Huc)_{I-\frac{1}{2}}^{I+\frac{1}{2}} \frac{1}{\Delta\alpha} - \Delta t (Hvc)_{J-\frac{1}{2}}^{J+\frac{1}{2}} \frac{1}{\Delta\beta}$$

$$- \Delta t (H\Omega' C)_K^{K+\frac{1}{2}} \frac{2}{\Delta\sigma} + D_H \Delta t \left( H \frac{\partial c}{\partial \alpha} \right)_{I-\frac{1}{2}}^{I+\frac{1}{2}} \frac{1}{\Delta\alpha} + D_H \Delta t \left( H \frac{\partial c}{\partial \beta} \right)_{J-\frac{1}{2}}^{J+\frac{1}{2}} \frac{1}{\Delta\beta}$$

$$+ D_v \Delta t \left( \frac{\partial c}{\partial \sigma} \right)_K^{K+\frac{1}{2}} \frac{2}{H\Delta\sigma} \quad (4-15)$$

Now,

$$-\Delta t (H\Omega C)_K^{K+\frac{1}{2}} \frac{2}{\Delta\sigma} = -\Delta t W_s(C)_K^{K+\frac{1}{2}} \frac{2}{\Delta\sigma} - \Delta t (H\Omega C)_K^{K+\frac{1}{2}} \frac{2}{\Delta\sigma}$$

Next, by inserting the boundary condition (4-4) into (4-15),

$$W_s C_K^n = \frac{D_v}{H} \frac{\partial c}{\partial \sigma} \Big|_K^{n, n+1, n-1} \quad \underline{\text{Top Boundary}}$$

Where,  $\frac{\partial c}{\partial \sigma} \Big|_{k+\frac{1}{2}}^{n, n+1, n-1} = \frac{C_{k+1}^n - (C_k^{n+1} + C_k^{n-1})/2}{\Delta \sigma}$

And,  $C_{k+\frac{1}{2}} \approx (C_k + C_{k+1})/2$

We finally obtain for the top boundary:

$$\begin{aligned}
 C_{I, J, K}^{n+1} &= \{ H_{I, J}^n C_{I, J, K}^n - (W_s \Delta t / \Delta \sigma) (C_{I, J, K}^n + C_{I, J, K+1}^n) \\
 &- \Delta t (H_{u, n}^n C_{I-\frac{1}{2}}^{n+1}) \frac{1}{\Delta \alpha} - \Delta t (H_{v, n}^n C_{J-\frac{1}{2}}^{n+1}) \frac{1}{\Delta \beta} + D_H \Delta t \cdot \\
 &(H_{I-\frac{1}{2}}^n \frac{\partial c^n}{\partial \alpha}) \frac{1}{\Delta \alpha} + D_H \Delta t (H_{J-\frac{1}{2}}^n \frac{\partial c^n}{\partial \beta}) \frac{1}{\Delta \beta} \\
 &- \frac{2 \Delta t}{\Delta \sigma} (H_{\Omega, n}^n C_k^{n+1}) + \frac{D_v \Delta t}{H^n (\Delta \sigma)^2} (2C_{k+1}^n - C_k^{n-1}) \} \\
 &/ (H_{I, J}^{n+1} + \frac{D_v \Delta t}{H^n (\Delta \sigma)^2}) \tag{4-16}
 \end{aligned}$$

Similarly, the bottom finite difference equation can be obtained by integrating over the bottom half-cell shown in Fig.4-2, that is,

$$\int_{\Delta t} \int_{\beta} \int_{\alpha} \int_{k-\frac{1}{2}}^k (\dots) \cdot \frac{H}{2} d\alpha d\beta d\sigma dt$$

The resulting finite difference equation with the bottom boundary condition (4-5)

$$\frac{D_v}{H} \frac{\partial c}{\partial \sigma} \Big|_k^n = W_s C_k^n (1-A)$$

inserted into the resulting finite difference equation yields for the bottom boundary:

$$\begin{aligned}
C_{I,J,K}^{n+1} = & \{ H_{I,J}^n C_{I,J,K}^n + (W_s \Delta t / \Delta \sigma) (C_{I,J,K}^n + C_{I,J,K-1}^n) \\
& - (2AW_s \Delta t / \Delta \sigma) C_k^n - \Delta t (H^n u^n c^n)_{I-\frac{1}{2}}^{I+\frac{1}{2}} \frac{1}{\Delta \alpha} - \Delta t (H^n v^n c^n)_{J-\frac{1}{2}}^{J+\frac{1}{2}} \cdot \\
& \frac{1}{\Delta \beta} + D_H \Delta t (H^n \frac{\partial c^n}{\partial \alpha})_{I-\frac{1}{2}}^{I+\frac{1}{2}} \frac{1}{\Delta \alpha} + D_H \Delta t (H^n \frac{\partial c^n}{\partial \beta})_{J-\frac{1}{2}}^{J+\frac{1}{2}} \frac{1}{\Delta \beta} \\
& - \Delta t (H^n \Omega^n c^n)_{k-\frac{1}{2}}^k \frac{2}{\Delta \sigma} + D_v \frac{\Delta t}{H^n (\Delta \sigma)^2} (C_k^{n-1} - 2C_{k-1}^n) \} \\
& / (H^{n+1} + \frac{D_v \Delta t}{H^n (\Delta \sigma)^2}) \quad (4-17)
\end{aligned}$$

Where for example,  $(Huc)_{I+\frac{1}{2}} = H_{I+\frac{1}{2}} u_{I+\frac{1}{2}} C_{I+\frac{1}{2}}$

$$H_{I+\frac{1}{2}} = (H_I + H_{I+1})/2$$

$$\begin{aligned}
C_{I+\frac{1}{2}} = & \frac{1}{2} \{ (C_{I,J,K} + C_{I+1,J,K})/2 + (C_{I+1,J,K} + C_{I,J,K} \\
& + C_{I+1,J,K-1} + C_{I,J,K-1})/4 \}
\end{aligned}$$

$$\begin{aligned}
u_{I+\frac{1}{2}} = & \frac{1}{2} \{ (u_{I,J,K} + u_{I+1,J,K})/2 \\
& + u_{I+1,J,K} + u_{I,J,K} + u_{I+1,J,K-1} + u_{I,J,K-1})/4 \}
\end{aligned}$$

Note, K-1 is replaced with K+1 for computing u and c at the bottom boundary.

Therefore, equations (4-16) and (4-17) are used instead of equation (4-1) for the top and bottom boundaries, respectively.

#### 4.5. Initial Conditions in Finite Difference Form

This section presents the finite difference form of the initial conditions for sediment transport and dissolved chemical transport.

##### 4.5.1. Initial Conditions for Sediment Transport

$$C(I,J,K) = 1 \quad \text{for } J=J_0 \quad \text{and } 1 \leq K \leq 5$$

Where  $J_0 = 7$  in the grid system shown in Fig.3-4.

$$C(I,J,K) = 0 \quad \text{for } J \neq J_0 \quad \text{and } 1 \leq K \leq 5$$

##### 4.5.2. Initial Conditions for Dissolved Chemical Transport

For instantaneous uniform concentration,

$$C(I,J,K) = 1 \quad \text{everywhere inside domain}$$

$$C(I,J,K) = 0 \quad \text{outside domain.}$$

For dye releases sites:

$$C(17,2,K) = 1 \quad \text{Black Creek}$$

$$C(7,6,K) = 1 \quad \text{Snapper Creek Canal}$$

$$C(20,2,K) = 1 \quad \text{Mowry Canal}$$

$$C(I,J,K) = 0 \quad \text{elsewhere.}$$

#### 4.6. Second Upwind Differencing of Horizontal Convection

##### Terms

It was learned in our numerical studies that the use of central differencing of the convective derivatives in equations (4-1), (4-16), and (4-17) resulted in negative concentrations. Lam (1975) points out that the central difference approximation will be over-estimating the advective flux so much that it often causes a negative concentration

to appear in the neighboring cell. To circumvent this problem we've used the so-called "second upwind" differencing method, or "donor cell" method introduced by Gentry, Martin and Daly (1966). Some sort of average interface velocities on each side of the grid cell are defined; and, then, the sign of these velocities determines, by upwind differencing which value of concentration,  $C$ , to use. Following Roache (1972), in one-dimensional notation,

$$\frac{\Delta C_I}{\Delta t} = - \frac{u_R c_R - u_L c_L}{\Delta x} \quad (4-18)$$

approximates  $\frac{\partial c}{\partial t} = - \frac{\partial (uc)}{\partial x}$

Where  $u_R = \frac{1}{2} (u_{I+1} + u_I)$

$u_L = \frac{1}{2} (u_I + u_{I-1})$

And,

$C_R = C_I$  for  $u_R > 0$ ,  $C_R = C_{I+1}$  for  $u_R < 0$

$C_L = C_{I-1}$  for  $u_L > 0$ ,  $C_L = C_I$  for  $u_L < 0$

For  $u_R > 0$ ,  $u_L > 0$ :

$$\frac{\Delta C_I}{\Delta t} = - \left( \frac{u_R C_I - u_L C_{I-1}}{\Delta x} \right) \quad (4-19)$$

For  $u_R < 0$ ,  $u_L < 0$ :

$$\frac{\Delta C_I}{\Delta t} = - \left( \frac{u_R C_{I+1} - u_L C_I}{\Delta x} \right) \quad (4-20)$$



For  $u_R > 0$ ,  $u_L < 0$ :

$$\frac{\Delta C_I}{\Delta t} = - \left( \frac{u_R C_I - u_L C_I}{\Delta x} \right) \quad (4-21)$$

For  $u_R < 0$ ,  $u_L > 0$ :

$$\frac{\Delta C_I}{\Delta t} = - \left( \frac{u_R C_{I+1} - u_L C_{I-1}}{\Delta x} \right) \quad (4-22)$$

Now for our case we have the following form for the horizontal convective terms,

$$\frac{\partial (Huc)}{\partial \alpha} \quad \text{and} \quad \frac{\partial (Hvc)}{\partial \beta}$$

Thus we've merely replaced  $u_R$  and  $u_L$  with  $(Hu)_R$  and  $(Hu)_L$  and  $(Hv)_R$  and  $(Hv)_L$ , where,

$$(Hu)_R = \frac{1}{2} (H_{I,J} + H_{I+1,J}) \cdot \frac{1}{2} (U_{I,J,K} + U_{I+1,J,K})$$

$$(Hu)_L = \frac{1}{2} (H_{I,J} + H_{I-1,J}) \cdot \frac{1}{2} (U_{I,J,K} + U_{I-1,J,K})$$

$$(Hv)_R = \frac{1}{2} (H_{I,J} + H_{I,J+1}) \cdot \frac{1}{2} (U_{I,J,K} + U_{I,J+1,K})$$

$$(Hv)_L = \frac{1}{2} (H_{I,J} + H_{I,J-1}) \cdot \frac{1}{2} (U_{I,J,K} + U_{I,J-1,K})$$

This method is both conservative and transportive and is more accurate than first upwind differencing.

#### 4.7. Total System Mass Algorithm

Now the proper solution to equation (3-30) for either sediment particle concentration or dissolved chemical concentration must satisfy conservation of mass for the domain of the bay, which includes settled out mass for a finite value of bottom deposition rate  $A$ , and includes tidal flushing. However, tidal flushing is really only significant for computer runs for more than several hours, and our numerical sediment transport studies were only run for several hours, since 90% deposition for the values selected for settling velocity,  $W_s$ , and deposition rate,  $A$ , occurred in less than 4 hours in all cases. Hence, tidal flushing was found to be only important in our long run numerical dye release studies as will be discussed in Section 7.

##### 4.7.1. Mass in Domain of Bay

The total mass remaining in the domain of the bay, less the mass settled out (of course this is equal to zero for conservative dissolved chemical transport) and the mass flushed out at the ocean-exchange area, is obtained as follows.

$$M_{I+\frac{1}{2}, J+\frac{1}{2}} = \bar{C} \cdot Vol \quad (4-23)$$

Where  $M_{I+\frac{1}{2}, J+\frac{1}{2}}$  = mass per grid cell

$\bar{C}$  = cell averaged concentration

Vol = grid cell volume

Where,

$$\bar{C} \equiv \frac{1}{H} \int_{Z=0}^H C(x, y, z, t) dz \quad (4-24)$$

But in the  $(\alpha, \beta, \sigma)$  coordinate system,

$$\bar{C} = \int_{\sigma=0}^1 C(\alpha, \beta, \sigma, t) d\sigma \quad (4-25)$$

And, then

$$\text{Vol} = \Delta\alpha \cdot \Delta\beta \cdot H_{I+\frac{1}{2}, J+\frac{1}{2}} \quad (4-26)$$

Where, further

$$H_{I+\frac{1}{2}, J+\frac{1}{2}} = (H_{I, J} + H_{I+1, J} + H_{I, J+1} + H_{I+1, J+1})/4 \quad (4-27)$$

Hence, the mass left in the domain of the bay  $M(t)$  is,

$$M(t) = \sum_J \sum_I M_{I+\frac{1}{2}, J+\frac{1}{2}} \quad (4-28)$$

#### 4.7.2. Settled Out Mass Algorithm

For the case of bottom deposition of sediment particles on the bed, we have for the mass settled out per grid cell:

$$SM_{I+\frac{1}{2}, J+\frac{1}{2}} = AC_{I+\frac{1}{2}, J+\frac{1}{2}, K=5} \cdot W_s \cdot \Delta\alpha \cdot \Delta\beta \cdot \Delta t \quad (4-29)$$

$$\text{Where } C_{I+\frac{1}{2}, J+\frac{1}{2}, K} = (C_{I, J, K} + C_{I+1, J, K} + C_{I, J+1, K} + C_{I+1, J+1, K})/4 \quad (4-30)$$

Thus, the total mass settled out in the domain of the bay  $SM(t)$  is given by,

$$SM(t) = \sum_J \sum_I SM_{I+\frac{1}{2}, J+\frac{1}{2}} \quad (4-31)$$

#### 4.7.3. Total System Mass Without Flushing

By combining equations (4-28) and (4-31) we have a numerical check on our solution for sediment transport, that is

$$M(t) + SM(t) = \text{Const.} = M(t=0) \quad (4-32)$$

Of course this ignores tidal flushing, but for our numerical sediment transport studies, flushing is actually zero. This is true since 90% deposition of sediment particles occurred during flood tide, and flushing only occurs during ebb tide!

#### 4.7.4. Computation of Percent of Tidal Flushing

The fraction of mass left in the bay during tidal flushing is defined as,

$$X(t) = \frac{M(t)}{M(t=0)} \quad (4-33)$$

Then the percent of tidal flushing is defined as,

$$P \equiv \% \text{ tidal flushing} = (1 - X) \times 100\% \quad (4-34)$$

This of course, is not valid for sediment transport which would be,

$$P = \left(1 - \frac{M(t) + SM(t)}{M(t=0)}\right) \times 100\% \quad (4-35)$$

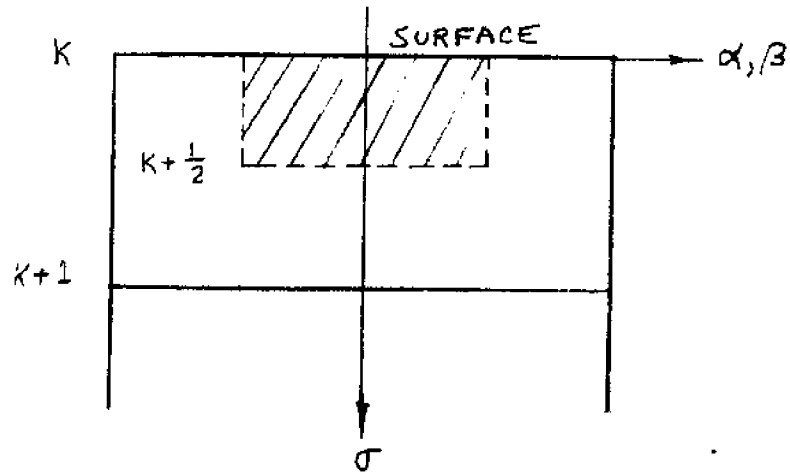


Fig.4-1 Top Half-Cell for Concentration Equation.

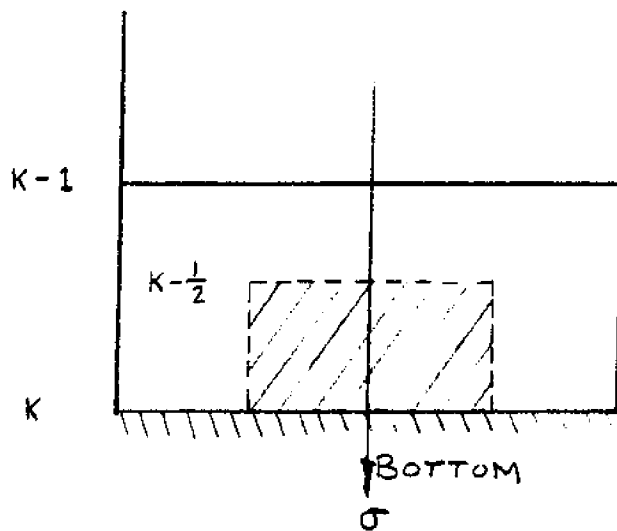


Fig.4-2 Bottom Half-Cell for Concentration Equation.

## 5. Coupling of Velocity Field and Surface Height Variations to Concentration Equation

The governing species concentration equation was coupled to the conservation of momentum equations and the surface height equation for the sediment transport studies; however, a previously obtained magnetic tape of numerical solutions of the velocity field and surface heights was coupled to the concentration equation for conservative, dissolved chemical transport studies. This latter method holds the surface heights and velocity field constant over each half-hour, and, thus the concentration equation is the only equation solved by the computer. This method was employed to save considerable computation time, since the numerical dissolved chemical flushing studies are run for two weeks of simulated time in order to obtain large flushing out of the bay. Lam (1975) followed a similar method of storing computed currents on magnetic tapes for inputting into the simulation of dispersion conservative substances such as chloride, and, the nonconservative substance phosphorus in Lake Erie.

### 5.1. Staggered Grid System for Computing Velocity Field and Surface Heights for Storage on Magnetic Tape for Dissolved Chemical Transport

The hydrodynamic equations and boundary conditions were expressed in the Richardson Lattice. Figure 5-1 shows a schematic of this staggered grid system. A Richardson lattice is used for the staggered grid arrangement of system variables  $\eta, u, v$  and  $\Omega$ . As already noted in Chapter 3 with

this type of grid arrangement, the horizontal velocity components  $u$  and  $v$  appear on solid boundaries only as normal velocities. That is, no conditions on tangential velocity components is specified on the boundaries. Section 3.3.2 and 3.4 in Chapter 3 present the appropriate boundary and initial conditions which were used to obtain numerical solutions for  $\eta, u, v$  and  $\Omega$ .

#### 5.2. Numerical Solutions of the Hydrodynamic Model used for Coupling to the Dissolved Chemical Transport Equation

The values of  $\eta$  (or  $H=h + \eta$ ),  $u, v$ , and  $\Omega$  used in equation (3-29) were obtained using wind and tide data bases for April 15, 1975. The hydrodynamic numerical model was run for two complete tidal cycles over 24 hours. However, to ignore "transient effects" prominent after start-up, the second tidal cycle results were repeated twice. The results were then stored on magnetic tape every half-hour.

The results of this simulation run are now presented in detail. First, the tide level variations at the tide gage locations used by Schneider (1969) are illustrated in Fig. 5-2 through 5-7 for a value of  $Kv=20.0 \text{ cm}^2/\text{sec}$ . The agreement at these tide gage locations is quite good both in terms of relative high and low tide values, and relative phasing between the tide data base and the model predictions. It must be noted at this point that we're comparing a statistically averaged data base to a computer model run using tide and wind data input for a particular day (i.e. April 15, 1975). Thus, the comparison for  $Kv=20.0 \text{ cm}^2/\text{sec}$  is really quite

good.

Figs. 5-8 through 5-11 shows the surface currents and lines of constant surface height predicted by the model every 6 hours in order to illustrate the tidal exchange at the inlet over a complete tidal cycle. As can be seen the bay is quite sensitive to the tidal driving force at the inlet. Figs. 5-12 and 5-13 show a plot of horizontal velocity, at various depths, as a function of time, at a point in the northern part of the bay and at a point in the southern part of the bay. As can be seen the currents are all in the same direction with varying depth as time proceeds; and furthermore the direction of the current is in the direction determined by the tidal current at the inlet. The wind effect has not reversed the current at either of these bay locations, and, therefore, the bay can be said to be tide dominated. Fig. 5-14 indicates the phase relationship between the tide height and the tidal current at the inlet. It can be seen that the current at the inlet does not reverse with increasing depth, and that the phase relationship indicates that the current and the tide height are out of phase owing to reflection of the surface waves at the west shoreline of the bay.

### 5.3. Calibration of Hydrodynamic Model used for Dissolved Chemical Transport Studies

The velocities were calibrated by using Wang's (1977) current data base for the South Biscayne Bay. After a thorough comparison and analysis of the model results for



various values of  $K_v$ , a value of  $K_v=20.0^2\text{cm} / \text{sec}$  was selected as the final value to use for generating our input magnetic tape. See Appendix E for velocity calibration.

#### 5.4. Interpolation of Staggered Grid Variables for Obtaining Solutions of the Dissolved Chemical Transport Equation

As shown in Fig.5-1 the variables  $H$ (or  $\eta$ )  $u, v$ , and  $\Omega$  are not located at the integral nodes in the full grid system. However, the concentration,  $C$ , is computed at these integral nodes, and, hence, the hydrodynamic variables must be interpolated in order to obtain values at these integral node points in the full grid system. The interpolation scheme used is as now follows.

1.  $u, v, \Omega$ , and  $H$  are used only at  $(I, J, K)$  integral nodes in the full (unstaggered) grid system for the concentration equation.

2.  $u, v, \Omega$ , and  $H$  are obtained from the values in the staggered grid system as follows:

$$u(I, J, K) = \{u(I, J-1, K) + u(I, J, K)\} / 2$$

$$v(I, J, K) = \{v(I-1, J, K) + v(I, J, K)\} / 2$$

$$H(I, J) = \{H(I-1, J) + H(I, J-1) + H(I, J) + H(I-1, J-1)\} / 4$$

$$\Omega(I, J, K) = \{\Omega(I, J, K) + \Omega(I-1, J, K) + \Omega(I, J-1, K) + \Omega(I-1, J-1, K)\} / 4$$

### 5.5. Numerical Solutions of the Hydrodynamic Model used for Coupling to the Sediment Transport Equation

The hydrodynamic model used in the sediment transport studies is given in Section 3.2.3. with variable  $K_v$  and  $D_v$  as given in Eq.3-1. A time step  $\Delta t=2$  min was used. Figs. 5-15 through 5-18 indicate the surface currents predicted by this model for 1 hour, 2 hours, 3 hours and 4 hours after start-up. As can be seen the flow field is strongly determined by the inlet current, and note that the southern part of the bay exhibits to a large degree uniform flow, whereas the northern part of the bay exhibits more of an irregular velocity pattern. The effect of these resulting velocity fields upon the sediment transport will be discussed in Section 6.2 to follow.

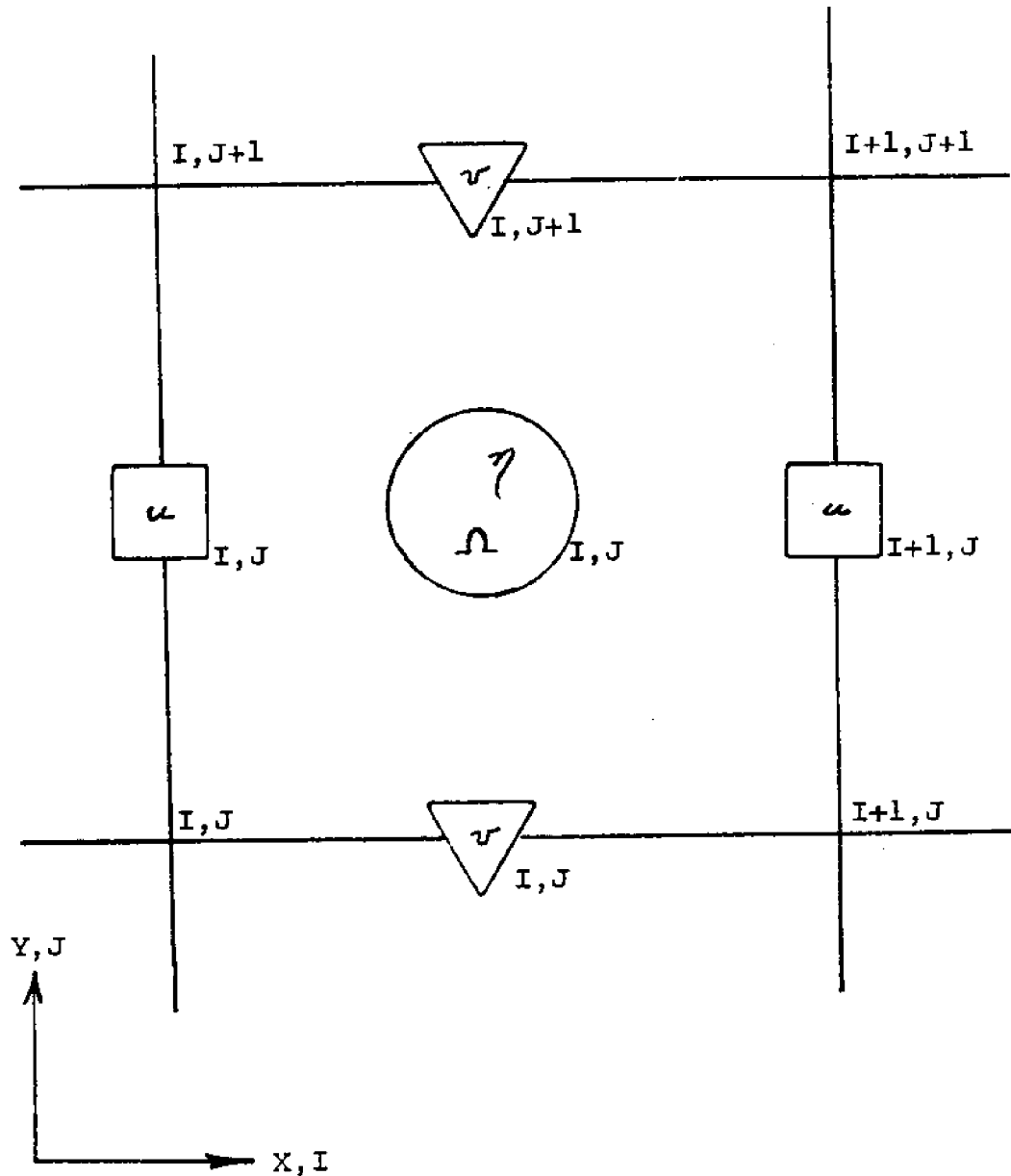
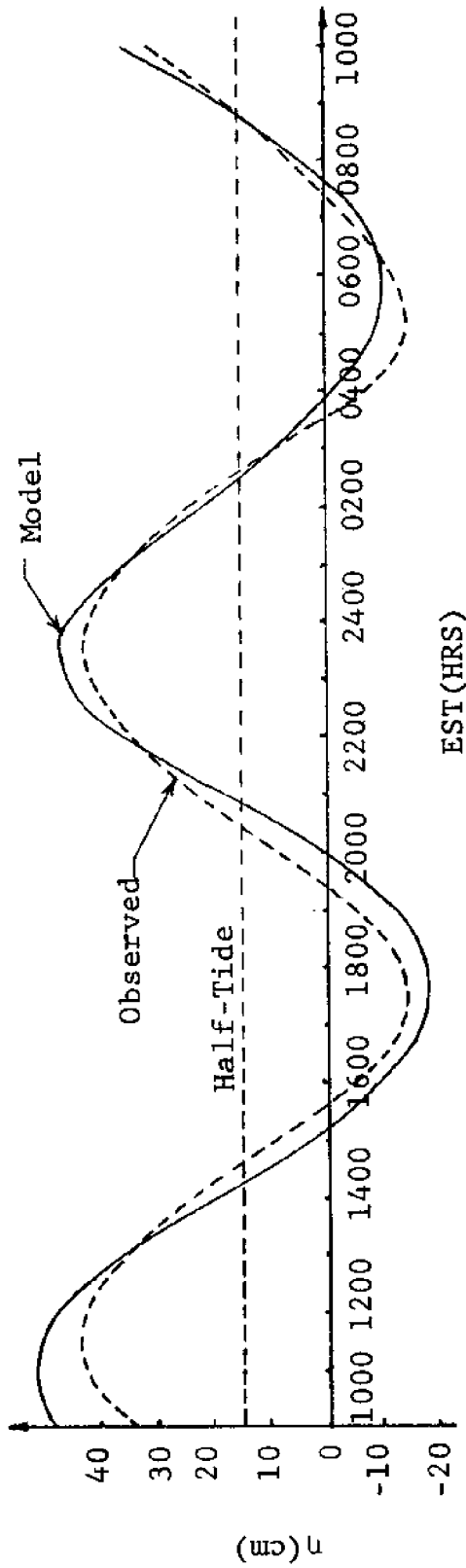


Fig. 5-1 Indexing system in the horizontal plane, Richardson Lattice.

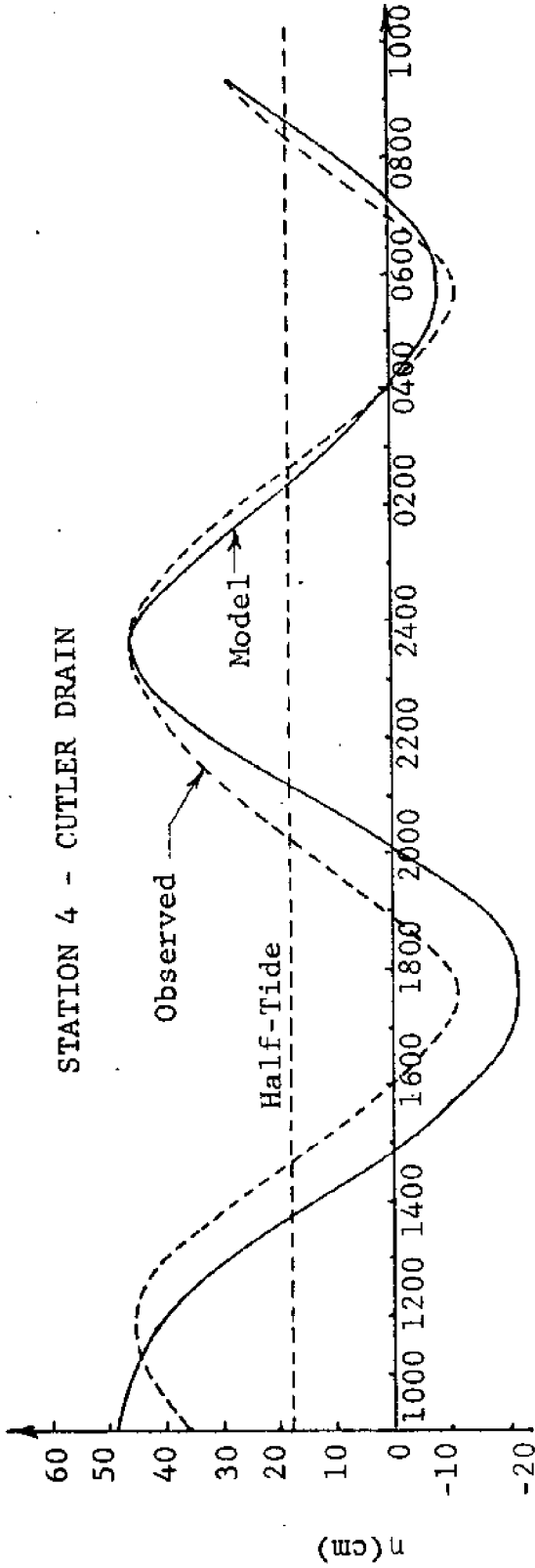
Fig. 5-2 Tide Levels, Observed vs. Model

STATION 2 - COCONUT GROVE



STATION 4 - CUTLER DRAIN

EST (HRS)

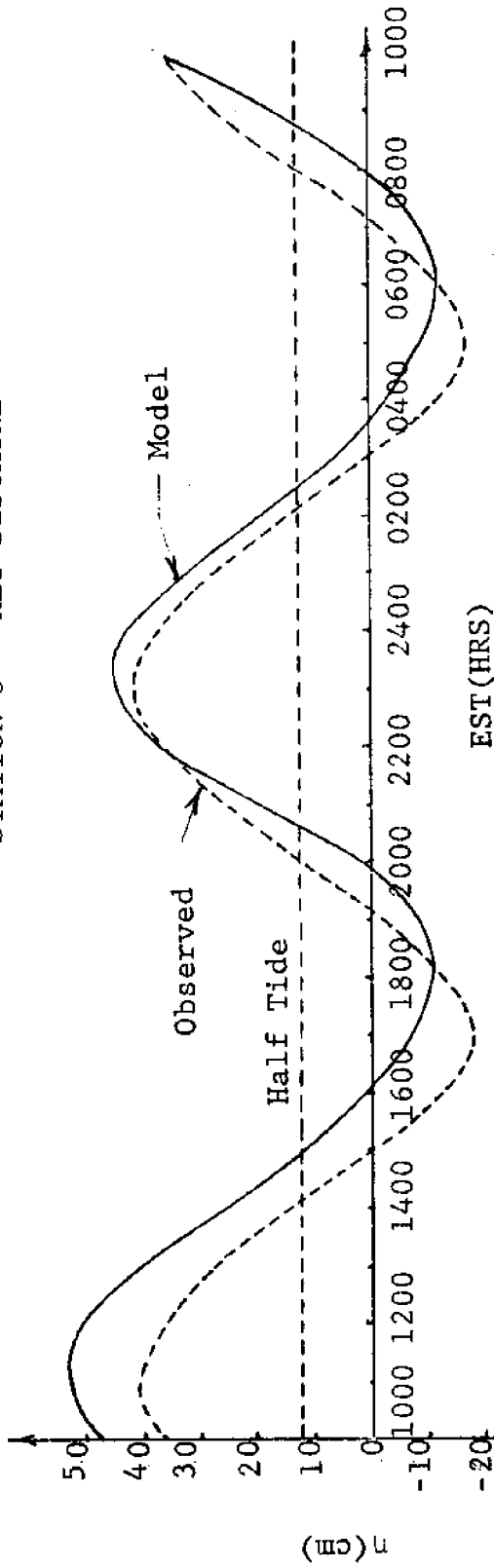


EST (HRS)

Fig. 5-3 Tide Levels, Observed vs. Model

Fig. 5-4 Tide Levels, Observed vs. Model

STATION 3 - KEY BISCAIYNE



STATION 5 - HOMESTEAD

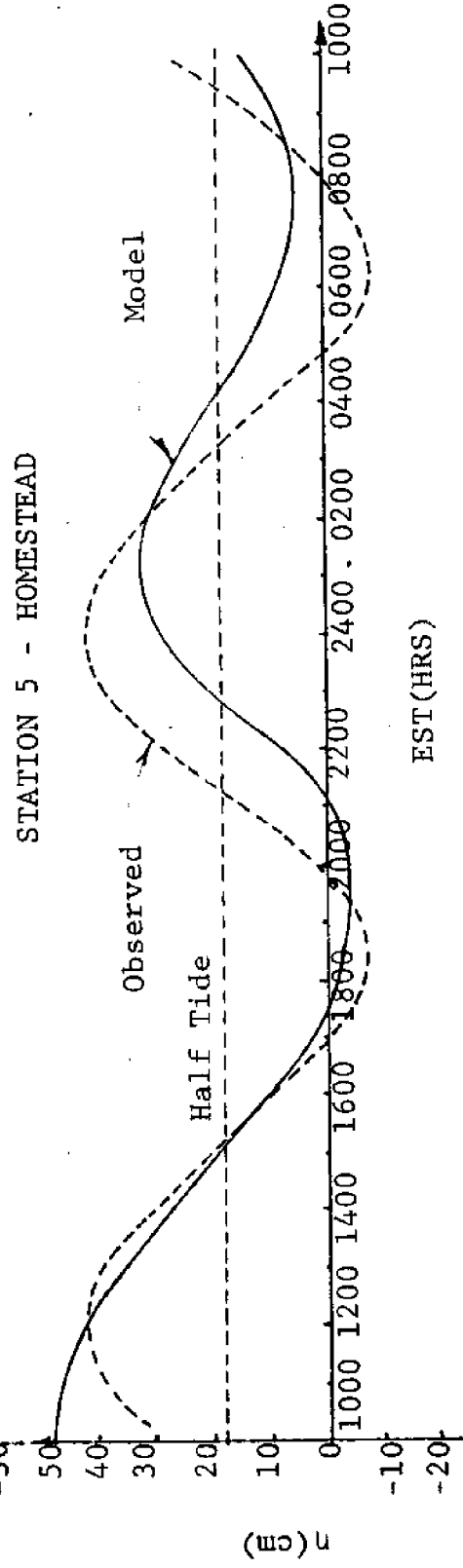


Fig. 5-5 Tide Levels, Observed vs. Model

Fig.5-6 Tide Levels, Observed vs. Model

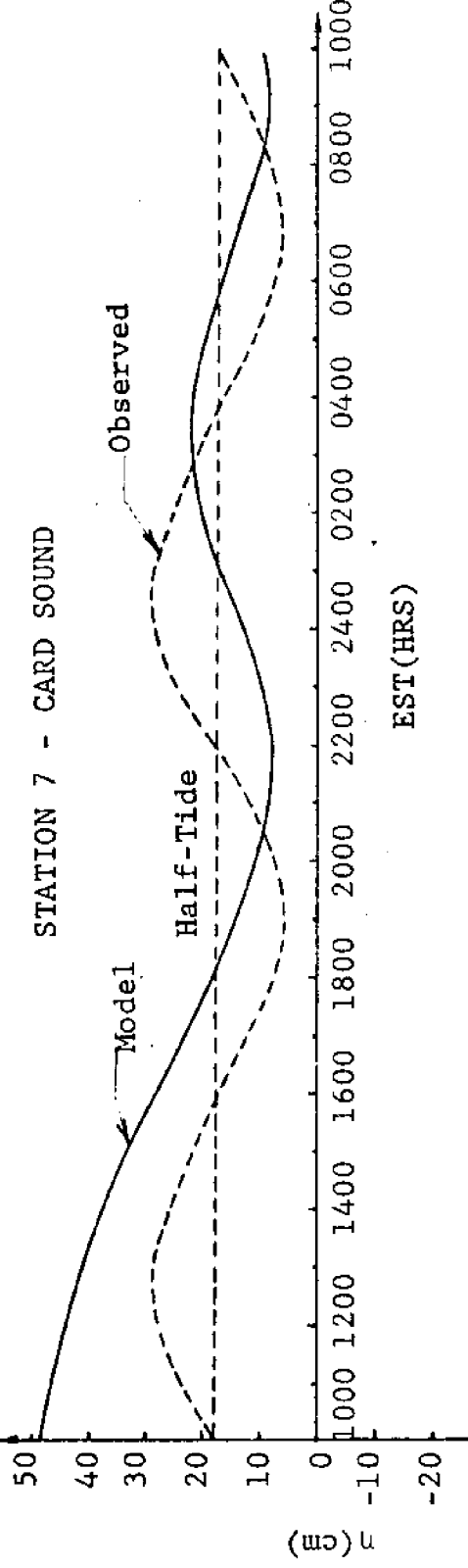
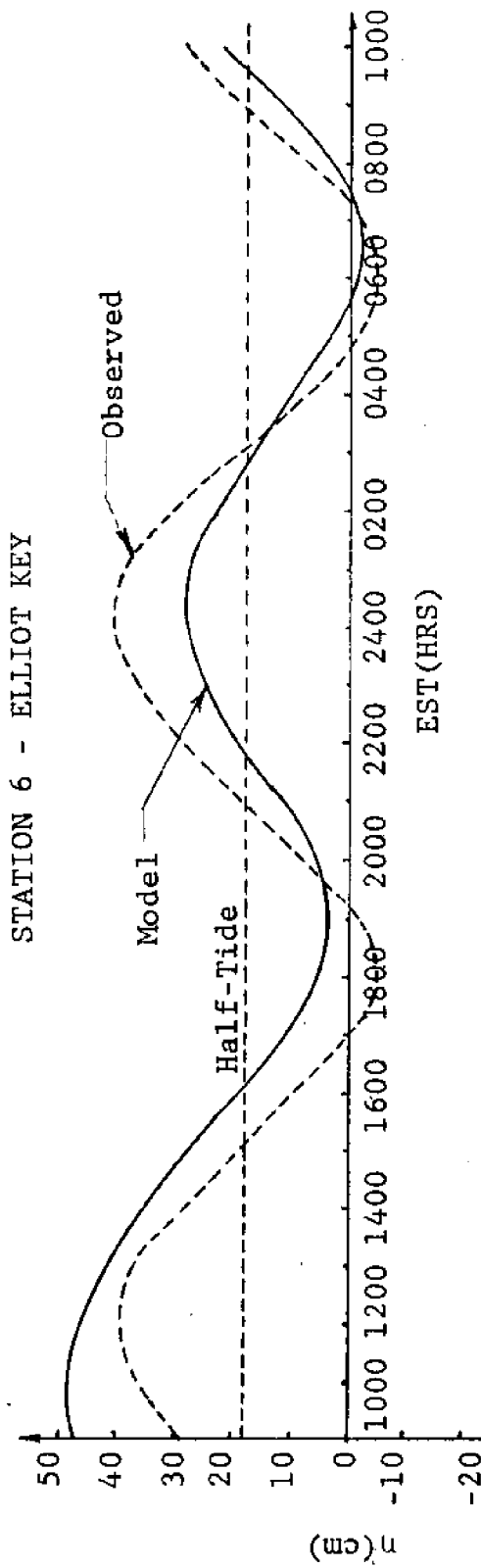


Fig.5-7 Tide Levels, Observed vs. Model

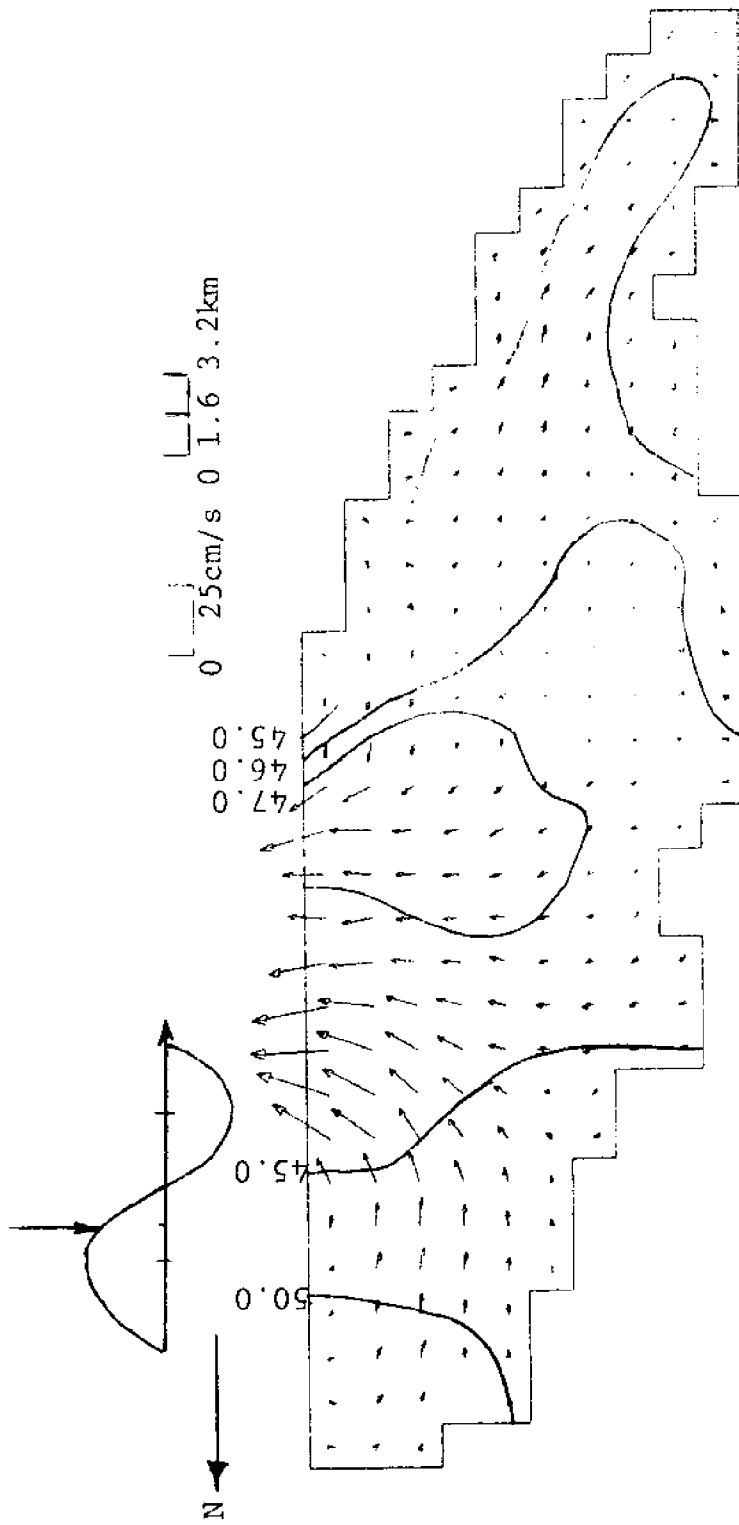


Fig. 5-8 Computed Surface Currents and Surface Elevations (cm) for Calibrated Model, 1.5 hours after High Tide on April 15, 1975.

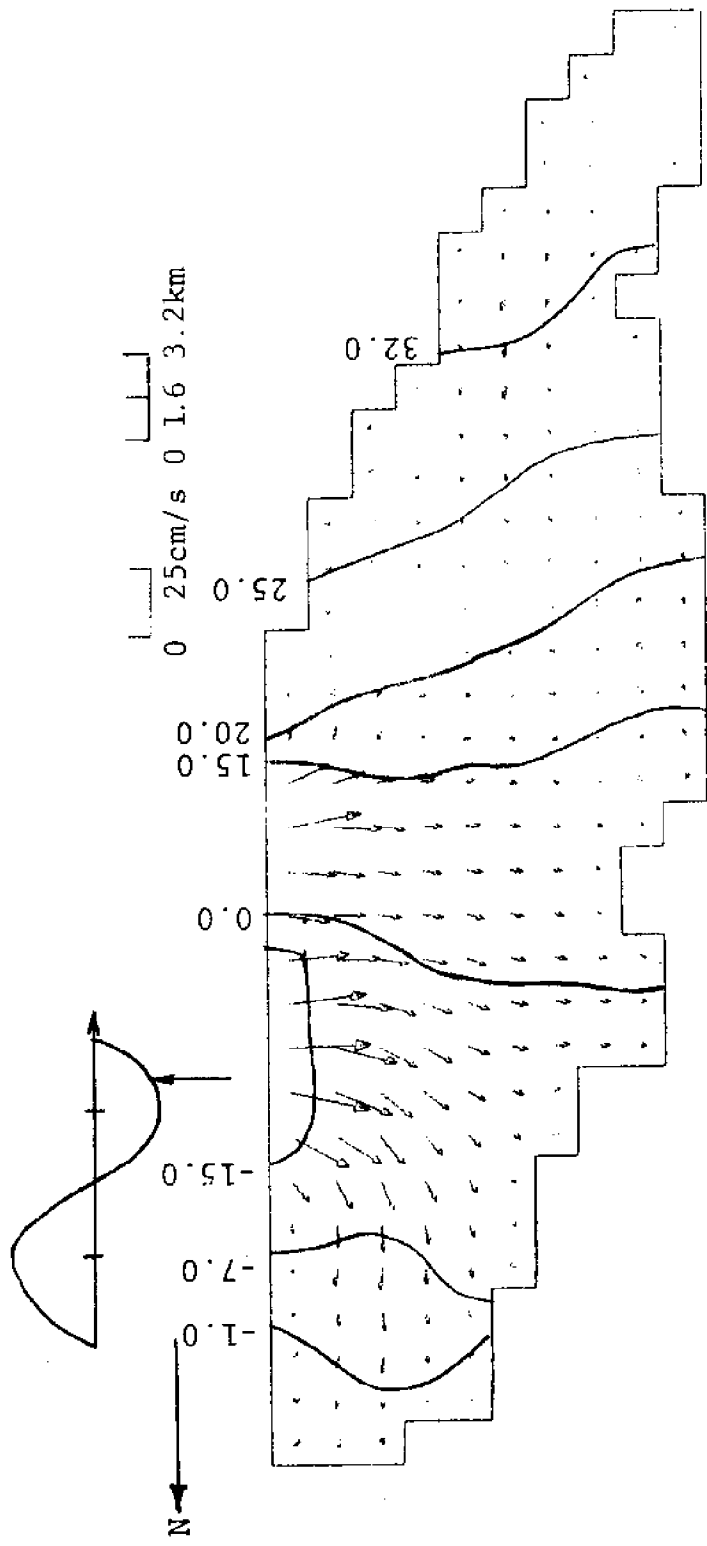


Fig. 5-9 Computed Surface Currents and Surface Elevations (cm) for Calibrated Model, 7.5 hours after High Tide on April 15, 1975.



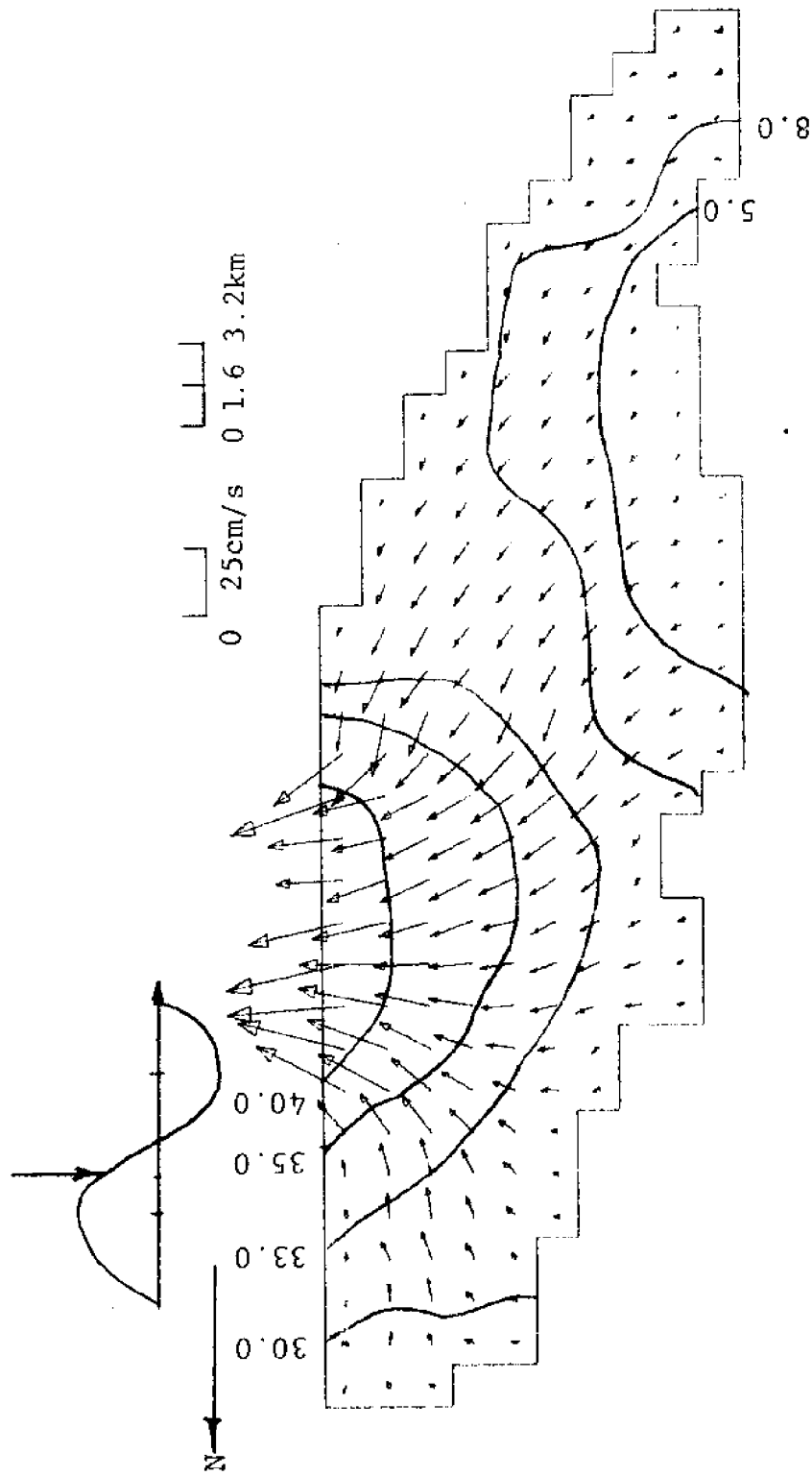


Fig. 5-10 Computed Surface Currents and Surface Elevations (cm) for Calibrated Model, 13.5 hours after High Tide on April 15, 1975.

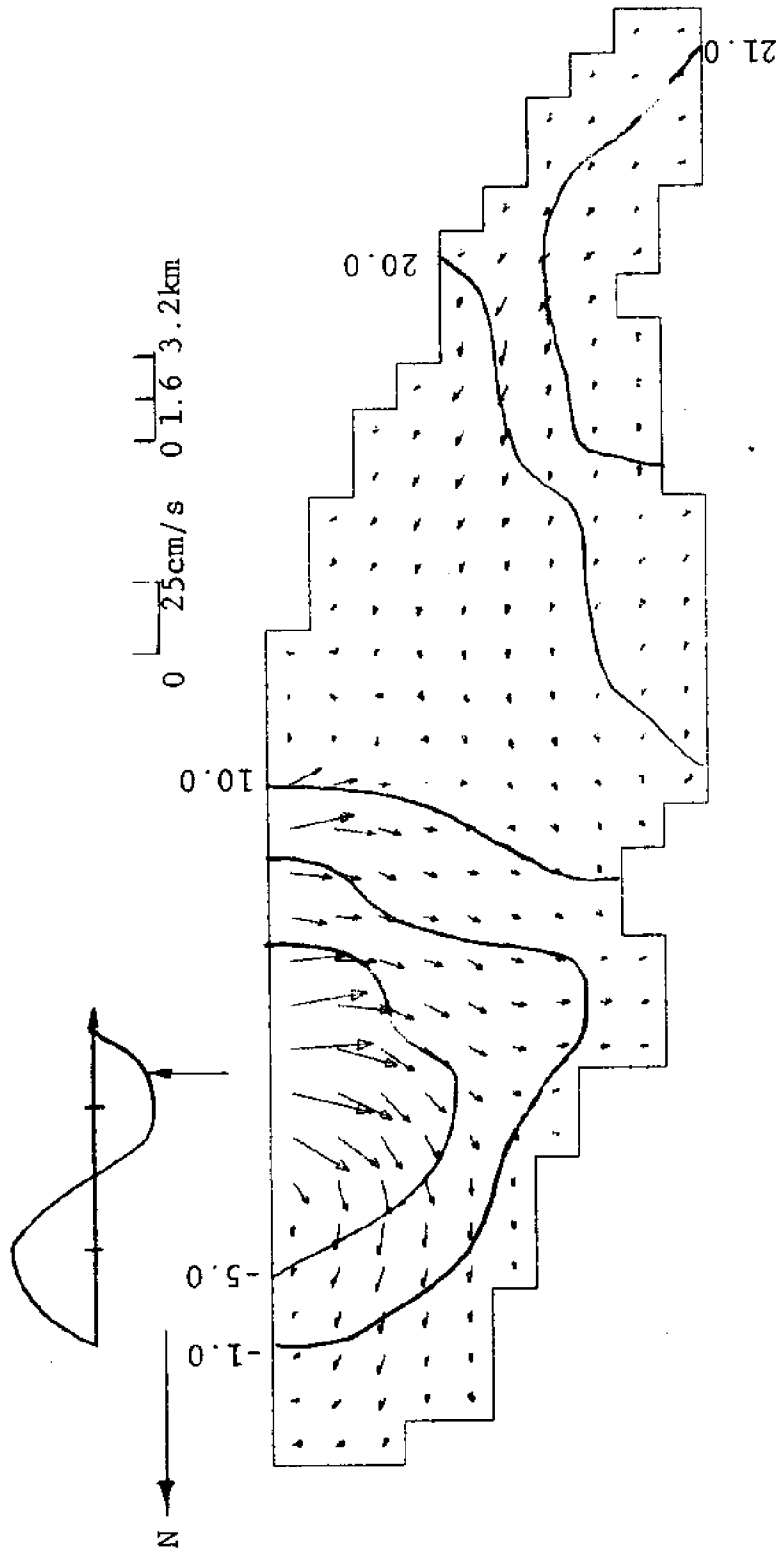


Fig. 5-11 Computed Surface Currents and Surface Elevations (cm) for Calibrated Model, 19.5 hours after High Tide on April 15, 1975.

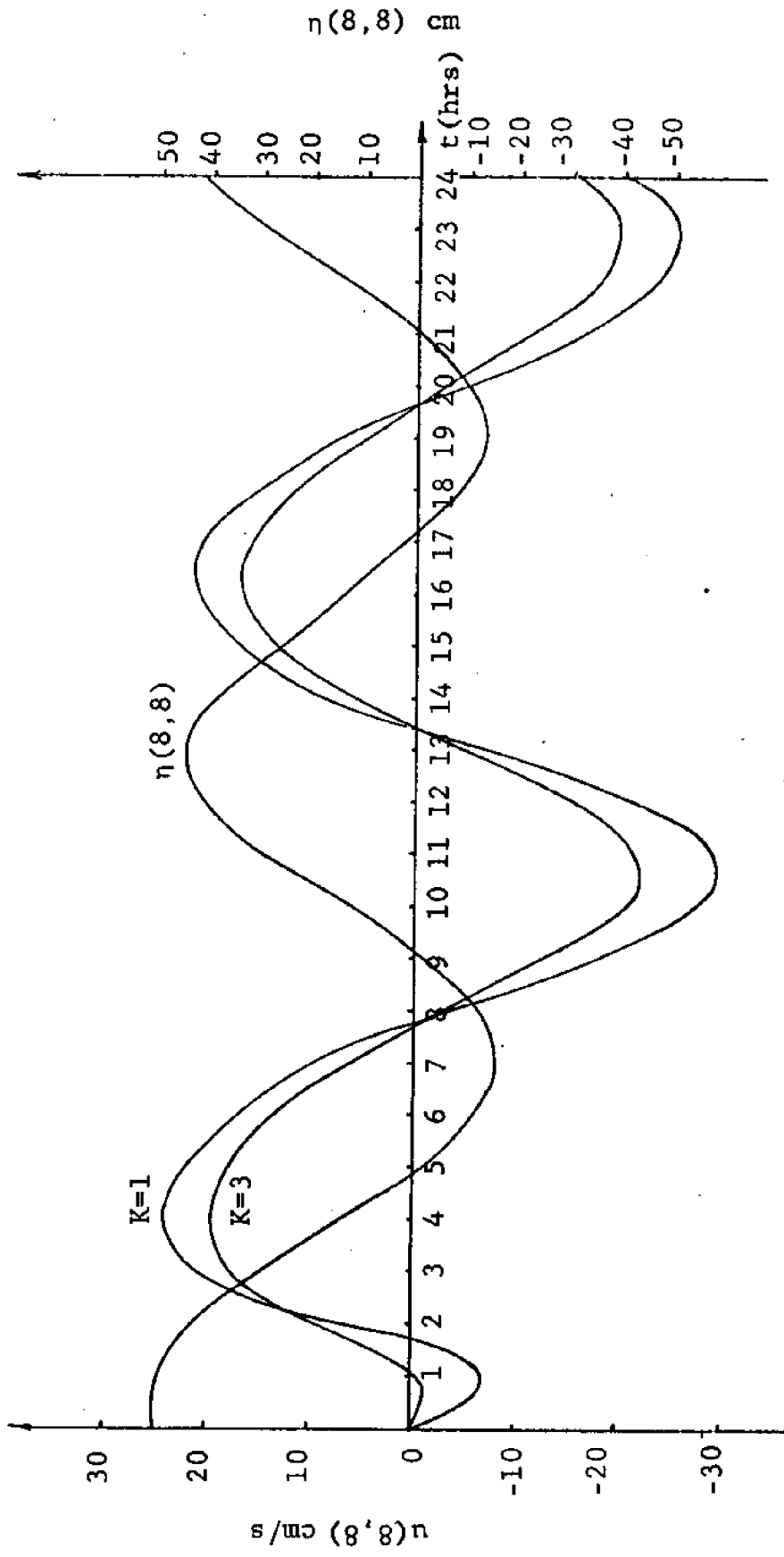


Fig. 5-12 u-component of Velocity and  $\eta$  vs. Time at  $I=8$ ,  $J=8$ .

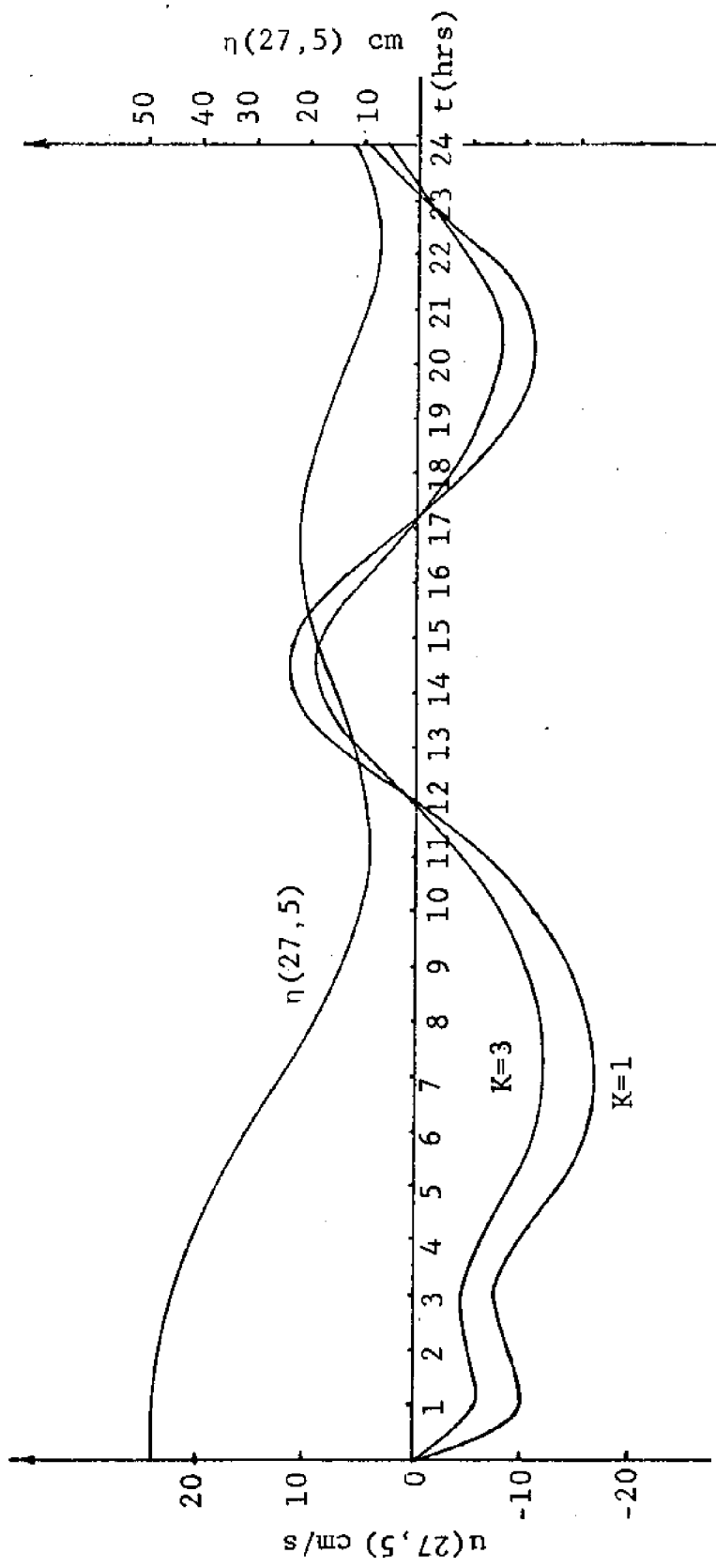


Fig. 5-13 u-component of Velocity and  $\eta$  vs. Time at  $I=27$ ,  $J=5$ .

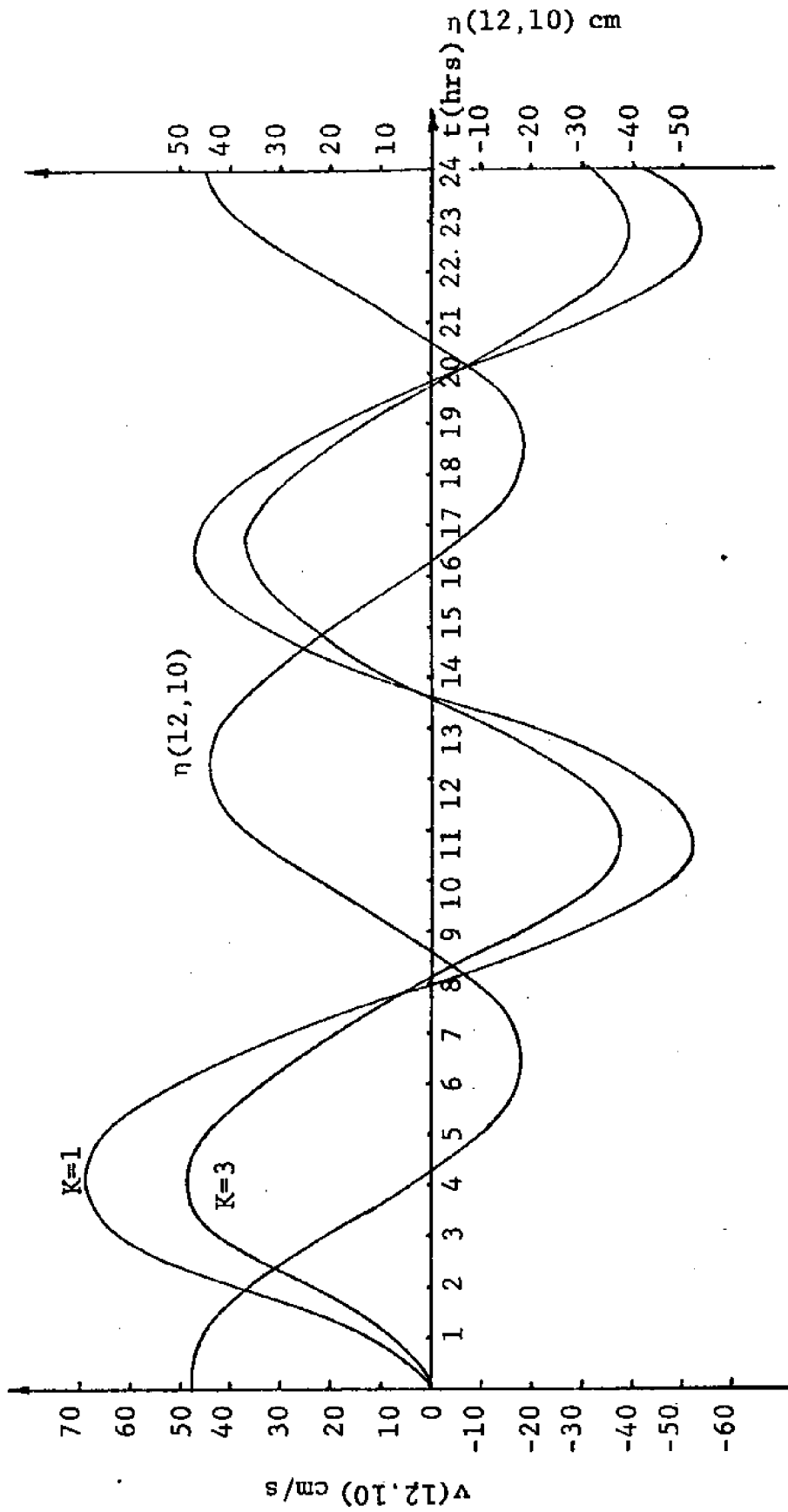


Fig. 5-14 v-component of Velocity and  $\eta$  vs. Time at I=12, J=10 (Inlet).

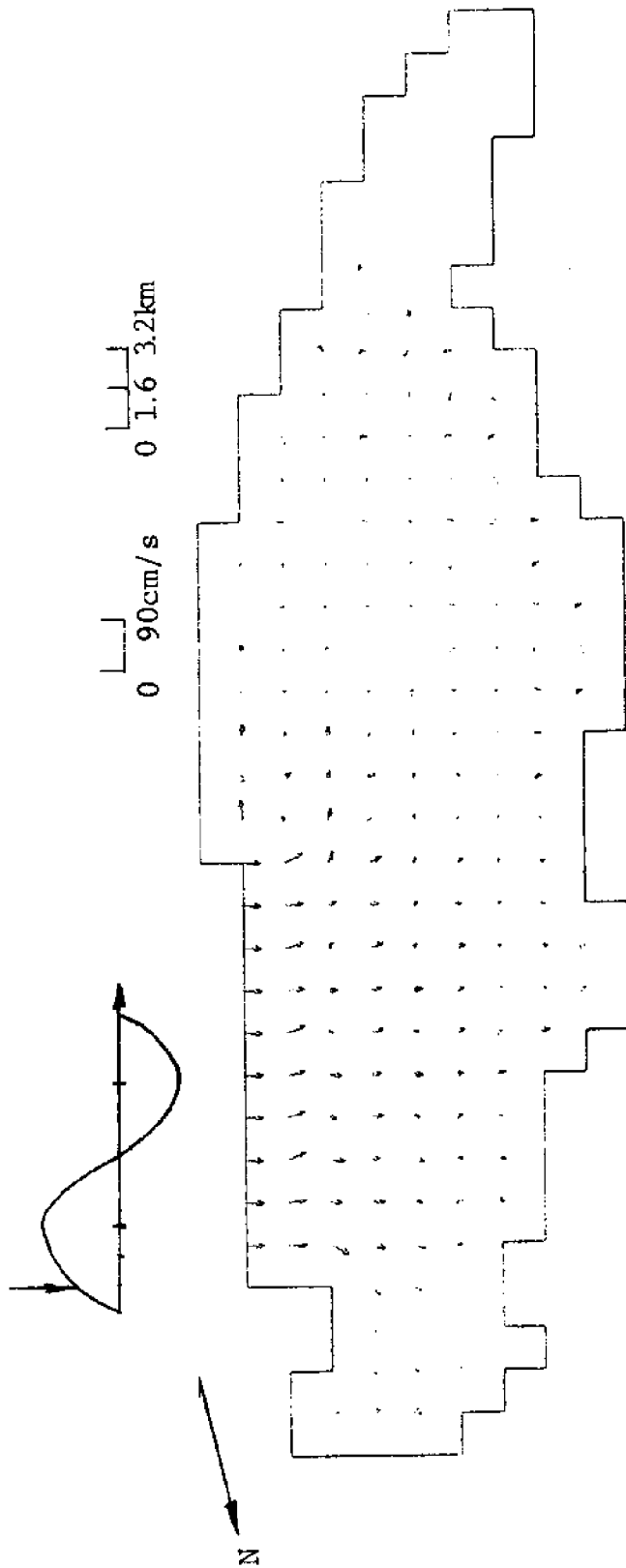


Fig. 5-15 Computed Surface Currents for Uncalibrated Model in Rotated Grid System, 1 hour from Start-Up on April 15, 1975.

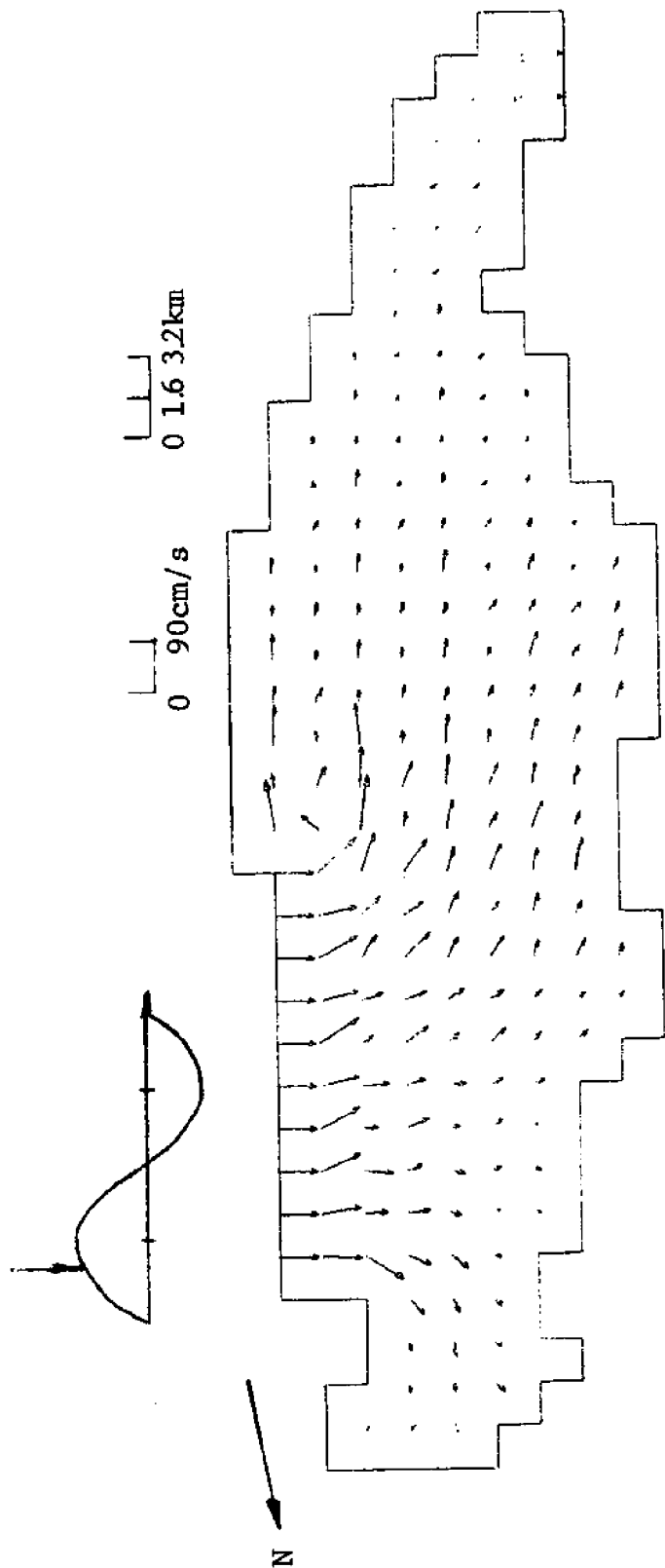


Fig. 5-16 Computed Surface Currents for Uncalibrated Model in Rotated Grid System, 2 hours from Start-Up on April 15, 1975.

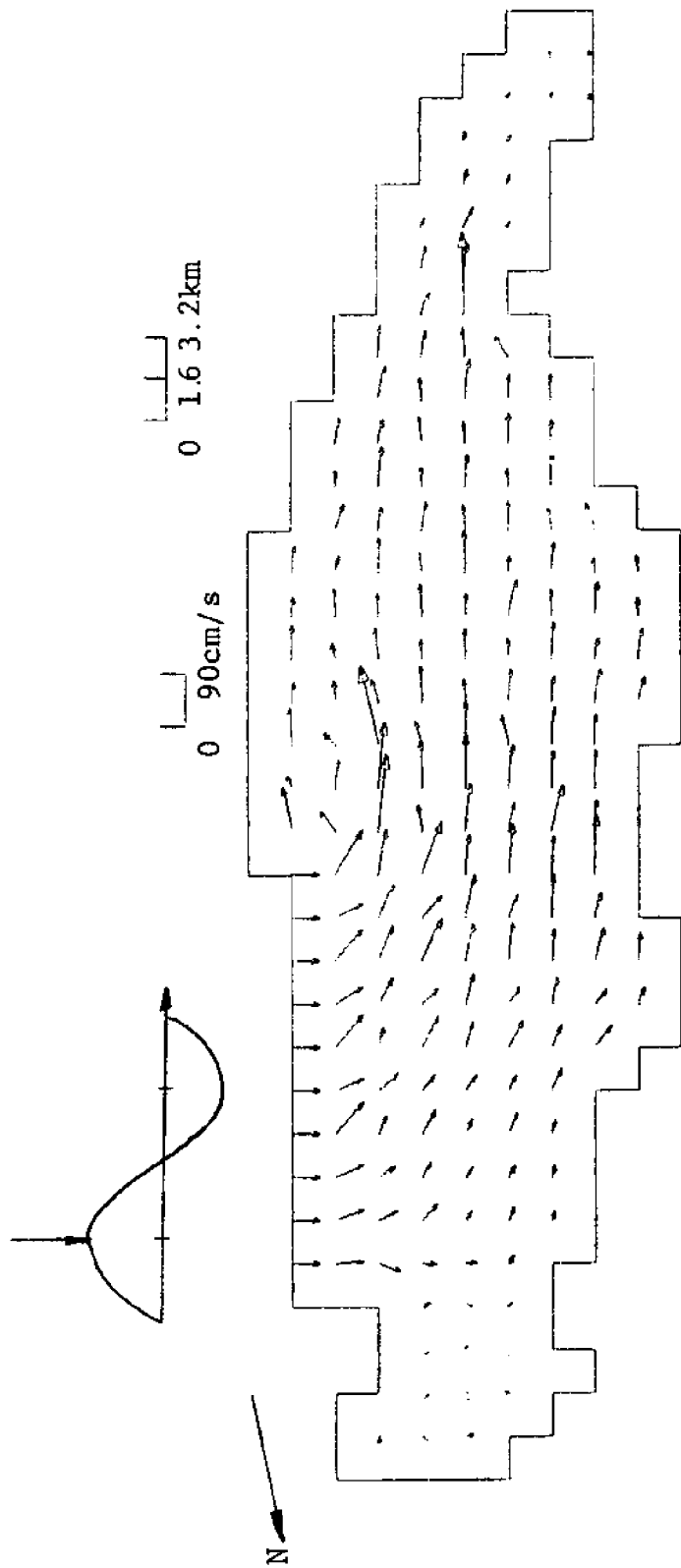


Fig. 5-17 Computed Surface Currents for Uncalibrated Model in Rotated Grid System, 3 hours from Start-Up on April 15, 1975.



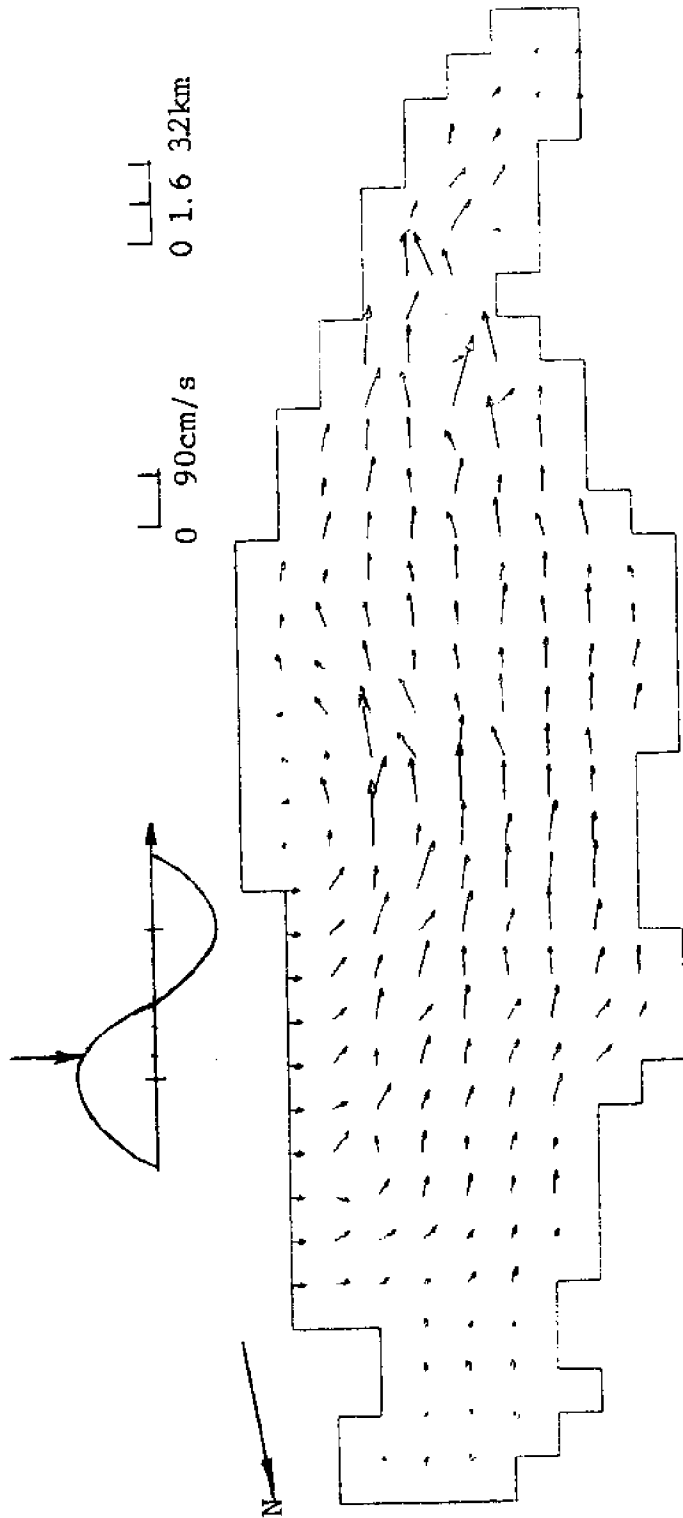


Fig. 5-18 Computed Surface Currents for Uncalibrated Model in Rotated Grid System, 4 hours from Start-Up on April 15, 1975.

## 6. Results for Sediment Transport

### 6.1. Grid System for Studying Intracoastal Waterway Channel in South Biscayne Bay

The grid system for these numerical sediment transport studies is shown in Fig. 3-4. This grid system for the South Biscayne Bay was constructed such that the intracoastal waterway channel goes through the nodes. This was essential for specifying an initial condition. Note, this grid system is rotated  $20^{\circ}$  clockwise with respect to due North. The rotation of the grid system affected the values of the wind stresses, but causes no change in the Coriolis parameter  $f$ . Appendix C gives the details of the effects of this rotation of  $20^{\circ}$  clockwise from due North. Note, the horizontal grid size is  $\Delta x = \Delta y = 1.6$  km.

### 6.2. Computer Runs for Different Values of Settling Velocity and Bottom Deposition Rate for An Instantaneous Line Source

The concentration equation for the first case of sediment transport, Eq. 3-30, was run coupled to the hydrodynamic model given in Section 3.2.3, with variable  $K_v$  and  $D_v$  as given in Eq. 3-1, a time step  $\Delta t = 2$  min, was used. The computer model was run for an instantaneous line source along the intracoastal waterway channel, as given in section 4.5.1. See Figs. 5-15 through 5-18 for the coupled velocity field!

The values of settling velocity,  $W_s$ , and for bottom deposition rate,  $A$ , were varied to gain physical insight into the governing mechanisms of sediment transport.

The computer runs were as follows:

- a).  $W_s = .04, A = 0.9$
- b).  $W_s = .02, A = 0.9$
- c).  $W_s = .04, A = 0.3$

Now Fig.6-1 illustrates the sediment particle concentration distribution at the surface,  $K=1$ , for a J-transect at  $I=13$ , so that the effect of the inlet could be studied. The above noted three cases were plotted in Fig.6-1 for a period of one hour and two hours, respectively. It can be readily seen that doubling the settling velocity,  $W_s$ , strongly affects the distribution of sediment particles, although the affect of tripling the deposition rate,  $A$ , is relatively minor. Secondly, it can be seen that the effect of the advection from the incoming tidal current significantly skews the concentration distribution at  $I=13$ , which is a J-transect normal to the inlet. This advection effect is greater demonstrated in Fig.6-2 for  $W_s=.02$  and  $A= .9$  for increasing the time period from 1 hour to 2 hours and then to 3 hours. Note, further, that 90% deposition occurred at 4 hrs. 46 min. for  $W_s = .02, A=.9$ , at 3 hours 40 min. for  $W_s =.04, A=.3$ , and at 2 Hrs. 4 min. for  $W_s =.04, A=.9$ . However, the skewing caused by the incoming tidal current is most pronounced for  $W_s=.02, A=0.9$ .

Now Fig.6-3 shows the concentration distribution at the surface,  $K=1$ , for a J-transect at  $I=21$ . At this J-transect the flow field is aligned with the intracoastal waterway, and, hence, the skewing effect has vanished. Again we can see that the settling velocity is much more

dominant than the deposition rate. Fig.6-4 clearly shows that the surface concentration distribution is strongly time dependent, this being due mainly to bottom deposition - which depends more strongly on gravitational settling than on deposition rate, A.

Fig.6-5 illustrates sediment particle concentration distributions at various depths for two J-transects at I=13 and at I=21. This case is for  $W_s=.02$  and  $A=.9$ . The skewing effect again is clearly observed for I=13, and is virtually nonexistent for I=21. Both distributions vary somewhat the same with respect to depth, since the depth dependent variation is mostly dependent on settling velocity and deposition rate. Fig.6-6 indicates that the vertical profiles decrease sharply with increasing time, and the influence of advection is less significant than for horizontal concentration variations, due to the rapid turbulent mixing vertically.

## 7. Results for Dissolved Constituent Transport

### 7.1. Grid System for Studying Dissolved Chemical Transport

The grid system for studying dissolved chemical transport is shown in Fig.7-1. This grid system has already been used by Lee and Sengupta (1976) for investigating the tide and wind driven circulation in the South Biscayne Bay. Note, that this grid system is aligned toward due North, and the horizontal grid size is  $\Delta x = \Delta y = 1.6$  km. As already noted in section 3.1.5. the coarse resolution of this grid size eliminates the inclusion of sidewall boundary layers.

Also, note that the inlet (ocean-exchange area) is not recessed one grid step as for the grid system used to study sediment transport in the South Biscayne Bay. Otherwise the two grid system are rather similar.

### 7.2. Definition of Flushing

The fraction of tidal flushing has already been defined in section 4.7.4. as,

$$x(t) = \frac{M(t)}{M(t=0)} \quad (7-1)$$

This, of course, is only true for conservative dissolved chemicals in the bay system. However, to better appreciate our flushing results, one may also use tidal prism theory to compute the flushing performance of the bay. Following Lo(1976), the concentration of the dissolved chemical constituent after N tidal cycles is given by:

$$C = C_0 \left( \frac{v}{v + \alpha p} \right)^N \quad (7-2)$$

Where  $\alpha$  = Mixing coefficient

$p$  = Volume of water in tidal prism

$v$  = Volume of water in bay at low tide.

### 7.3. Flushing Rates for Dissolved Chemical Transport

The flushing rates for the three dye release sites; Snapper Creek Canal, Black Creek and Mowry Canal are shown in Figures 7-2, 7-3 and 7-4. Figure 7-5 shows the flushing rate for a uniform distribution of dissolved chemical. Note, that a time step  $\Delta t=6$  min. was used; and the computer program was run for a period of 2 weeks of simulation time for each case.

As can be seen in reviewing these figures, Black Creek and Mowry Canal dye release sites indicate the largest amount of flushing, whereas the Snapper Creek Canal dye release site indicates the least amount of tidal flushing. The flushing rate of the uniform distribution of dissolved chemical indicates a greater rate of flushing, initially, than either Black Creek or Mowry Canal dye release sites. This is attributable to the large region of dissolved chemical affected in the vicinity of the ocean-exchange area. It is interesting to observe that Black Creek and Mowry Canal are near-shoreline dye release sites relatively far from the ocean-exchange area, and that Snapper Creek Canal is directly across from the ocean-exchange area. However, this curious result cannot be further examined without a data base on long-term flushing rates. This data base does not exist at the present time.

As can be seen in Figs.7-2, 7-3, 7-4 and 7-5, after two weeks of simulation, the dye initially at Black Creek and at Mowry Canal has been 93% flushed out of the

bay, whereas the dye initially at Snapper Creek Canal has only been 32% flushed out of the bay. The uniform distribution flushed 80% in 2 weeks of simulation time.

#### 7.4. Model Dye Release Site Studies

In this section the model results for simulating the dispersion of injected dye at three shoreline locations is presented and compared with Wang's (1977) data base. Figs 7-6 through 7-9 illustrate the comparison for Snapper Creek, Figs 7-10 through 7-12 are for Black Creek, and Figs. 7-13 through 7-15 are for Mowry Canal.

The dye release experiments were performed as follows:

1. Snapper Creek Canal (7,6)

5 gallons of rhodamine WT (20%) were injected at 6:45 EST on November 2, 1977 in 8 feet of water and tracked for 10.5 hours.

2. Black Creek (17,2)

1 gallon of rhodamine WT (20%) was injected at 9:10 EST on December 7, 1977 in 3½ feet of water and tracked for 29 hours.

3. Mowry Canal (20,2)

2 gallons of rhodamine WT (20%) were injected 10:00 EST on December 20, 1977 in 3 feet of water and tracked for 24 hours.

The computations for specifying the model dye release reference concentrations were performed as follows.

1. Volume of Initial Line Source

$$V_o = (H \cdot \Delta x \cdot \Delta y) / 4, \quad (7-3)$$

2. Reference Value of Dye Concentration

$$C_{\text{ref}} = \frac{V_R}{V_o} \times 10^9 \text{ PPB} \quad (7-4)$$



where  $V_R$  = # gallons of rhodamine WT (20%)

and PPB = parts of rhodamine WT (20%) per billion parts of water.

Now, Table 7-1 presents the values of  $V_R$ ,  $V_O$ ,  $C_{ref}$  for the 3 dye release sites.

TABLE 7-1

SITE	$V_R$ (cm <sup>3</sup> )	$V_O$ (cm <sup>3</sup> )	$C_{ref}$ (PPB)	Grid Pt.
Snapper Creek Canal	$22.73 \times 10^3$	$1.56 \times 10^{12}$	14.6	(7,6)
Black Creek	$4.55 \times 10^3$	$6.83 \times 10^{11}$	6.7	(17,2)
Mowry Canal	$9.09 \times 10^3$	$5.85 \times 10^{11}$	15.5	(20,2)

Now the model results will be compared with Wang's data base. Note that the actual dye injection points correspond quite closely with the grid points used in the model runs, and, therefore, the comparisons are meaningful. Furthermore, high tide used for the model runs are not in phase with high tide occurring on the three different dye release experiments. However, spreading of the dye can be considered both qualitatively and quantitatively meaningful in terms of the basic transport processes, the dominant two being vertical diffusion and horizontal convection.

\* Figs.7-6 through 7-9 shows relatively good agreement between the model predictions and the measured values for Snapper Creek Canal. The corresponding lines of rhodamine WT (20%) are in good agreement, thus lending much merit to

\* The model source in Figs.7-6 through 7-15 has been located by interpolation of grid location of line source and the boundary, and the source strength has been adjusted accordingly. This was done for the sake of comparison.

the computer model for dissolved chemical transport.

Furthermore, the rate of spreading of the dye is in surprisingly good agreement with Wang's measured values, thus verifying that the model formulation properly takes account of the dominant transport processes in the South Biscayne Bay.

Figs.7-10 through 7-12 present the comparison for Black Creek. Initially, the model does not yield some of the measured values of lines of rhodamine WT (20%) dye, however this is due to the lack of resolution of the model due to the relatively large grid size  $\Delta x=1.6$  km. But, as can be seen in Fig.7-12 the rate of spreading of the dye is in quite good agreement with the measured values. Thus, again it has been demonstrated that the model properly takes account of the dominant transport processes for dissolved chemical dispersion.

Figs.7-13 through 7-15 present the comparison for Mowry Canal. Initially, the values of rhodamine WT (20%) are in good agreement, noting again that the actual dye injection point is slightly different than the model initial line source of dye release. As time proceeds, the comparison indicates that the model not only agrees favorably with regard to the amount of dye dispersed, but also simulates quite well the shape of the contours of the lines of varying amounts of dye:

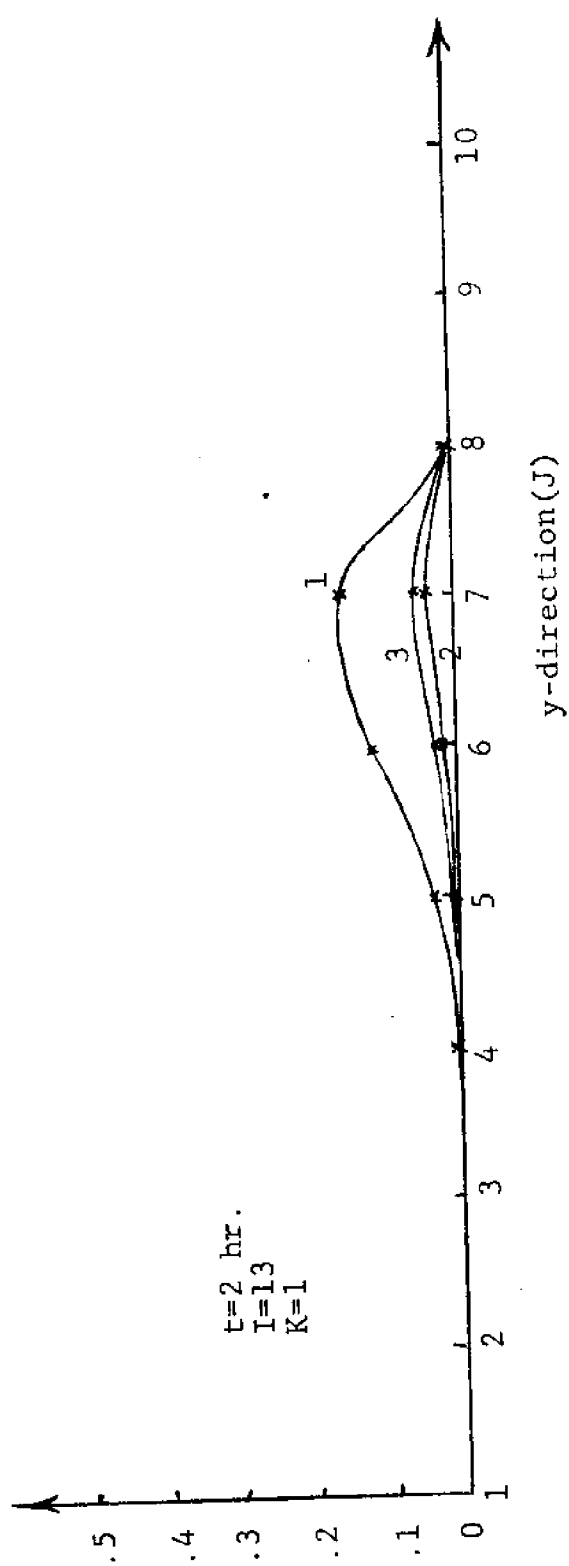
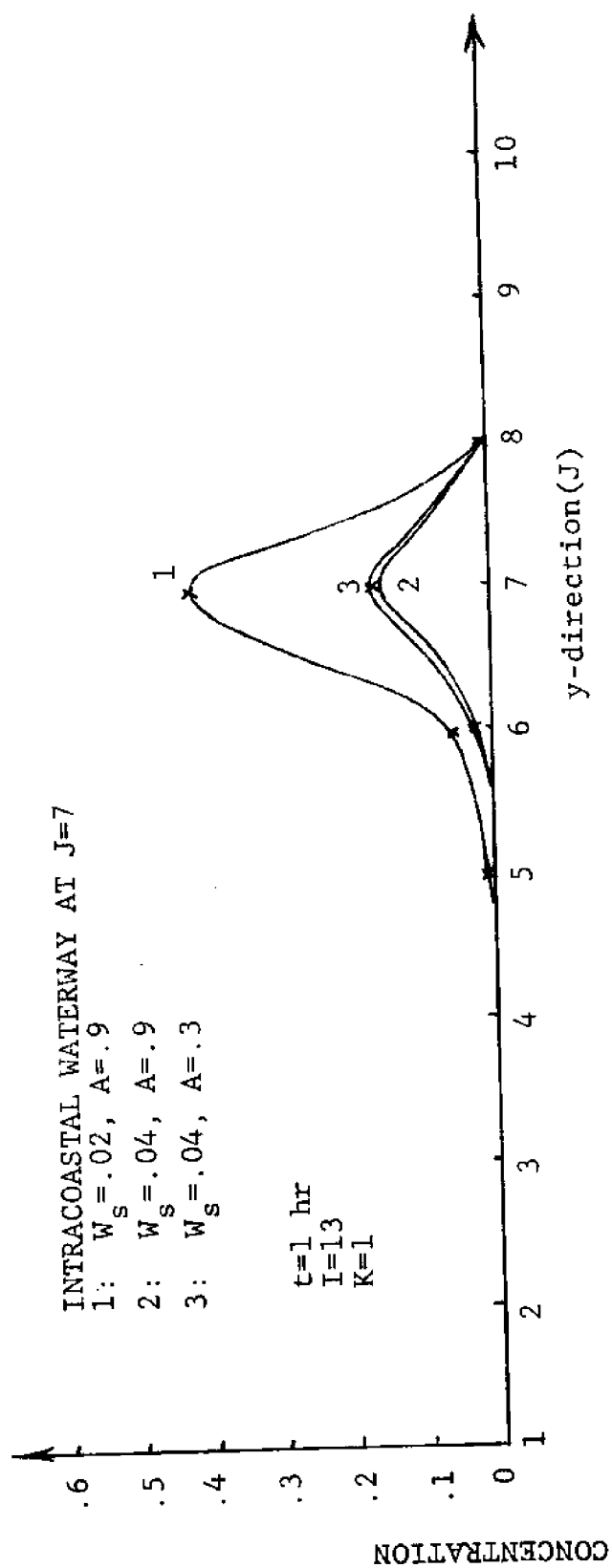


Fig. 6-1 Sediment Particle Concentration vs. y-direction at Surface at I=13.

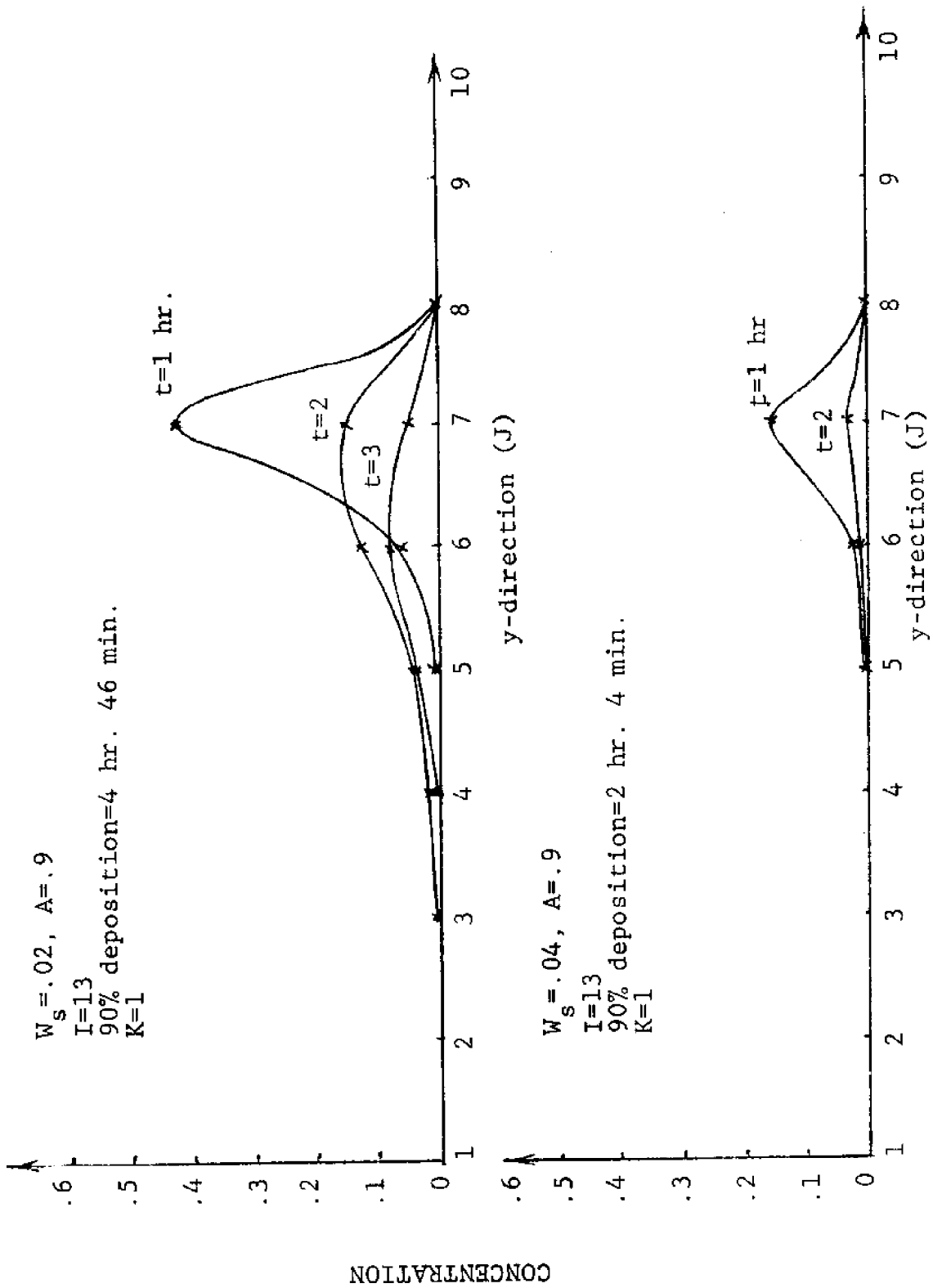


Fig. 6-2 Sediment Particle Concentration vs. y-direction at Surface at I=13.

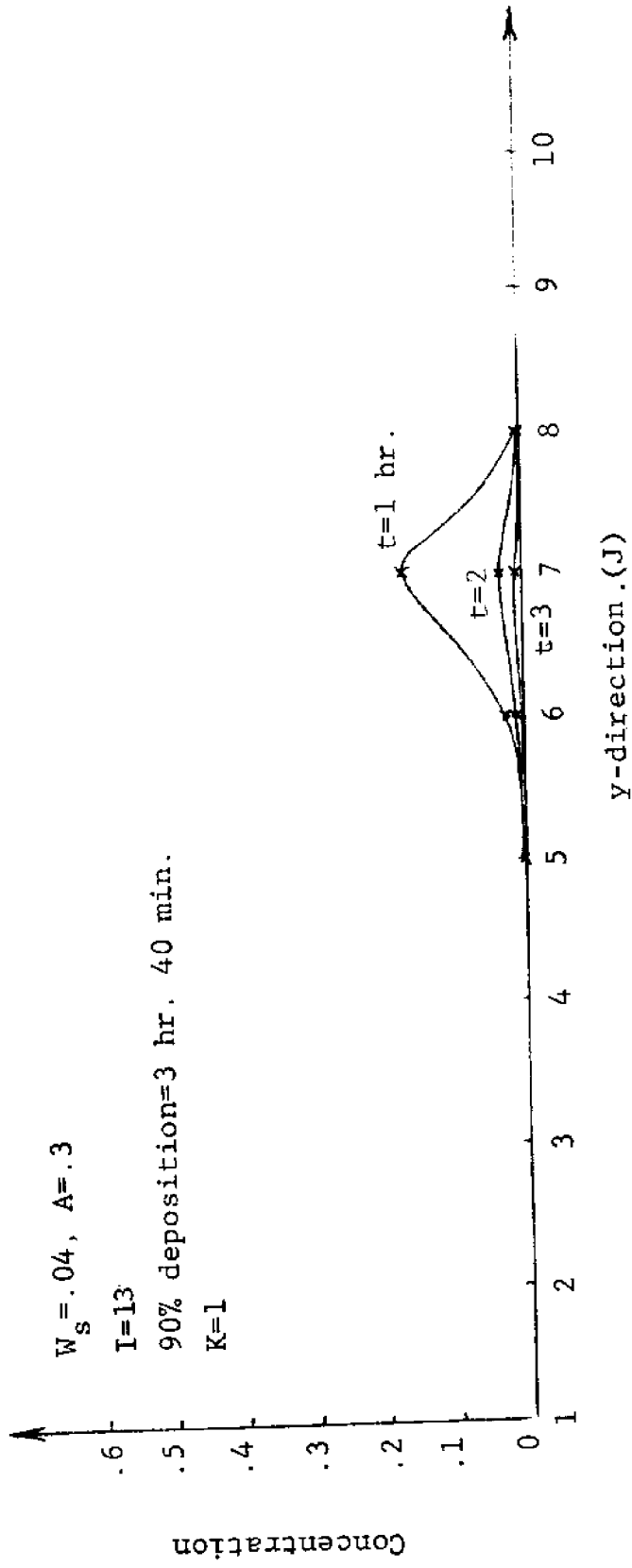


Fig. 6-2 (Continued)

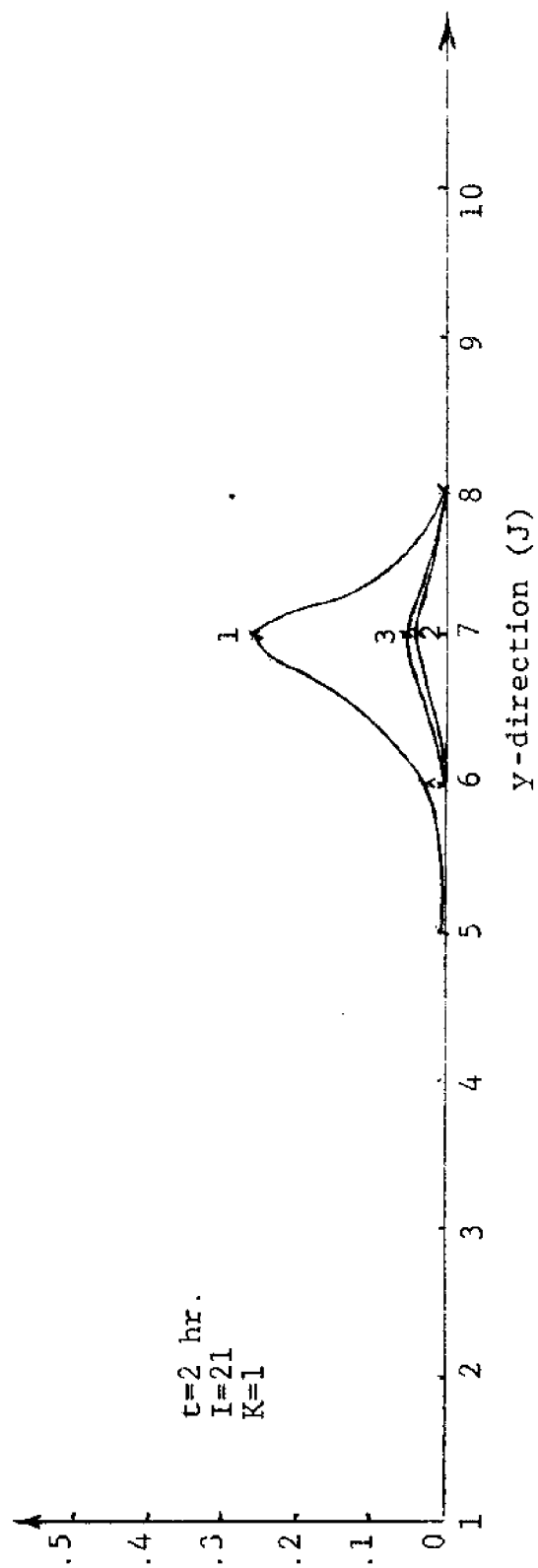
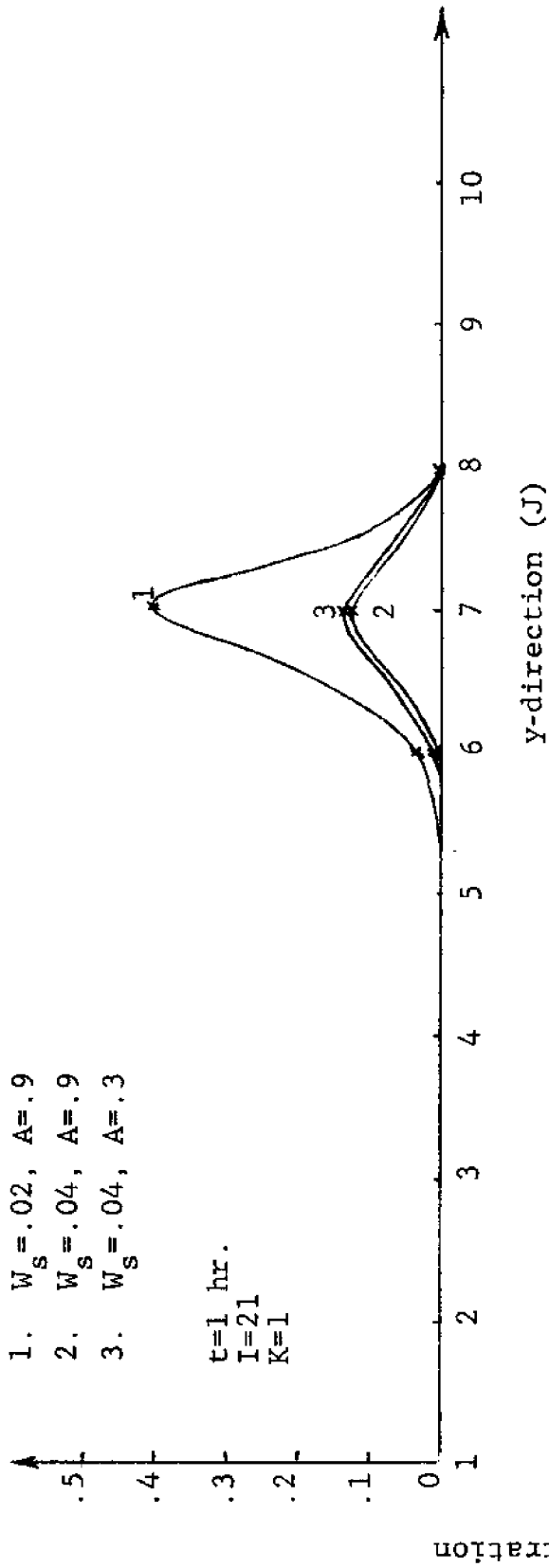


Fig.6-3 Sediment Particle Concentration vs. y-direction at Surface at  $I=21$ .

$W_s = .04$ ,  $A = .3$   
 $I = 21$   
90% deposition = 3 hrs. 40 min.  
 $K = 1$

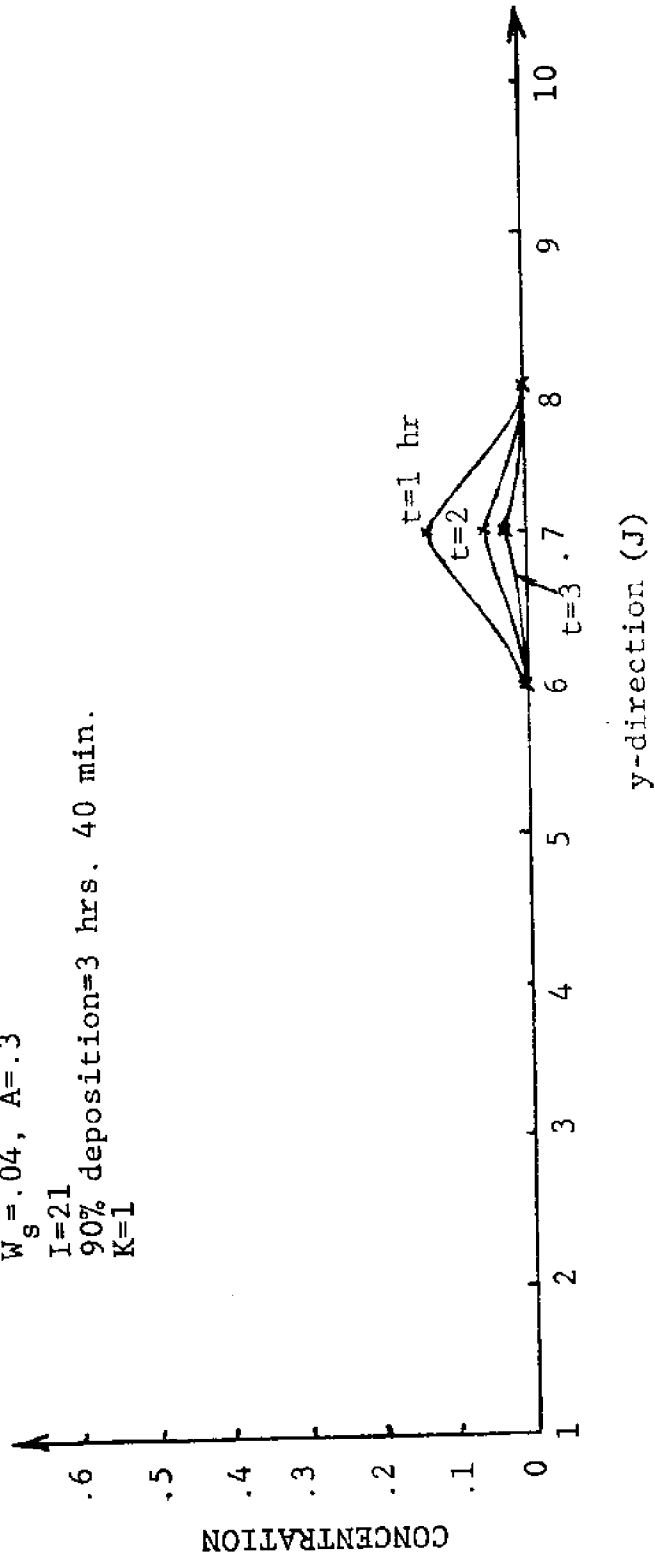


Fig. 6-4 Sediment Particle Concentration vs. y-direction at Surface at  $I=21$ .

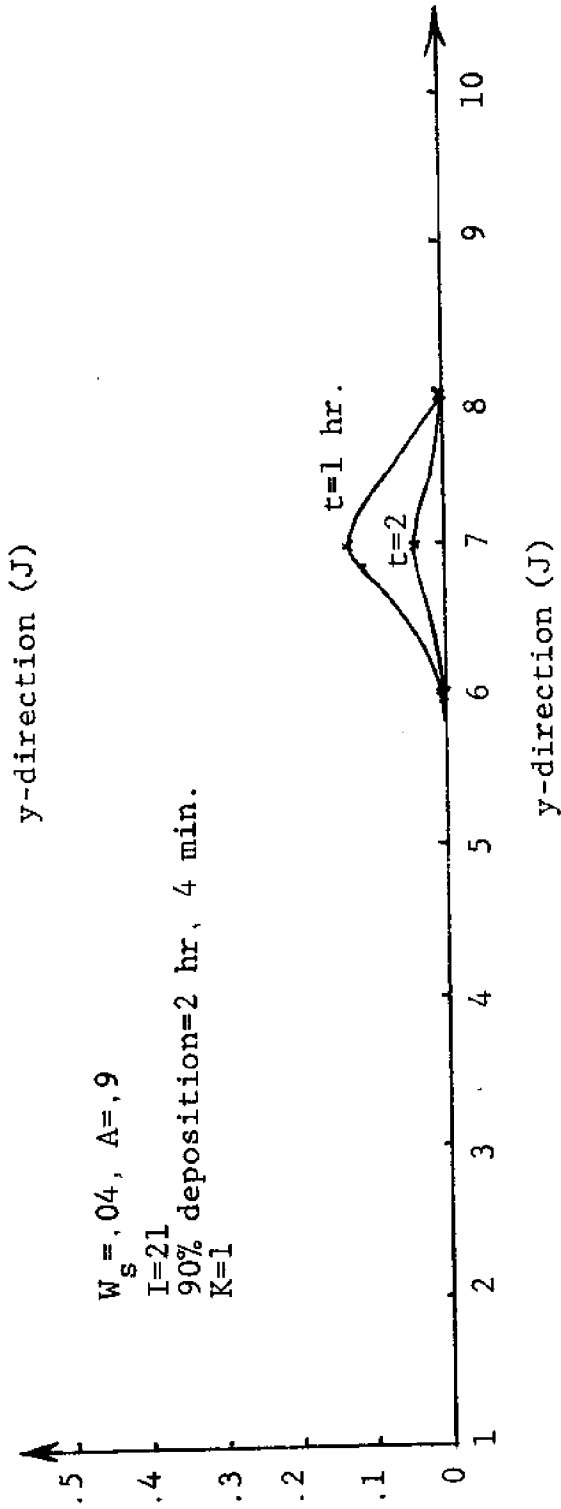
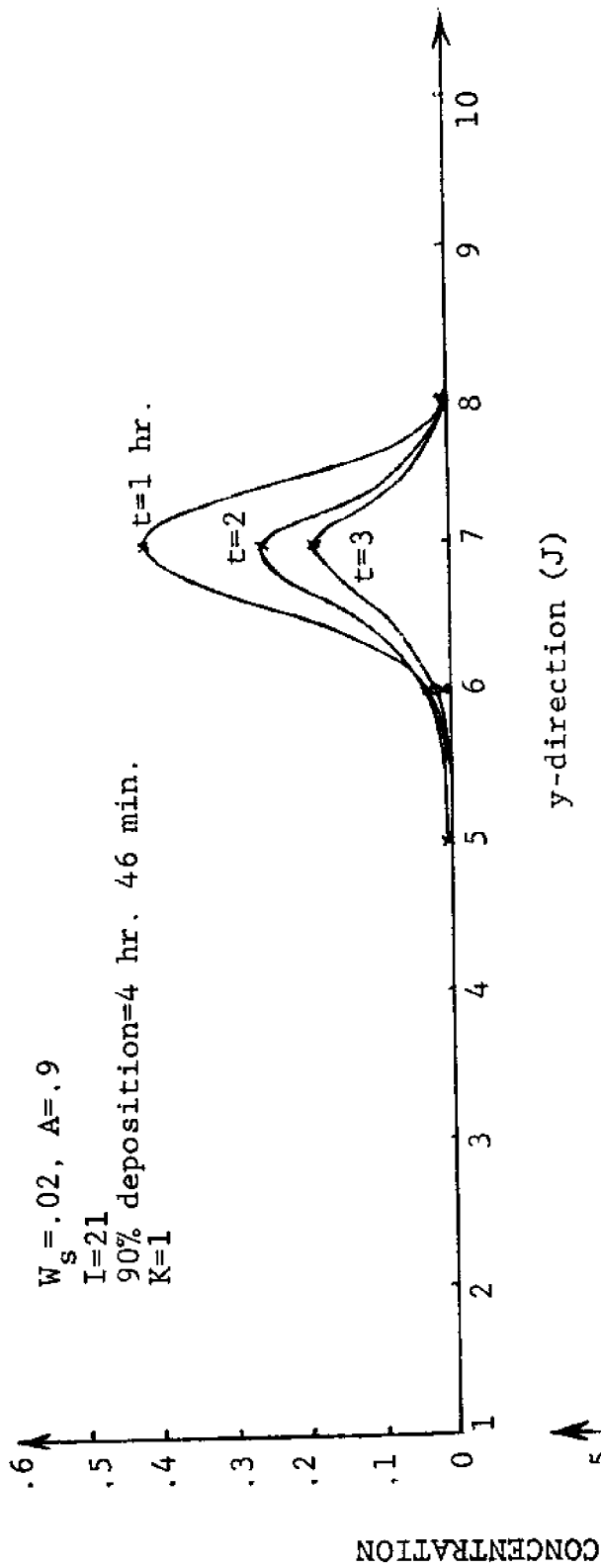


Fig. 6-4 (Continued)



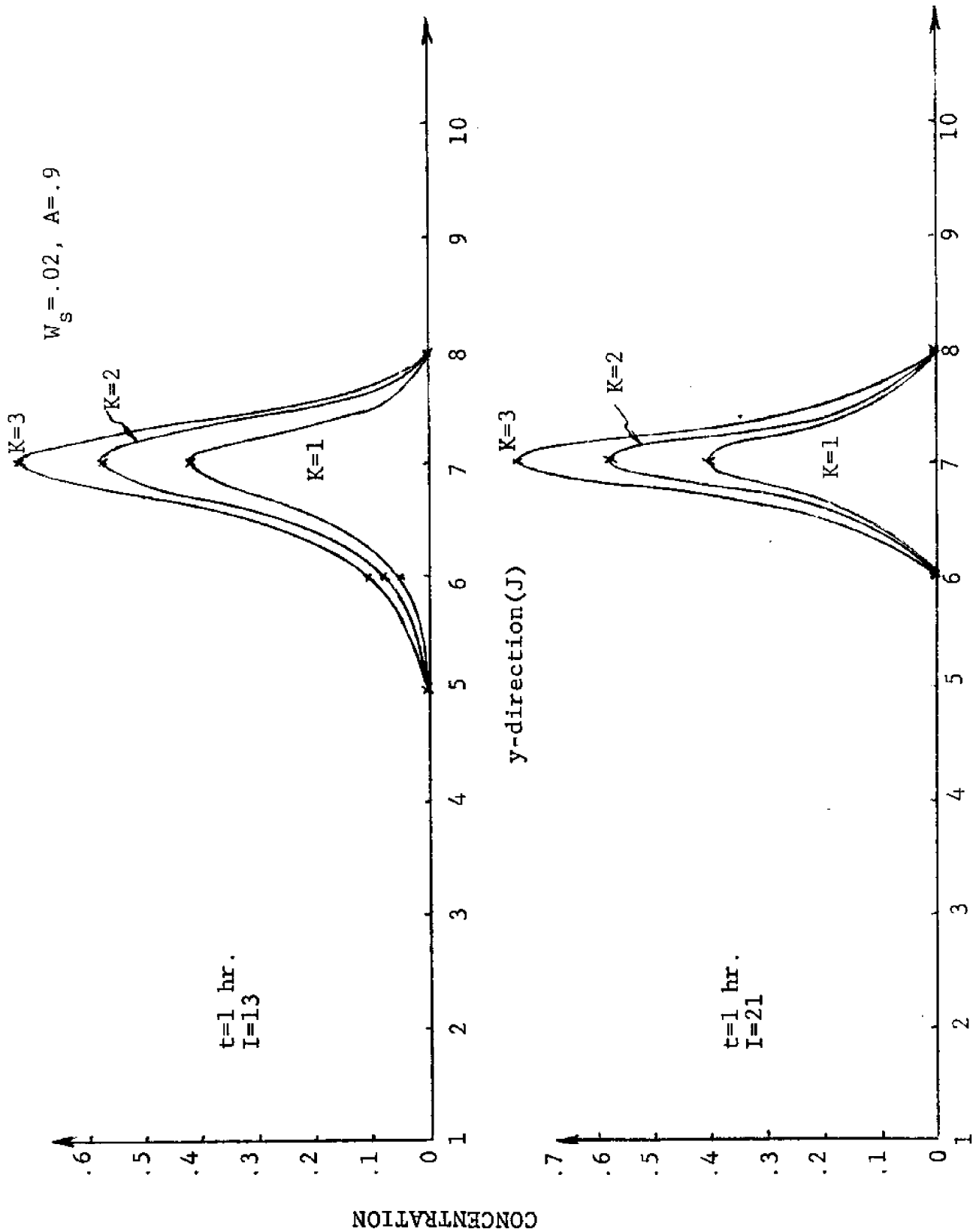
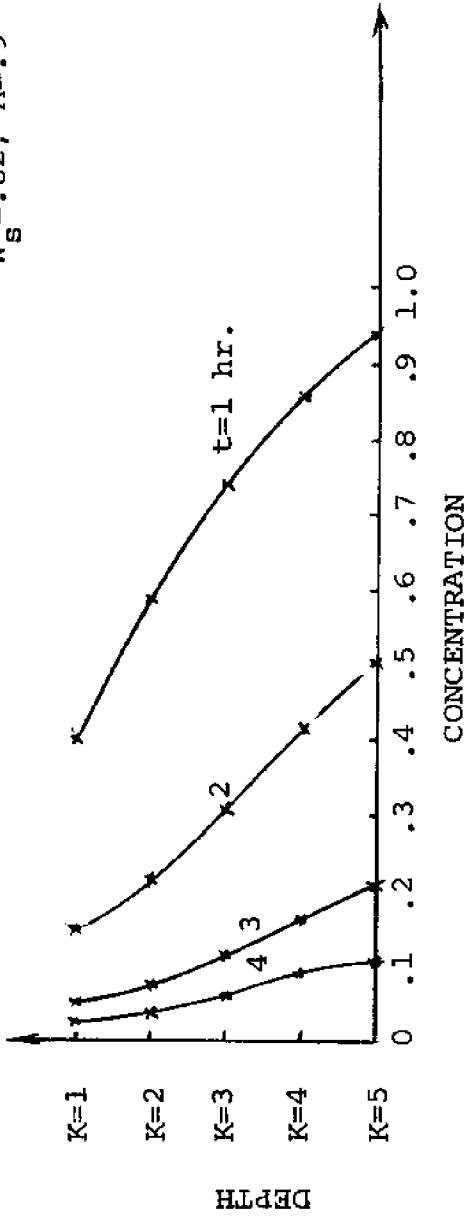


Fig.6-5 Sediment Particle Concentration vs. y-direction at Various Depths at I=13 and I=21.

I=13, J=7  
 $W_s = .02, A = .9$



I=21, J=7  
 $W_s = .02, A = .9$

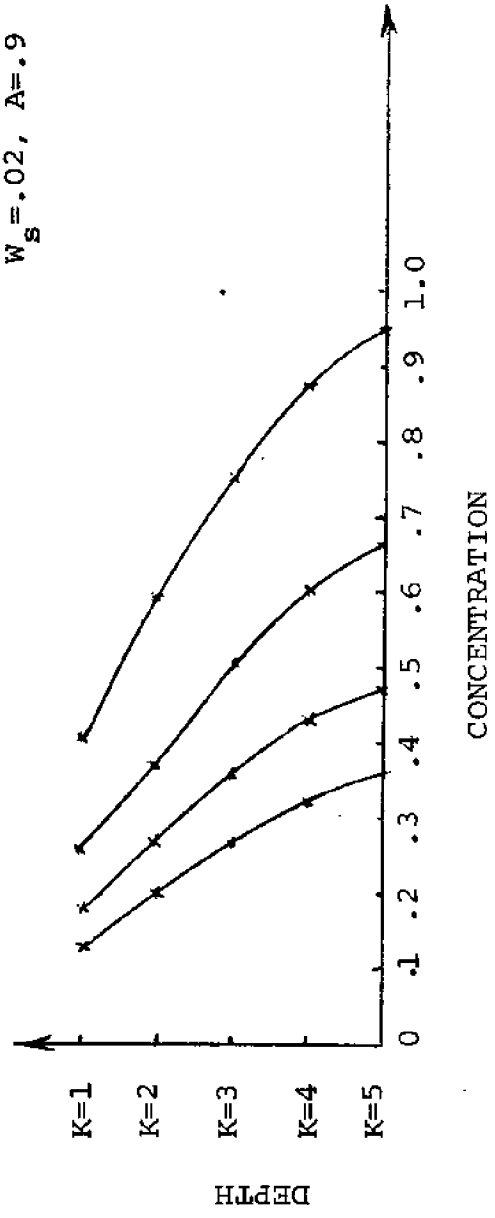


Fig.6-6 Vertical Sediment Particle Profiles at I=13 and I=21.

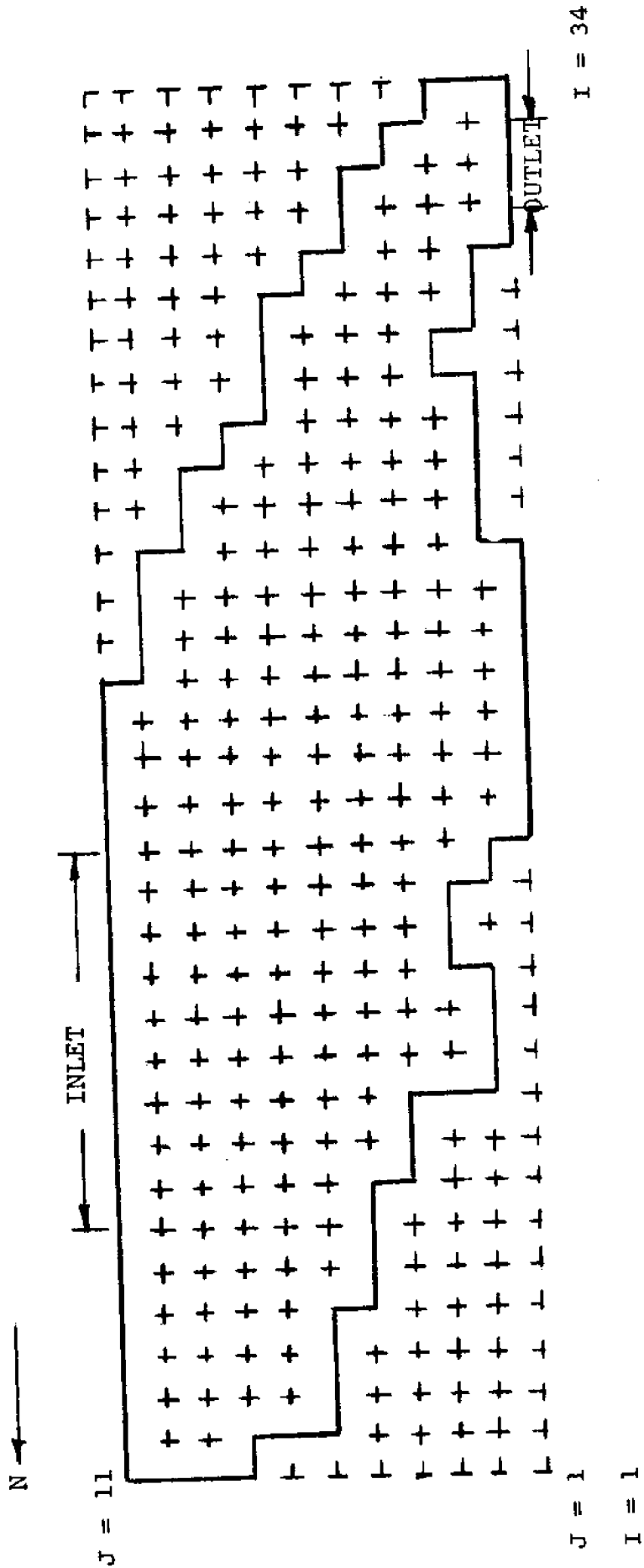


Fig. 7-1 Horizontal Grid System for Biscayne Bay used in Dissolved Chemical Transport.

$K_V=20 \text{ cm}^2/\text{s}$ , SNAPPER CREEK CANAL (7,6)

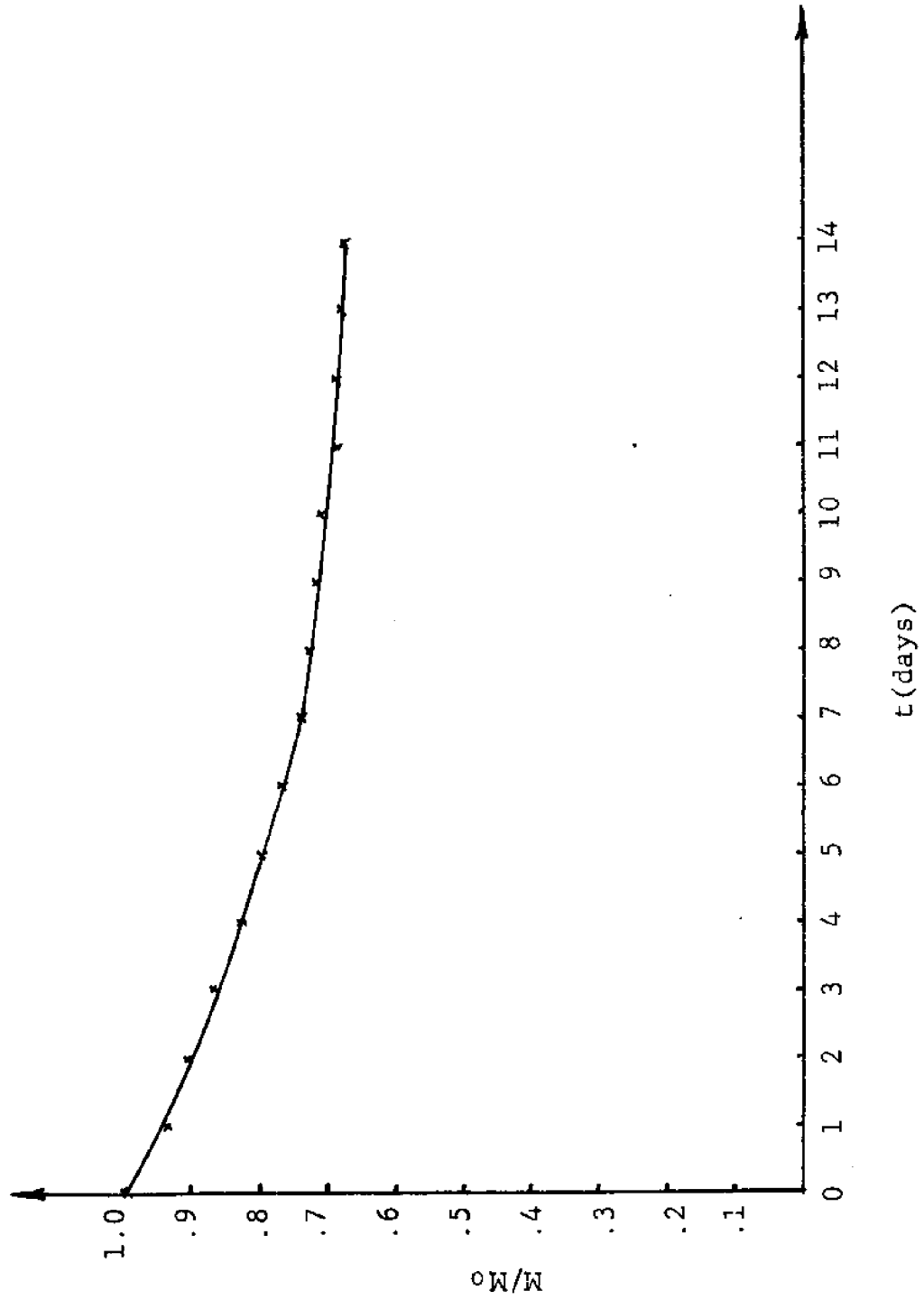


Fig. 7-2 Flushing Curve for Snapper Creek Canal Dye Release.

$KV=20 \text{ cm}^2/\text{s}$ , BLACK CREEK (17,2)

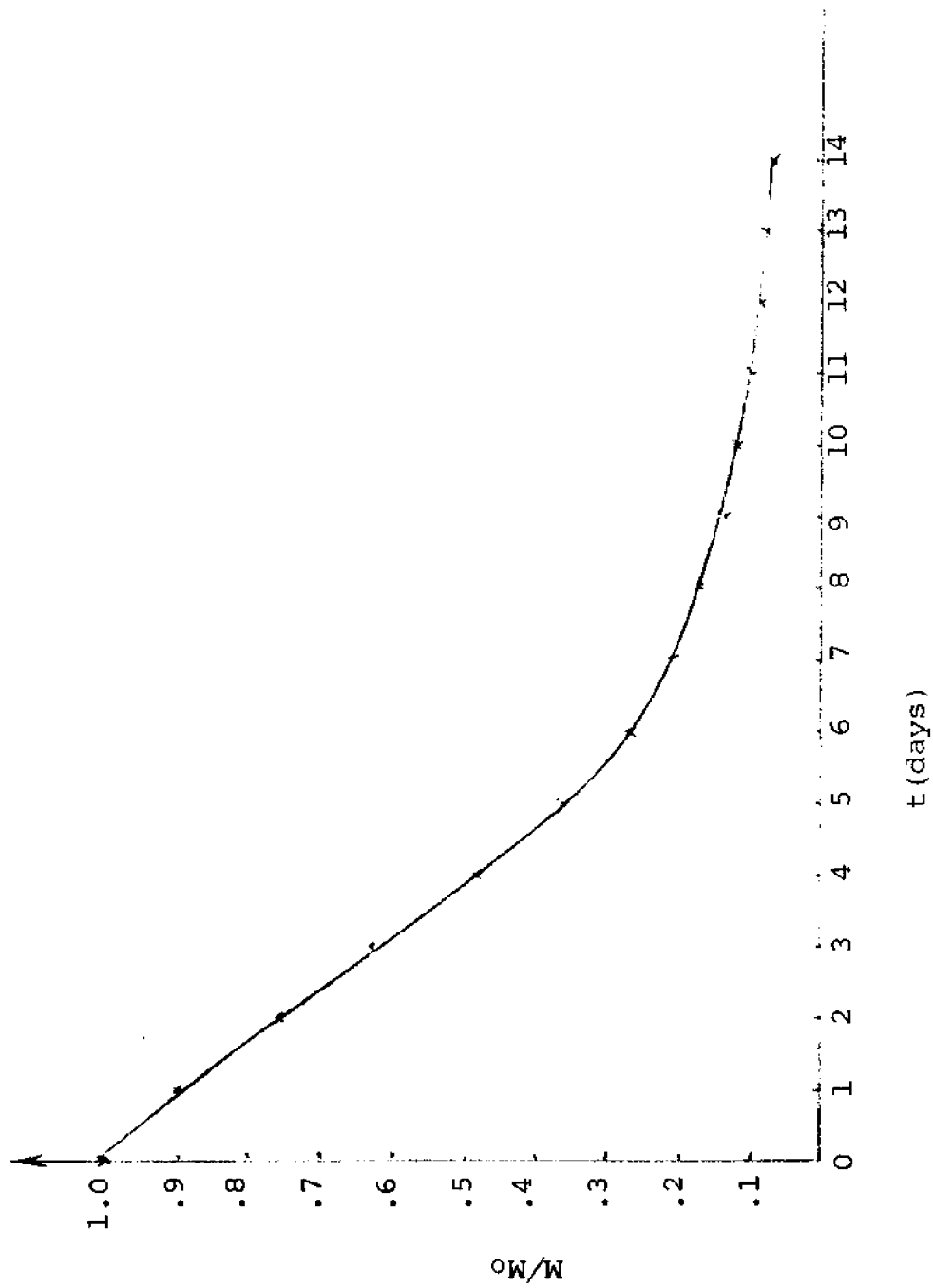


Fig.7-3 Flushing Curve for Black Creek Dye Release.

KV=20 cm<sup>2</sup>/s, MOWRY CANAL (20,2)

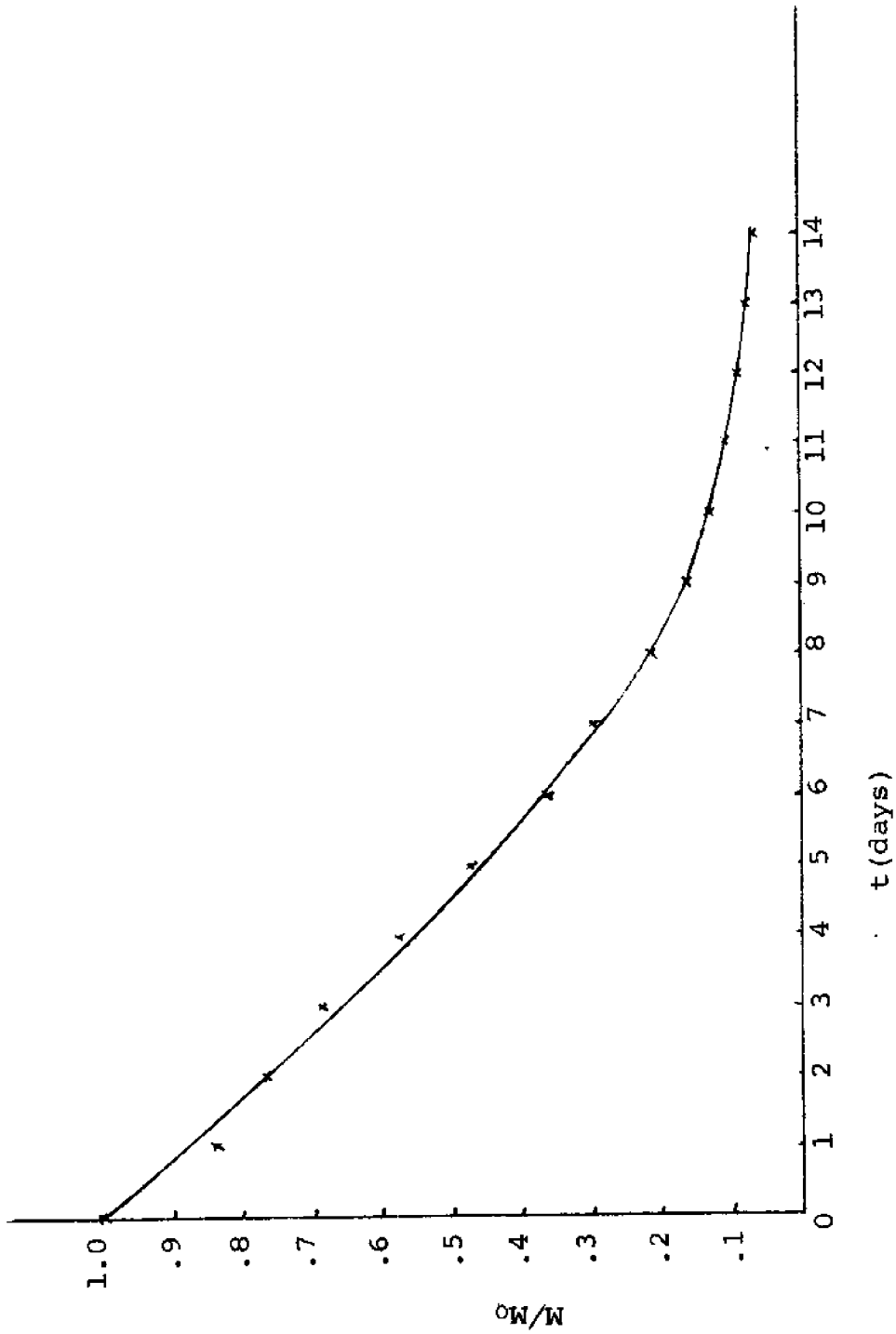


Fig.7-4 Flushing Curve for Mowry Canal Dye Release.

$K_v=20 \text{ cm}^2/\text{s}$ , UNIF. CONCENTRATION

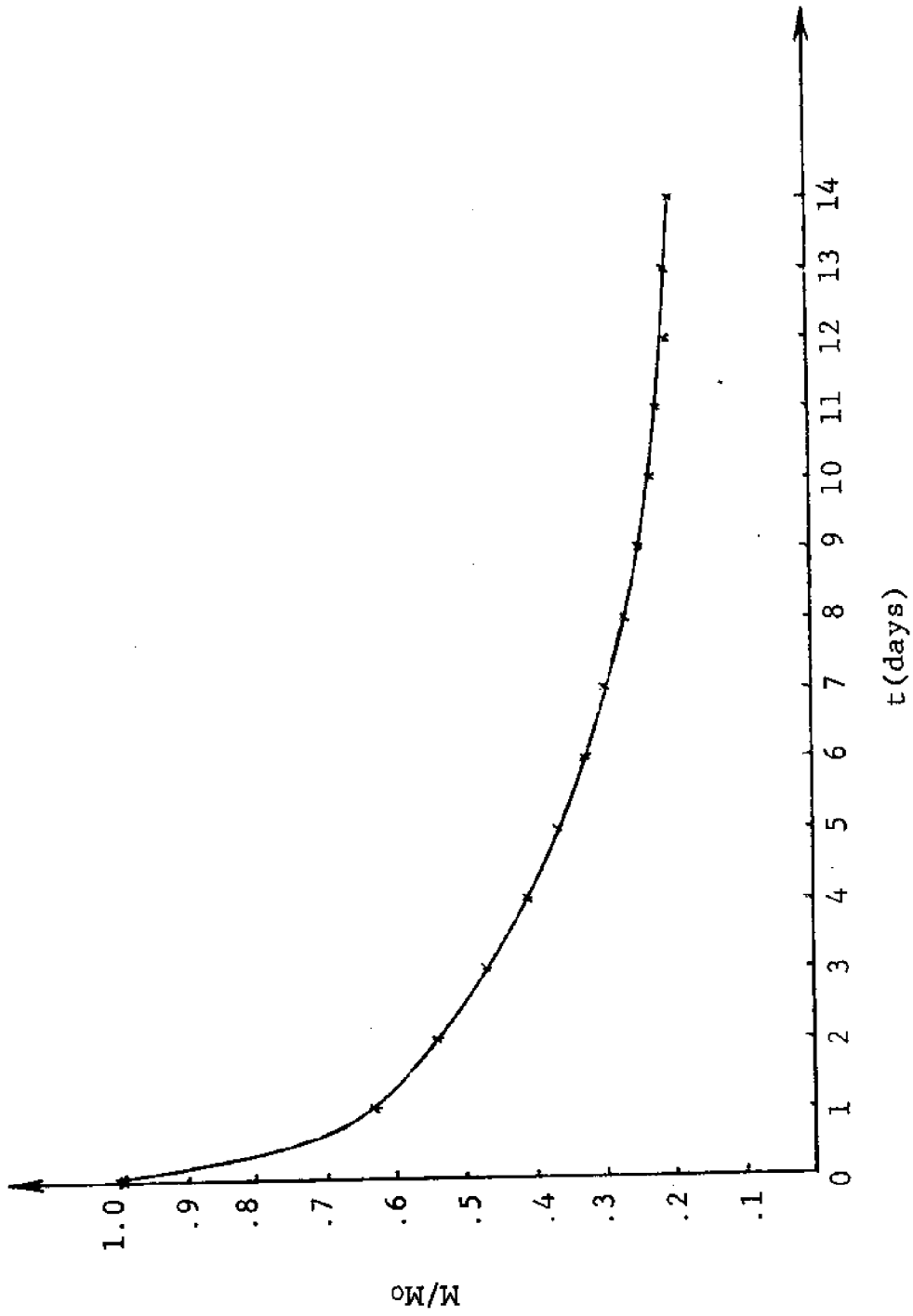
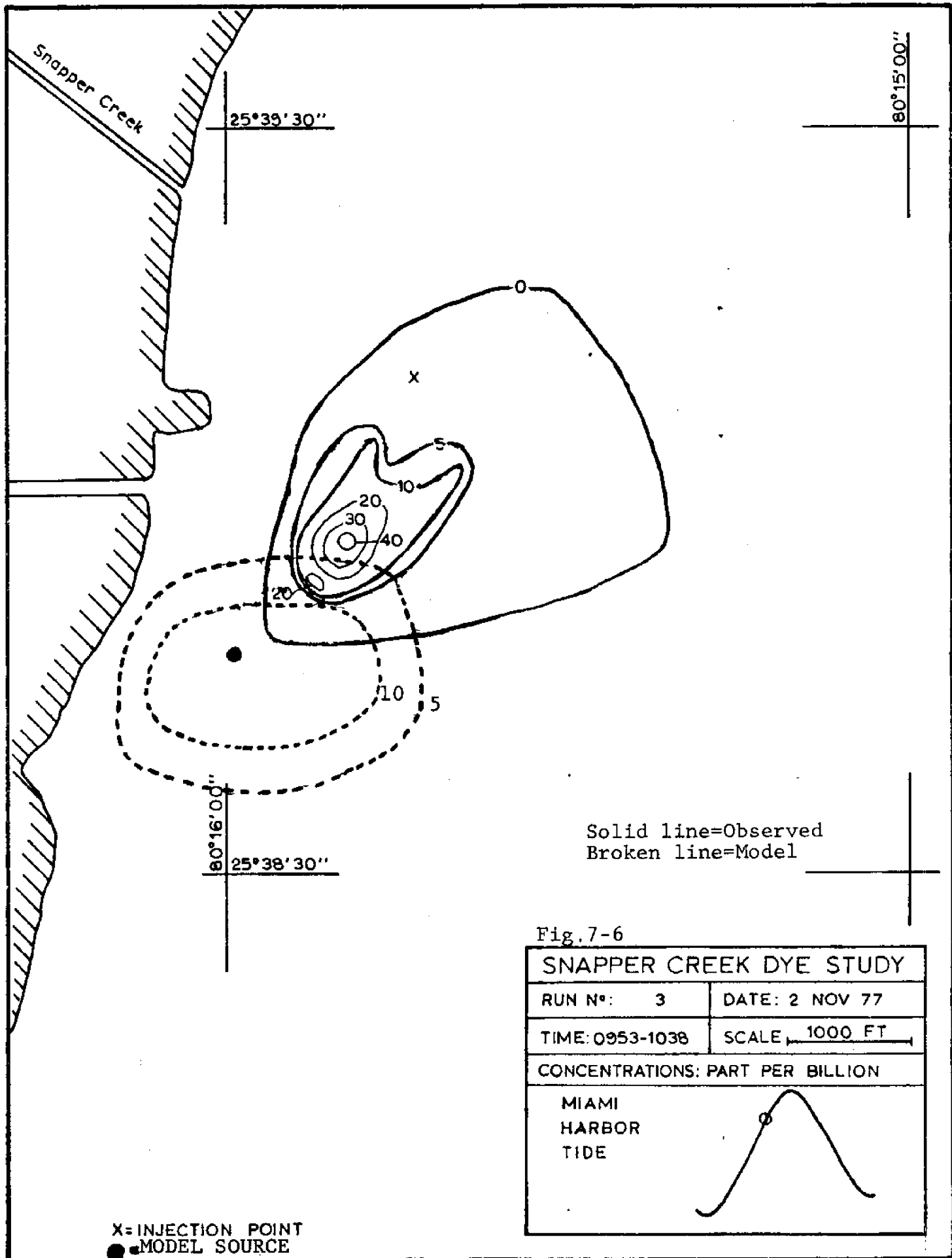
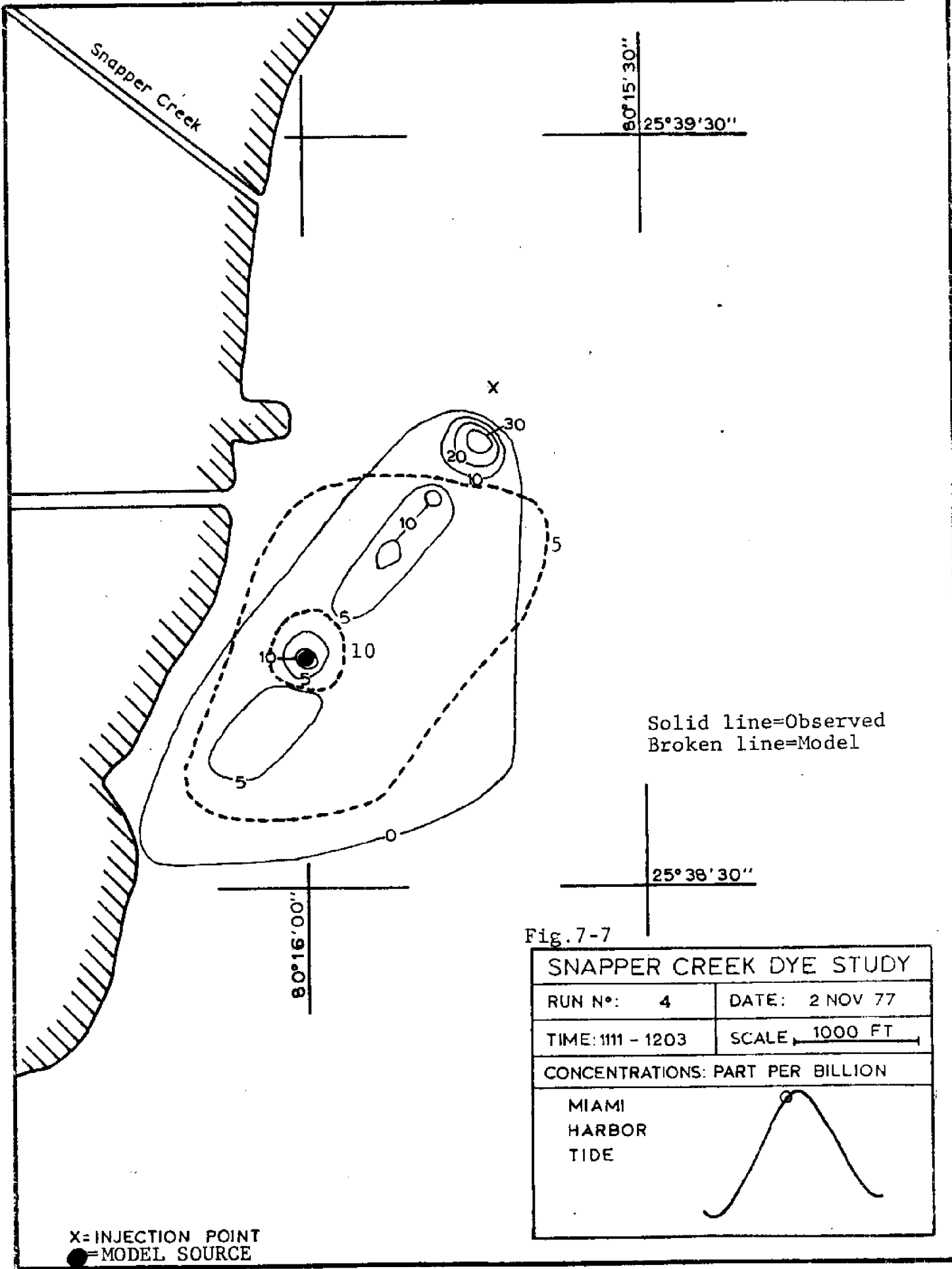
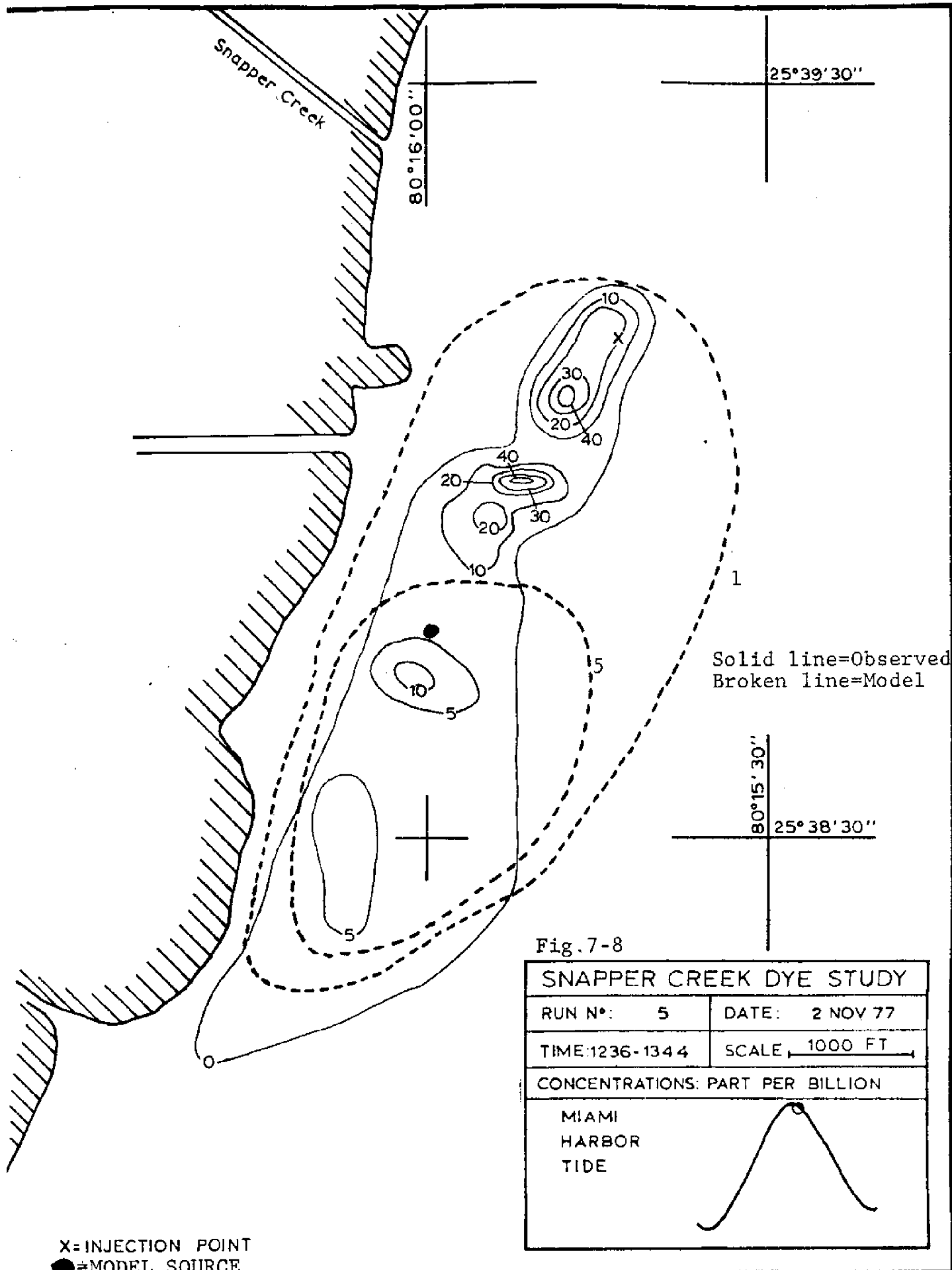


Fig.7-5 Flushing Curve for Uniform Concentration Distribution.



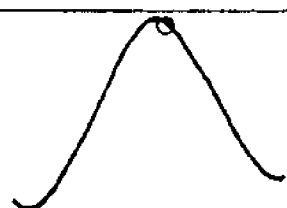




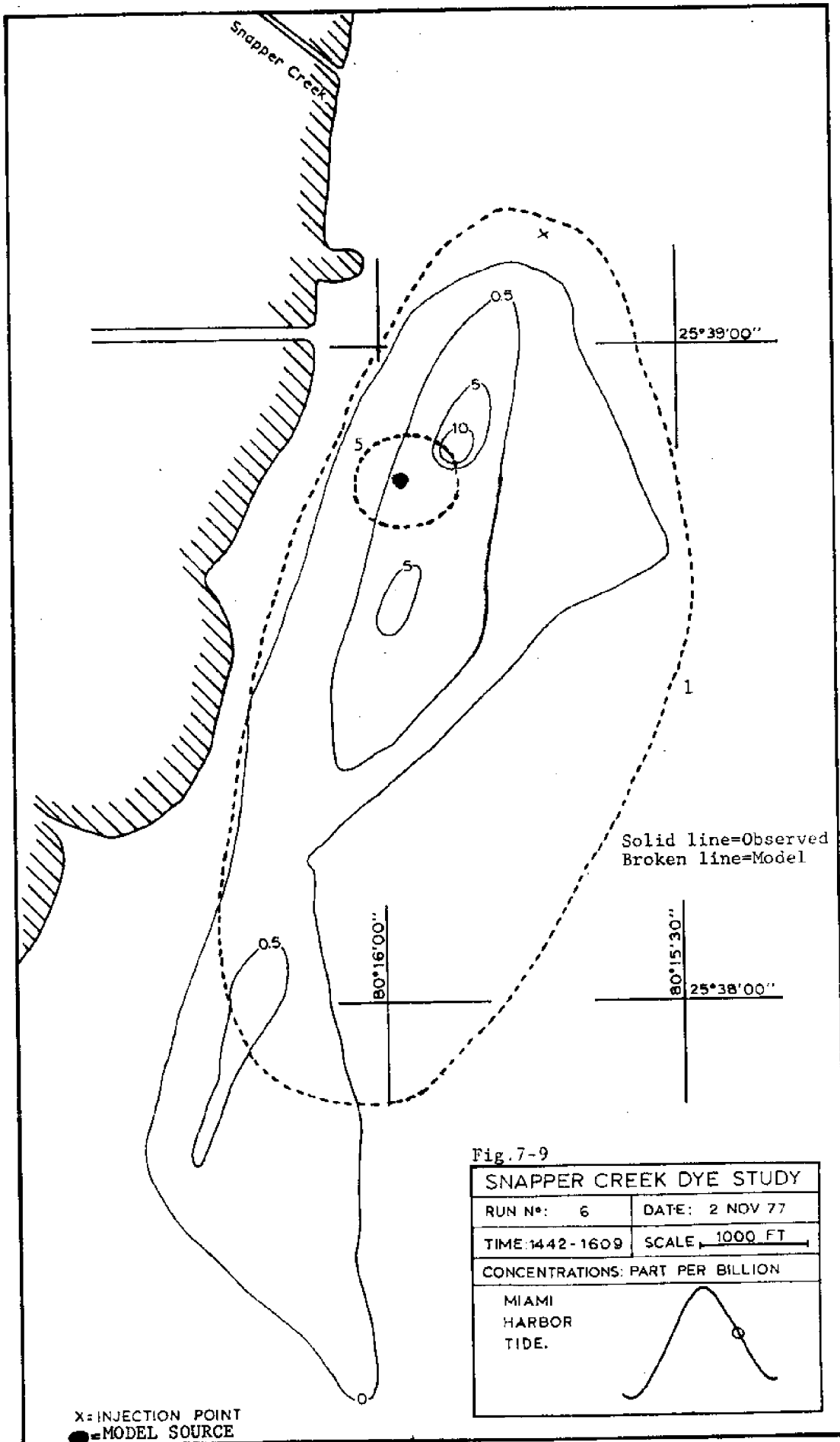


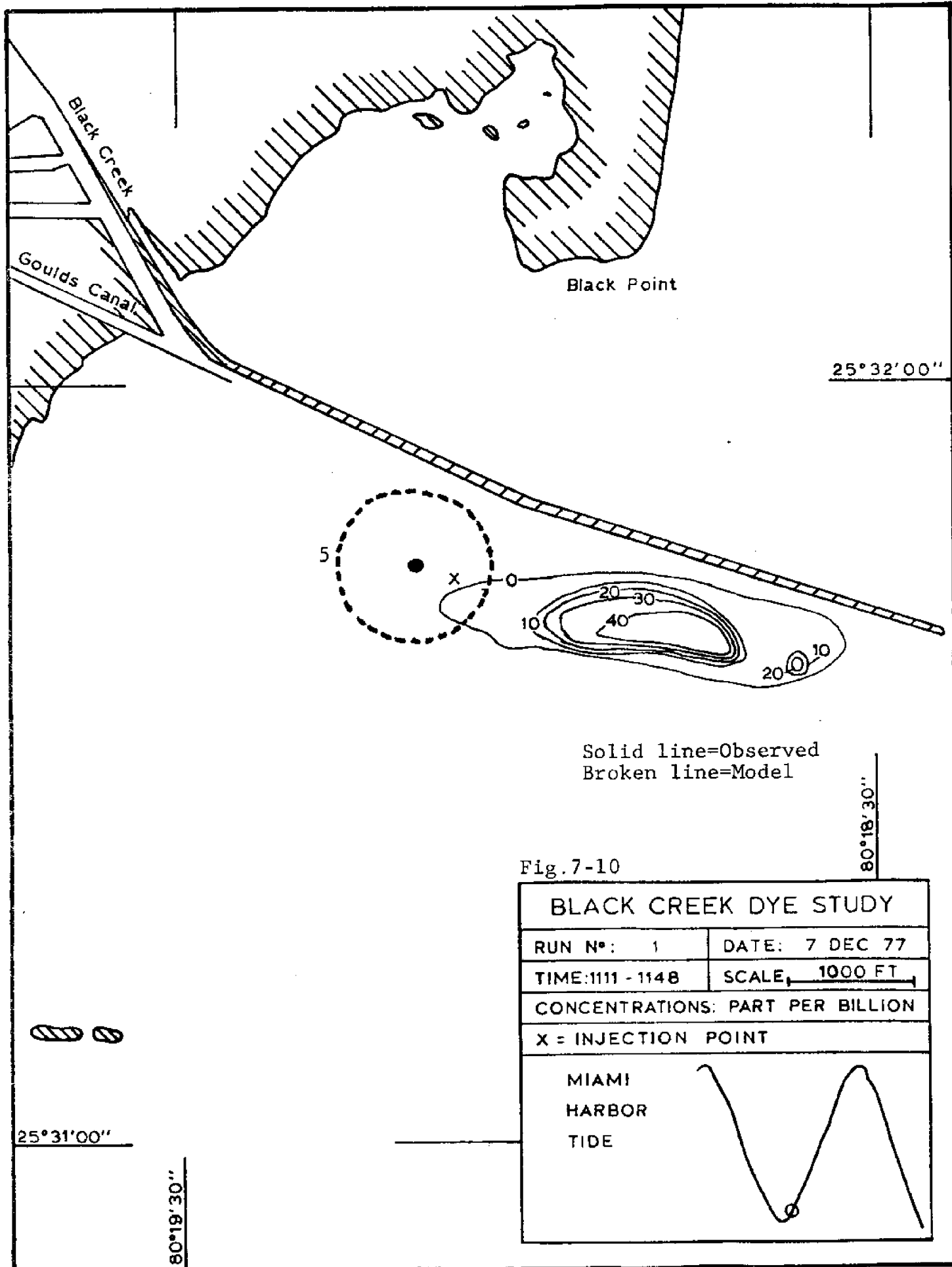
Solid line=Observed  
Broken line=Model

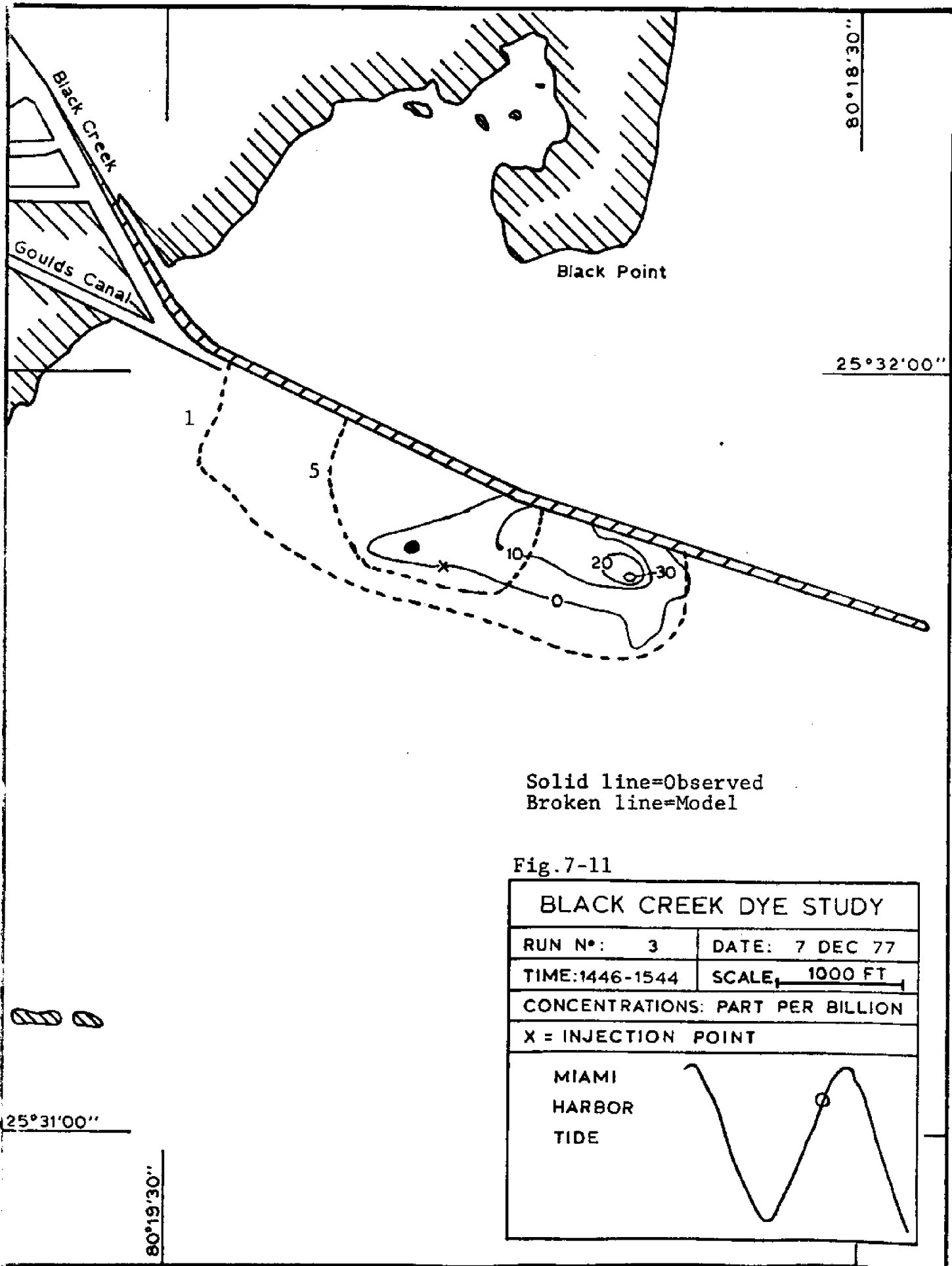
Fig.7-8

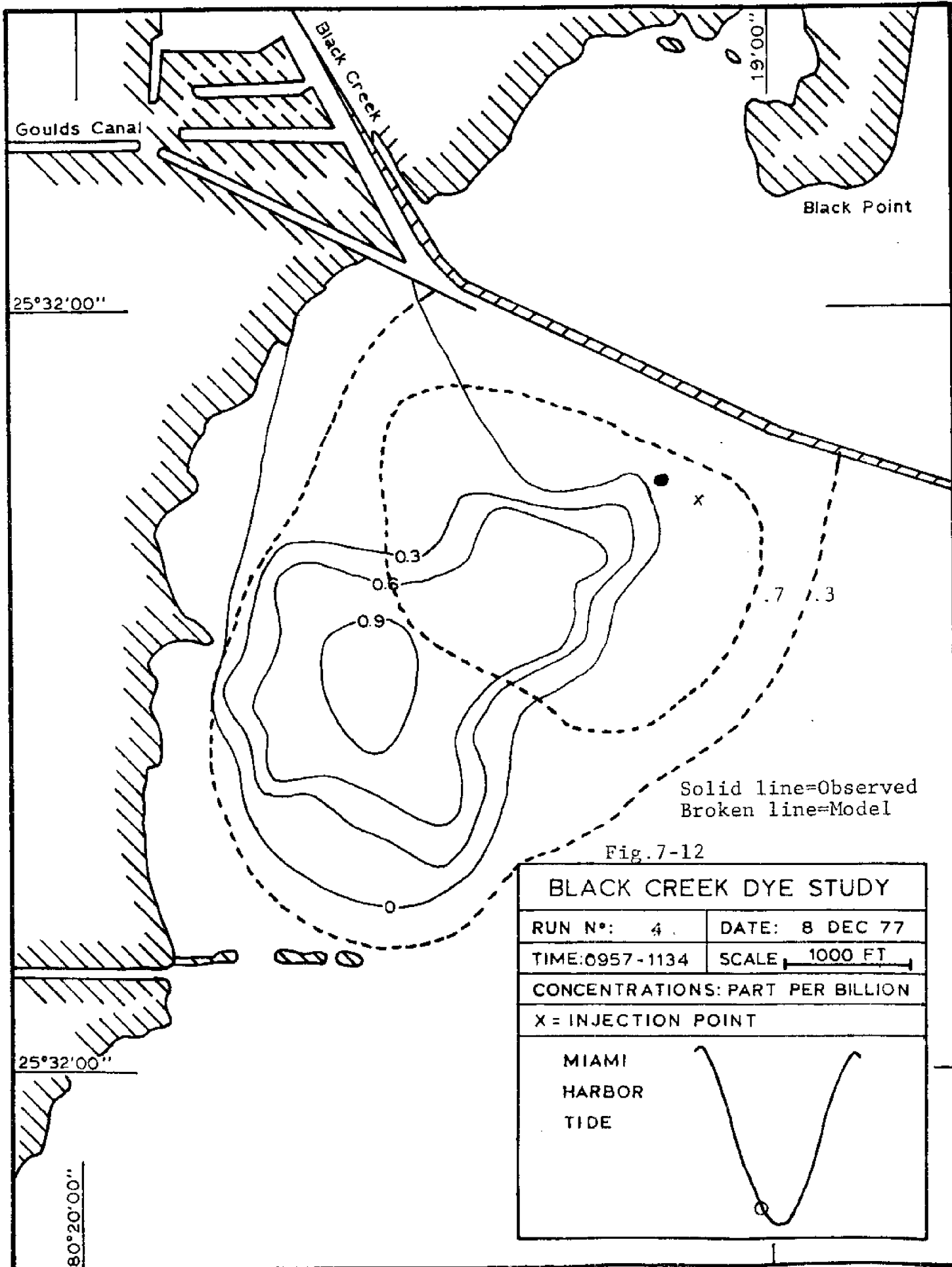
SNAPPER CREEK DYE STUDY	
RUN N°: 5	DATE: 2 NOV 77
TIME:1236-1344	SCALE: 1000 FT
CONCENTRATIONS: PART PER BILLION	
MIAMI HARBOR TIDE	

X=INJECTION POINT  
●=MODEL SOURCE





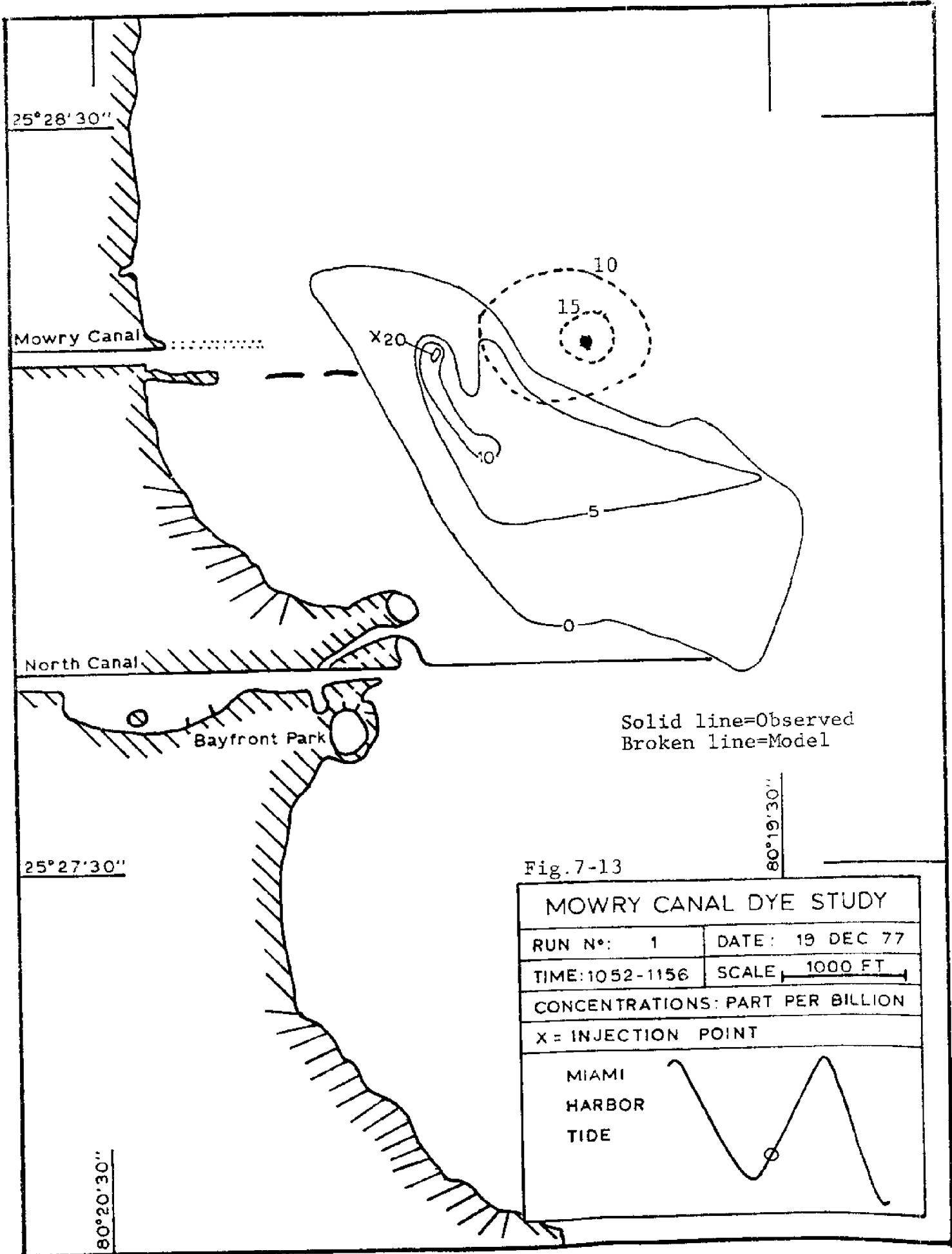


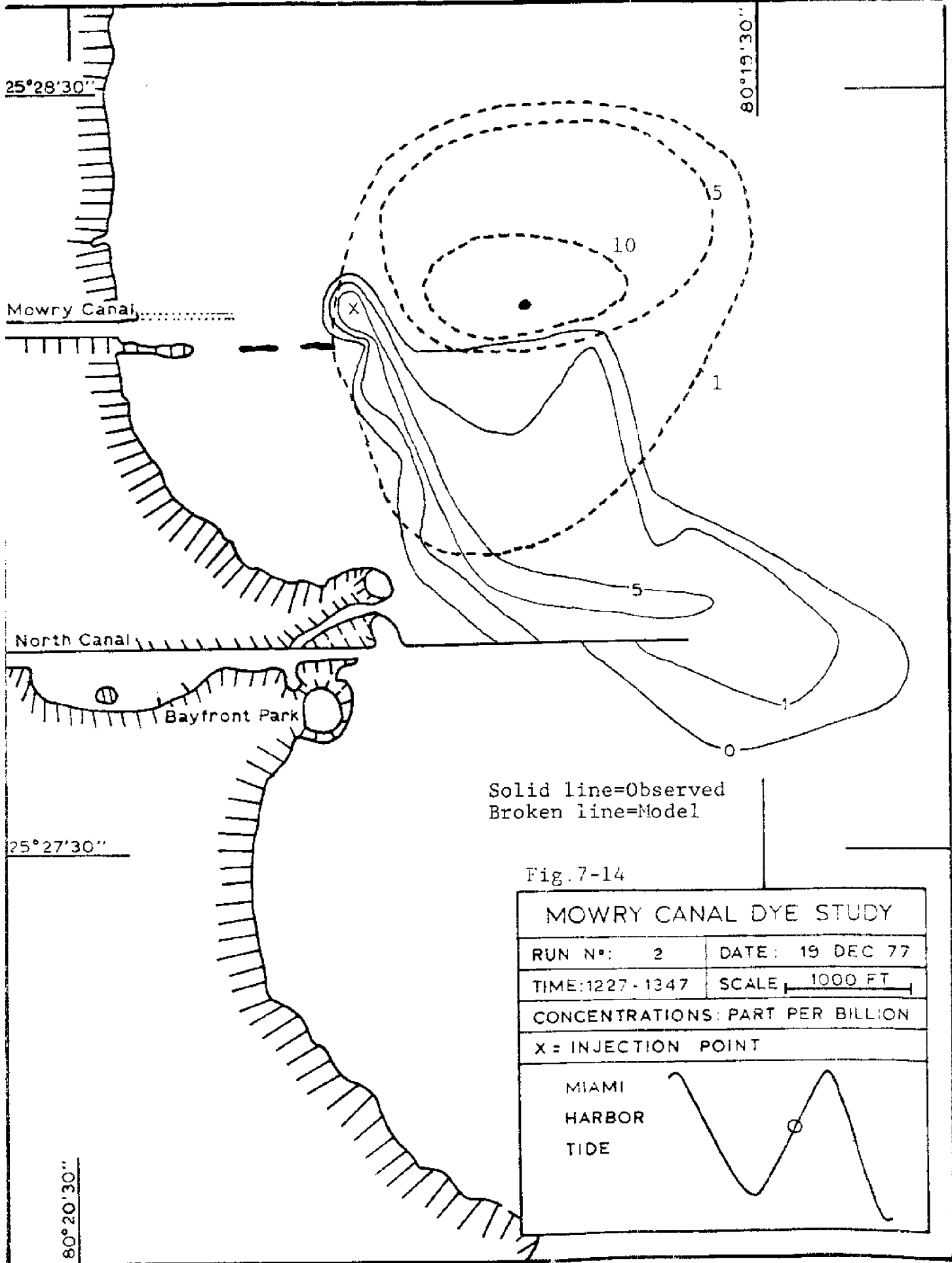


Solid line=Observed  
Broken line=Model

Fig.7-12

BLACK CREEK DYE STUDY	
RUN N°: 4	DATE: 8 DEC 77
TIME: 0957-1134	SCALE: 1000 FT
CONCENTRATIONS: PART PER BILLION	
X = INJECTION POINT	
MIAMI HARBOR TIDE	





Solid line=Observed  
 Broken line=Model

Fig. 7-14

MOWRY CANAL DYE STUDY	
RUN N°: 2	DATE: 19 DEC 77
TIME: 1227 - 1347	SCALE: 1000 FT
CONCENTRATIONS: PART PER BILLION	
X = INJECTION POINT	
MIAMI HARBOR TIDE	



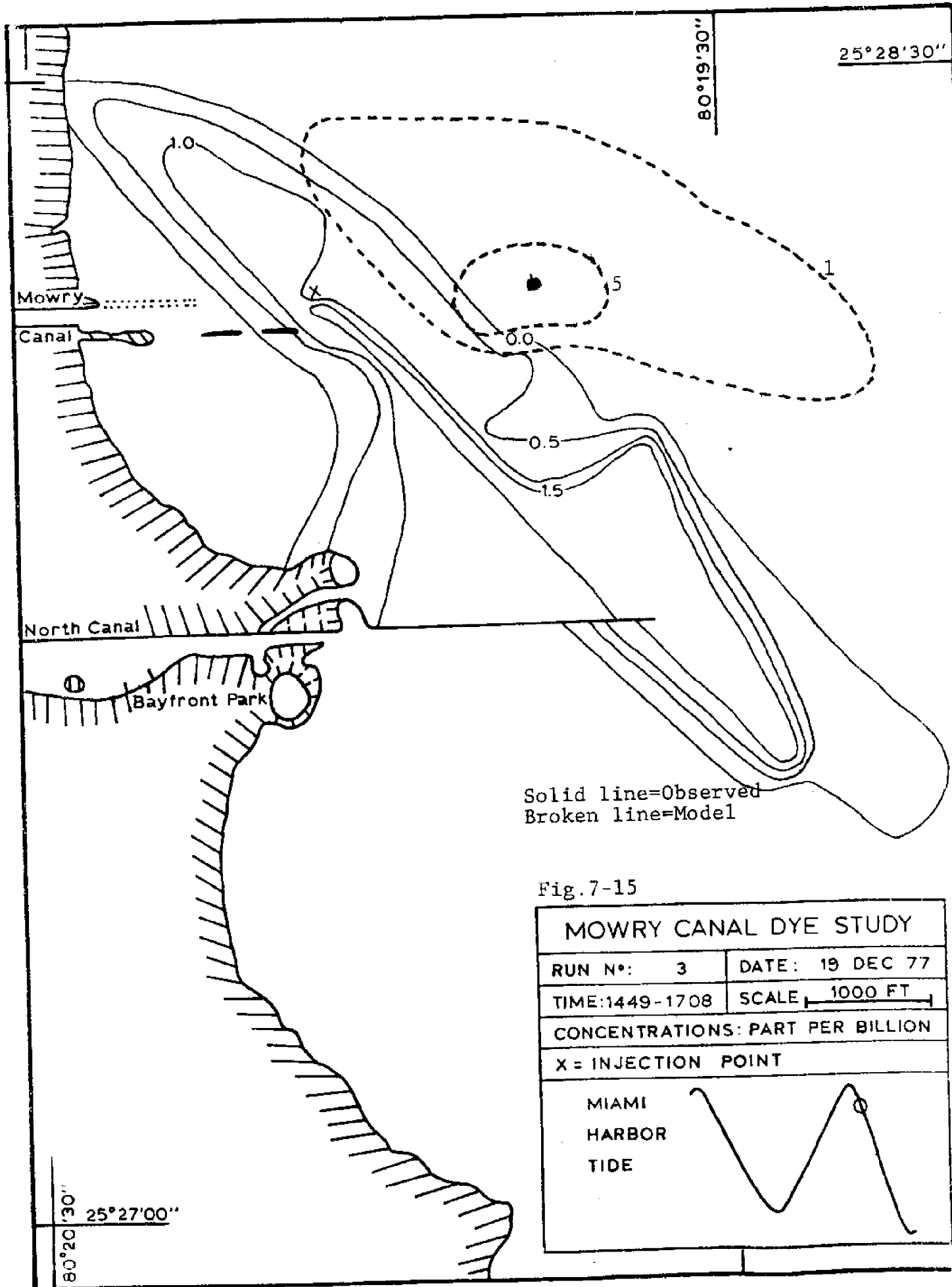


Fig.7-15

MOWRY CANAL DYE STUDY	
RUN N°: 3	DATE: 19 DEC 77
TIME: 1449-1708	SCALE: 1000 FT
CONCENTRATIONS: PART PER BILLION	
X = INJECTION POINT	
MIAMI HARBOR TIDE	

## 8.0. Discussion and Conclusions

### 8.1. Sediment Transport

The basic sediment transport processes, with associated boundary conditions, have been modelled. General features of the suspended sediment particle transport have been evaluated qualitatively, and the resulting behavior and dominant physical processes determined. The most rigorous hydrodynamic model used by other researchers is that of Sheng (1975). However, our model relaxes Sheng's "rigid-lid" approximation, by actually treating the bay's free surface behavior. Thus, the effects of variable tidal level for estuarine chemical and sediment transport has been accomplished by employing a three-dimensional, time-dependent free-surface model.

By varying the values of particle settling velocity and bottom deposition rate physical insight was gained with regard to the governing mechanisms of sediment transport. It has been learned that the resulting distribution of suspended sediment particles is much more strongly affected by varying settling velocity than by varying bottom deposition rate. Other researchers have not reported such findings. Sheng (1975), Apman and Rumer (1970), Hjelmfelt and Lenau (1970), Jobson (1970), Jobson and Sayre (1970), and Mei (1969).

The effects of ideal gravitational particle settling with variable settling velocity has not been discussed by the above researchers. However, Sheng (1975) and

Jobson (1970) have reported the results of using variable bottom deposition rate in their studies. Our investigation, vis-a-vis a thorough comparison with the state-of-the-art of research in sediment transport, is, therefore the most extensive with particular regard to rigorously modelling the hydrodynamic field of the environmental flow physics affecting the actual sediment transport and bottom deposition.

Further research into other physical processes of sediment transport, such as hindered particle settling, flocculation, and bed scour (or viscous turbulent entrainment), would be the next logical step in properly modelling sediment transport in geophysical flows. However, realistic descriptions of these complicated physical processes requires much more experimental research. Present descriptions are empirical in nature, Allen (1970), Raudkivi (1975), and relative interaction between these processes has not, as yet, been determined. Thus, until a better experimental base exists, introduction of these physics is a task not worth pursuing. The above mentioned researchers also limited their investigations to ideal gravitational particle settling, since in actual flows the data bases for sediment transport are virtually nonexistent.

## 8.2. Dissolved Chemical Transport

The hydrodynamic variables  $\eta, u, v,$  and  $\Omega$  were obtained using wind and tide data bases for April 15, 1975. The hydrodynamic model was run for two complete tidal cycles over 24 hours. The results were then stored on magnetic tape every  $\frac{1}{2}$  hour, and, subsequently coupled to the concentration equation to compute flushing rates of dissolved chemical dye releases and spreading of initial dye sources. A time step of 6 min. was obtained for these computer runs, and the dissolved chemical transport model was run for 2 weeks for three dye release sites, and for an initially uniform distribution. Upon velocity calibration a vertical eddy kinematic viscosity  $K_v=20.00 \text{ cm}^2/\text{sec}$  was used with a vertical eddy diffusivity  $D_v=20.00 \text{ cm}^2/\text{sec}$ .

As noted in Section 7.3 the dye injected at Black Creek and at Mowry Canal flushed 93% in 2 weeks of running the model program. The dye injected at Snapper Creek Canal flushed 32% as predicted by the model. The uniform distribution flushed 80% as predicted by the model. The greater rate of flushing of the first two sites is not amenable to further examination and subsequent verification without a corresponding data base on long-term flushing. However, these field experiments for flushing times have not been conducted as yet.

The model results for predicting the dispersion or "spreading" of injected rhodamine WT (20%) dye at these three shoreline locations is in quite good agreement with

Wang's (1977) measured values, both in terms of the relative shapes of the lines of constant concentration and in terms of the rate of spreading, that is, the quantitative values of the corresponding lines of rhodamine WT (20%) dye in PPB.

Thus a dissolved chemical transport model has been developed which yields flushing times and spreading of dye. However, presently no data base is available for verifying the flushing rates. The short term spreading of the dye, however, has yielded good agreement with an existing data base.

### 8.3. Conclusions

A three-dimensional, time-dependant free surface hydrodynamic model has been developed, which takes account of topographical and meteorological parameters, for the application to sediment transport and dissolved chemical transport in the South Biscayne Bay. Local tidal effects have been introduced into the mathematical model by applying a so-called primitive numerical boundary condition at the ocean-bay interface. Agreement with a statistically averaged tide data base, both at the ocean exchange area and at several shoreline locations, for a calibrated model (on the basis of velocity current data base) is quite good. Previous work by other researchers has not been truly three-dimensional, and ad hoc boundary conditions at the ocean-bay interface have been purely empirical. Both unstaggered and staggered hydrodynamic models have been used in these numerical dispersion studies.

Basic sediment transport processes, with associated boundary conditions, have been modelled. General features of the suspended particle sediment transport have been evaluated qualitatively, and the behavior of the dominant physical mechanisms determined. Our investigation of sediment transport is the most extensive in regard to rigorously modelling the hydrodynamic field. Further research into other physical processes of sediment transport, namely, hindered particle settling, flocculation and bottom bed turbulent entrainment, requires detailed, controlled laboratory experiments and extensive field data collection. Consequently, this investigation, like the work of other researchers, limited the physics to ideal gravitational settling, and a bottom boundary condition which neglects turbulent entrainment.

Dye release numerical studies at several shoreline locations have been conducted, and model predictions for non-reactive (conservative), dissolved chemical dispersion have been obtained. Flushing times of the injected dye has been obtained for the calibrated hydrodynamic model, however, no data base exists for the South Biscayne Bay with which to compare our model predictions. Thus a further verification effort is required with respect to long-term flushing calculations. The model is deemed to be of merit, both qualitatively and quantitatively, with respect to the numerical dye release studies, and the good agreement with Wang's (1977) dye release experiments.

The model can be directly applied to numerical studies of nutrient, and other biochemical processes, as well as to a variety of contaminant transport studies. However, further effort is necessary to ensure quantitative agreement with respect to long-term flushing and to sediment transport.

## REFERENCES

1. Allen, J.R.L., Physical Processes of Sedimentation, American Elsevier Publishing Company, New York, 1970.
2. Apmann, R.P. and Rumer, R.R., Jr., "Diffusion of Sediment in Developing Flow", Journal of the Hydraulics Division, Proceeding of ASCE, Vol. 96, HY1, 1970.
3. Barenblatt, G.I., "Motion of Suspended Particles in Turbulent Flow", Prikl. Matem. Mekh., 17, No.3, 1953.
4. Barenblatt, G.I., "Motion of Suspended Particles in Turbulent Flow Occupying a Half-Space or Plane Channel of Finite Depth", Prikl. Matem. Mekh., 19, No.1, 1955.
5. Blumberg, A.F., "Numerical Model of Chesapeake Bay", Journal of the Hydraulics Division, American Society of Civil Engineers, 1977a.
6. Blumberg, A.F., "Numerical Model of Estuarine Circulation", Journal of the Hydraulics Division, American Society of Civil Engineers, 1977b.
7. Camp, T.R., "Sedimentation and the Design of Settling Tanks", ASCE Transactions, Paper No. 2285, 1946.
8. Carter, C.V., "The Hydro-Thermal Characteristics of Shallow Lakes", Ph.D. Dissertation, University of Miami, 1977.
9. Dean, A.M. and Verma, A.P., "Numerical Modelling of Hydromechanics of Bay Systems", Dept. of Coastal and Oceanographic Engineering, University of Florida, 1969.
10. Einstein, A., "Investigations on the Theory of the Brownian Movement", Ph.D. Dissertation, Zurich Polytechnic, 1905, also Dover Publications, New York, 1956.
11. Fischer, H.B., "Mixing and Dispersion in Estuaries", Annual Review of Fluid Mechanics, Vol.8, 1976.
12. Freeman, N.G., Hale, A.M., and Danard, M.B., "A Modified Sigma Equations Approach to the Numerical Modelling of Great Lakes Hydrodynamics", Journal of Geophysical Res., Vol.77, No.6, 1972.
13. Gemmel, R.S., "Mixing and Sedimentation", Water Quality and Treatment, The American Water Works Association, McGraw-Hill, 1971.



14. Gentry, R.A., Martin, R.E., and Daly, B.J., "An Eulerian Differencing Method for Unsteady Compressible Flow Problems", Journal of Computation Physics, Vol.1, 1966.
15. Hjelmfelt, A.T. and Lenau, C.W., "Non-Equilibrium Transport of Suspended Sediment", Journal of the Hydraulics Division, Proc. of ASCE, Vol.96, HY7, 1970.
16. Jobson, H.E., "Predicting Concentration Profiles in Open Channels", Proc. ASCE, Vol.96, HY10, 1970.
17. Jobson, H.E. and Sayre, W.W., "Vertical Transfer in Open Channel Flow", Proc. ASCE, Vol.96, HY3, 1970.
18. Ketchum, B.H., "Distribution of Coliform bacteria and other Pollution in Tidal Estuaries", Sewage Ind. Wastes, 27, 1955.
19. Lam, D.C.L., "Computer Modelling of Pollutant Transports in Lake Erie", Water Pollution, 1975.
20. Lee, S.S. and Sengupta, S., Three-Dimensional Thermal Pollution Models, NASA CR-144858, 1977.
21. Lo, K.M., King, T.G., and Cooper, A.S., "A Computer Modelling Study to Assess the Effects of a Proposed Marina on a Coastal Lagoon", Proceedings of the Conference on Environmental Modelling and Simulation", 1976.
22. Lumley, J.L., "Some Problems Connected with the Motion of Small Particles in Turbulent Fluid", Ph.D. Dissertation, Johns Hopkins University, 1957.
23. Mei, C.C., "Non-Equilibrium Diffusion of Suspended Sediment", Journal of the Hydraulics Division, Proc. ASCE, Vol.95, HY1, 1969.
24. Monin, A.S. and Yaglom, A.M., Statistical Fluid Mechanics, MIT Press, 1971.
25. Murray, S.P., "Settling Velocities and Vertical Diffusion of Particles in Turbulent Water", Journal of Geophysical Res., Vol.75, 9, 1970.
26. Neumann, G. and Pierson, W.J., Jr., Principles of Physical Oceanography, Prentice-Hall, 1966.
27. Phillips, N.A., "A Coordinate System Having Some Special Advantages for Numerical Forecasting", Journal of Meteorology, Vol.14, 1957.

28. Raudkivi, A.J., Loose Boundary Hydraulics, Pergamon Press, 1975.
29. Reid, R.O. and Bodine, B.R., "Numerical Model for Storm Surges in Galveston Bay", Journal of Waterways and Harbors Division, Proc, ASCE, 1968.
30. Roache, J.P., Computational Fluid Dynamics, Hermosa Publishers, 1972.
31. Sayre, W.W., "Dispersion of Mass in Open-Channel Flow", Hydraulics Papers, Colorado State University, Fort Collins, Colorado, 1968.
32. Schneider, J.J., "Tidal Relations in the South Biscayne Bay", U.S. Geological Survey, 1969.
33. Sengupta, S. and Lick, W., "A Numerical Model for Wind Driven Circulation and Temperature Fields in Lakes and Ponds", FTAS/TR-74-99, Case Western Reserve University, 1974.
34. Sengupta, S., Lee, S.S., and Bland, R., "Three-Dimensional Model Development for Thermal Pollution Studies", Proceedings at the EPA Conference on Modelling, Cincinnati, 1976.
35. Sengupta, S., Lee, S.S., and Miller, H.P., "Three Dimensional Free Surface Model for Transport Processes in Biscayne Bay", Computational Methods in Geophysical Mechanics, ASME, AMD-Vol.25, 1977.
36. Sheng, Y.P., "The Wind-Driven Currents and Contaminant Dispersion in the Near-Shore of Large Lakes", Report H-75-1, Dept. of Earth Sciences, Case Western Reserve University, 1975.
37. Sheng, Y.P. and Lick, W., "Currents and Contaminant Dispersion in the Nearshore Region and Modification by a Jetport", Journal Great Lakes Res., 1976.
38. Tchen, C.M., "Mean Value and Correlation Problems Connected with the Motion of Small Particles Suspended in a Turbulent Fluid", Ph.D. Dissertation, Delft, 1947.
39. Wang, J.D., Private Communication, Univ. of Miami, RSMAS, 1977.

## APPENDIX A

### SETTLING VELOCITY IN A TURBULENT FLOW FIELD

The settling velocity has been determined in our work by assuming quiescent laminar flow not in the Stokes regime, that is, for  $Re > 1$ , from Gemmel (1971)

$$W_s^2 = \frac{8}{3} \frac{gr}{C_d} \left( \frac{\gamma_s - \gamma_w}{\gamma_w} \right) \quad (A-1)$$

And,

$$C_d = \frac{24}{Re} + \frac{3}{Re^{\frac{1}{2}}} + 0.34 \quad (A-2)$$

For  $Re > 1$  (note,  $C_d = \frac{24}{Re}$  for Stokes creeping flow)

Jobson et al (1970) concluded that turbulence increased the average settling velocity by about 5%. Whereas, Murray (1970) concluded that the average settling velocity as determined by experiment in various turbulent flow fields is reduced by as much as 30% below the corresponding quiescent laminar settling velocity. Since no convincing criteria have been presented indicating the limitations of assuming that the mean value of the particle settling velocity is unaffected by turbulent fluctuations of the fluid, we have computed its value on the basis of quiescent conditions.

## APPENDIX B

### FLUID AND PARTICLE EDDY TRANSPORT COEFFICIENTS

The fluid eddy diffusion coefficients,  $D_H$  and  $D_V$ , is assumed to be the same as that of the particles, both suspended and dissolved (or neutrally buoyant). Sayre (1968) concluded that small sediment particles (diameter less than 0.1 mm) very nearly follow the turbulent fluctuations, and, hence, have a diffusion coefficient nearly equal to that of the fluid. It is tacitly assumed that the particles are sufficiently dilute in the fluid, such that

$$D_H \text{ particle} = D_H \text{ fluid} \quad (\text{B-1})$$

$$D_V \text{ particle} = D_V \text{ fluid} \quad (\text{B-2})$$

Einstein (1905) concluded that dissolved molecules and suspended particles are identical in their diffusive behavior at great dilution. For long diffusion times, Tchen (1947) showed, by studying the motion of a small particle suspended in a turbulent fluid, that for a homogeneous turbulent field of infinite extent, the eddy diffusion coefficient for the particle is the same as that of the fluid.

APPENDIX C  
WIND STRESSES AND CORIOLIS PARAMETER IN  
ROTATED GRID SYSTEM

The grid system as shown in Fig.6-1 has been rotated  $20^{\circ}$  clockwise with respect to due North. This was done in order to align the intracoastal waterway channel with the grid nodes for ease in specifying an instantaneous line source of stirred up sediment particles.

Now for the angle of rotation  $\alpha=20^{\circ}$ , we have the following relationships for wind stresses.

S Direction of Wind

$$\tau_{xz} = -\tau \cos \alpha \quad (C-1)$$

$$\tau_{yz} = -\tau \sin \alpha \quad (C-2)$$

SSW Direction of Wind

$$\tau_{xz} = -\tau \cos(22.5^{\circ} - \alpha) \quad (C-3)$$

$$\tau_{yz} = +\tau \sin(22.5^{\circ} - \alpha) \quad (C-4)$$

WNW Direction of Wind

$$\tau_{xz} = \tau \sin(22.5^{\circ} - \alpha) \quad (C-5)$$

$$\tau_{yz} = \tau \cos(22.5^{\circ} - \alpha) \quad (C-6)$$

NW Direction of Wind

$$\tau_{xz} = \tau \sin(45^{\circ} - \alpha) \quad (C-7)$$

$$\tau_{yz} = \tau \cos(45^{\circ} - \alpha) \quad (C-8)$$

The Coriolis parameter  $f = 2\Omega \sin \phi$  is not effected by the rotation of  $\alpha=20^{\circ}$  as can be easily shown. The Navier-Stokes equations in a non-inertial reference can be expressed in terms of the Coriolis parameter  $f$  (in the Northern

Hemisphere) as:

$$\frac{D\vec{v}}{Dt} + 2\vec{\Omega} \times \vec{v} = \dots \quad (C-9)$$

Where  $\vec{v} = u\hat{i} + v\hat{j} + w\hat{k}$

Now referring to Fig.C-1 we see that  $2\vec{\Omega} \times \vec{v}$  can be resolved into the x,y, and z directions, respectively. Thus,

$$\vec{\Omega} = \Omega \cos \phi \hat{j} + \Omega \sin \phi \hat{h} \quad \text{in the Northern Hemisphere}$$

And, hence,

$$2\vec{\Omega} \times \vec{v} = (2w\Omega \cos \phi - 2v\Omega \sin \phi) \hat{i} + 2u\Omega \sin \phi \hat{j} - 2u\Omega \cos \phi \hat{k}$$

But  $f = 2\Omega \sin \phi$  and therefore,

$$2\vec{\Omega} \times \vec{v} = (2w\Omega \cos \phi - fv) \hat{i} + fu \hat{j} - 2u\Omega \cos \phi \hat{k}$$

Now resolving  $\frac{D\vec{v}}{Dt}$  into u,v,w components we have:

$$\frac{Du}{Dt} + 2w\Omega \cos \phi - fv = \dots \quad (C-10)$$

$$\frac{Dv}{Dt} + fu = \dots \quad (C-11)$$

$$\frac{Dw}{Dt} - 2u\Omega \cos \phi = \dots \quad (C-12)$$

But in most geophysical flows and particularly for the South Biscayne Bay,

$$u \gg w \quad \text{Hence } 2w\Omega \cos \phi \text{ is neglected.}$$

$$v \gg w$$

And, we have neglected (C-12) by invoking the hydrostatic approximation. Now, let our non-inertial coordinate system (x,y,z) be rotated through an angle  $\alpha=20^\circ$  clockwise with respect to due North. Referring to Fig.C-2 we rotate x,y to x',y' in some x,y plane perpendicular

to z. Then, for components of  $\Omega$  along  $x'$ ,  $y'$  and  $z (=z')$  we can use direction cosines, such that,

$$\begin{aligned}\vec{\Omega} \cdot \hat{i}' &= \Omega \cos \gamma \text{ in } x' \text{ - direction } (\gamma \text{ unknown}) \\ \vec{\Omega} \cdot \hat{j}' &= \Omega \cos \theta \text{ in } y' \text{ - direction } (\theta \text{ unknown}) \\ \vec{\Omega} \cdot \hat{k}' &= \Omega \cos \beta = \Omega \cos (90^\circ - \phi) = \Omega \sin \phi \text{ in} \\ & z \text{ - direction.}\end{aligned}$$

Then  $\vec{\Omega}$  in  $(x', y', z')$  is expressed as,

$$\vec{\Omega} = \Omega \cos \gamma \hat{i}' + \Omega \cos \theta \hat{j}' + \Omega \sin \phi \hat{k}' \quad (C-13)$$

And, consequently,

$$\begin{aligned}2\vec{w} \times \vec{v} &= 2 \{ (w \Omega \cos \theta - v \Omega \sin \phi) \hat{i}' + (u \Omega \sin \phi \\ & - w \Omega \cos \gamma) \hat{j}' + (v \Omega \cos \gamma - u \Omega \cos \theta) \hat{k}' \}\end{aligned}$$

Again for  $w \ll u$ ,  $w \ll v$  and replacing  $\frac{Dw}{Dt} = \dots$  with hydrostatic equation we arrive at,

$$\frac{Du}{Dt} - fv = \dots$$

$$\frac{Dv}{Dt} + fu = \dots$$

Where  $f = 2\Omega \sin \phi$ . Therefore, by invoking the hydrostatic approximation, we see that rotation of the grid system has negligible effect upon the Coriolis forces.

APPENDIX D  
CONVECTIVE AND DIFFUSIVE TERMS  
IN  $(\alpha, \beta, \sigma)$  COORDINATE SYSTEM

The transformation of the convective and diffusive terms from the  $(x, y, z)$  coordinate system to the  $(\alpha, \beta, \sigma)$  coordinate system will now be presented.

CONVECTIVE

Consider the  $u$ -momentum equation in the  $(x, y, z)$  coordinate system - only the convective terms:

$$\frac{\partial u}{\partial t} + u \frac{\partial u}{\partial x} + v \frac{\partial u}{\partial y} + w \frac{\partial u}{\partial z} = 0 \quad (D-1)$$

now by a partial derivative expansion we obtain,

$$\frac{\partial u}{\partial x} = \frac{\partial u}{\partial \alpha} + \frac{1}{H} \frac{\partial \eta}{\partial \alpha} \frac{\partial u}{\partial \sigma} - \frac{\sigma}{H} \frac{\partial H}{\partial \alpha} \frac{\partial u}{\partial \sigma} \quad (D-2)$$

$$\frac{\partial u}{\partial y} = \frac{\partial u}{\partial \beta} + \frac{1}{H} \frac{\partial \eta}{\partial \beta} \frac{\partial u}{\partial \sigma} - \frac{\sigma}{H} \frac{\partial H}{\partial \beta} \frac{\partial u}{\partial \sigma} \quad (D-3)$$

$$\frac{\partial u}{\partial z} = \frac{1}{H} \frac{\partial u}{\partial \sigma} \quad (D-4)$$

then upon substituting equations (D-2), (D-3) and (D-4) into (D-1) we obtain:

$$\begin{aligned} & \frac{\partial u}{\partial t} + u \left\{ \frac{\partial u}{\partial \alpha} + \frac{1}{H} \frac{\partial \eta}{\partial \alpha} \frac{\partial u}{\partial \sigma} - \frac{\sigma}{H} \frac{\partial H}{\partial \alpha} \frac{\partial u}{\partial \sigma} \right\} \\ & + v \left\{ \frac{\partial u}{\partial \beta} + \frac{1}{H} \frac{\partial \eta}{\partial \beta} \frac{\partial u}{\partial \sigma} - \frac{\sigma}{H} \frac{\partial H}{\partial \beta} \frac{\partial u}{\partial \sigma} \right\} \\ & + (w/H) \frac{\partial u}{\partial \sigma} \end{aligned} \quad (D-5)$$

where,

$$w = \frac{dz}{dt} = H\Omega + (\sigma-1) \frac{d\eta}{dt} + \sigma \frac{dh}{dt} \quad (D-6)$$

Hence,



$$\begin{aligned}
& \frac{\partial u}{\partial t} + u \frac{\partial u}{\partial \alpha} + v \frac{\partial u}{\partial \beta} + \left\{ \frac{u}{H} \frac{\partial \eta}{\partial \alpha} \frac{\partial u}{\partial \sigma} - \frac{u\sigma}{H} \frac{\partial H}{\partial \alpha} \right. \\
& \quad \cdot \left. \frac{\partial u}{\partial \sigma} \right\} + \left\{ \frac{v}{H} \frac{\partial \eta}{\partial \beta} \frac{\partial u}{\partial \sigma} - \frac{v\sigma}{H} \frac{\partial H}{\partial \beta} \frac{\partial u}{\partial \sigma} \right\} \\
& \quad + \frac{1}{H} \frac{\partial u}{\partial \sigma} \left\{ H\Omega + (\sigma-1) \frac{d\eta}{dt} + \sigma \frac{dh}{dt} \right\} = 0 \quad (D-7)
\end{aligned}$$

The continuity equation in  $(x, y, z)$  is,

$$\frac{\partial u}{\partial x} + \frac{\partial v}{\partial y} + \frac{\partial w}{\partial z} = 0 \quad (D-8)$$

and can be easily shown to be expressed as follows in  $(\alpha, \beta, \sigma)$ :

$$\frac{\partial H}{\partial t} + \frac{\partial(Hu)}{\partial \alpha} + \frac{\partial(Hv)}{\partial \beta} + H \frac{\partial \Omega}{\partial \sigma} = 0 \quad (D-9)$$

Multiplying equation (D-9) by  $u$  we obtain:

$$u \frac{\partial H}{\partial t} + u \frac{\partial(Hu)}{\partial \alpha} + u \frac{\partial(Hv)}{\partial \beta} + uH \frac{\partial \Omega}{\partial \sigma} = 0 \quad (D-10)$$

Next, multiply equation (D-7) by  $H$  and obtain:

$$\begin{aligned}
& H \frac{\partial u}{\partial t} + Hu \frac{\partial u}{\partial \alpha} + Hv \frac{\partial u}{\partial \beta} + \left\{ u \frac{\partial \eta}{\partial \alpha} \frac{\partial u}{\partial \sigma} - u\sigma \frac{\partial H}{\partial \alpha} \frac{\partial u}{\partial \sigma} \right\} \\
& \quad + \left\{ v \frac{\partial \eta}{\partial \beta} \frac{\partial u}{\partial \sigma} - v\sigma \frac{\partial H}{\partial \beta} \frac{\partial u}{\partial \sigma} \right\} + \frac{\partial u}{\partial \sigma} \cdot \\
& \quad \left\{ H\Omega + (\sigma-1) \frac{d\eta}{dt} + \sigma \frac{dh}{dt} \right\} = 0 \quad (D-11)
\end{aligned}$$

Now, add equations (D-10) and (D-11),

$$\begin{aligned}
& H \frac{\partial u}{\partial t} + u \frac{\partial H}{\partial t} + Hu \frac{\partial u}{\partial \alpha} + u \frac{\partial(Hu)}{\partial \alpha} + Hv \frac{\partial u}{\partial \beta} \\
& \quad + u \frac{\partial(Hv)}{\partial \beta} + \left\{ u \frac{\partial \eta}{\partial \alpha} \frac{\partial u}{\partial \sigma} - u\sigma \frac{\partial H}{\partial \alpha} \frac{\partial u}{\partial \sigma} \right\} \\
& \quad + \left\{ v \frac{\partial \eta}{\partial \beta} \frac{\partial u}{\partial \sigma} - v\sigma \frac{\partial H}{\partial \beta} \frac{\partial u}{\partial \sigma} \right\} \\
& \quad + H\Omega \frac{\partial u}{\partial \sigma} + uH \frac{\partial \Omega}{\partial \sigma} + \left\{ (\sigma-1) \frac{\partial u}{\partial \sigma} \frac{d\eta}{dt} \right.
\end{aligned}$$

$$+ \sigma \frac{\partial u}{\partial \sigma} \frac{dh}{dt} \} = 0 \quad (D-12)$$

This reduces to,

$$\frac{\partial(Hu)}{\partial t} + \frac{\partial(Huu)}{\partial \alpha} + \frac{\partial(Huv)}{\partial \beta} + H \frac{\partial(u\Omega)}{\partial \sigma} + \Psi = 0 \quad (D-13)$$

where

$$\begin{aligned} \Psi = & u \frac{\partial u}{\partial \sigma} \left( \frac{\partial \eta}{\partial \alpha} - \sigma \frac{\partial H}{\partial \alpha} \right) + v \frac{\partial u}{\partial \sigma} \left( \frac{\partial \eta}{\partial \beta} - \sigma \frac{\partial H}{\partial \beta} \right) \\ & + (\sigma-1) \frac{\partial u}{\partial \sigma} \left( \frac{\partial \eta}{\partial t} + u \frac{\partial \eta}{\partial \alpha} + v \frac{\partial \eta}{\partial \beta} \right) + \sigma \frac{\partial u}{\partial \sigma} \cdot \\ & \left( \frac{\partial h}{\partial t} + u \frac{\partial h}{\partial \alpha} + v \frac{\partial h}{\partial \beta} \right) \end{aligned} \quad (D-14)$$

But upon simplification  $\Psi$  reduces to,

$$\Psi = (\sigma-1) \frac{\partial u}{\partial \sigma} \frac{\partial \eta}{\partial t} \quad (D-15)$$

Therefore the coordinate transformation of the convective terms (as illustrated by the u-momentum equation) is as follows:

$$\begin{aligned} \frac{\partial u}{\partial t} + u \frac{\partial u}{\partial x} + v \frac{\partial u}{\partial y} + w \frac{\partial u}{\partial z} \Rightarrow \frac{\partial(Hu)}{\partial t} + \frac{\partial(Huu)}{\partial \alpha} \\ + \frac{\partial(Huv)}{\partial \beta} + H \frac{\partial(u\Omega)}{\partial \sigma} + \underline{\underline{(\sigma-1) \frac{\partial u}{\partial \sigma} \frac{\partial \eta}{\partial t}}} \end{aligned} \quad (D-16)$$

The underlined term has been found to be quite small for the South Biscayne Bay, due to  $\frac{\partial \eta}{\partial t}$  being close to zero for numerical integration of the partial differential equation over a time step  $\Delta t \ll$  TIDAL CYCLE PERIOD OF THE BAY!

DIFFUSIVE

Again following equations (D-2), (D-3), and (D-4) the first order derivatives are:

$$\frac{\partial(\quad)}{\partial x} = \frac{\partial(\quad)}{\partial \alpha} + \frac{1}{H} \frac{\partial \eta}{\partial \alpha} \frac{\partial(\quad)}{\partial \sigma} - \frac{\sigma}{H} \frac{\partial H}{\partial \alpha} \frac{\partial(\quad)}{\partial \sigma} \quad (D-17)$$

$$\frac{\partial(\quad)}{\partial y} = \frac{\partial(\quad)}{\partial \beta} + \frac{1}{H} \frac{\partial \eta}{\partial \beta} \frac{\partial(\quad)}{\partial \sigma} - \frac{\sigma}{H} \frac{\partial H}{\partial \beta} \frac{\partial(\quad)}{\partial \sigma} \quad (D-18)$$

$$\frac{\partial(\quad)}{\partial z} = \frac{1}{H} \frac{\partial(\quad)}{\partial \sigma} \quad (D-19)$$

second order derivatives then become,

$$\begin{aligned} \frac{\partial}{\partial x} \left( \frac{\partial}{\partial x} \right) &= \frac{\partial \left( \frac{\partial}{\partial x} \right)}{\partial \alpha} + \frac{1}{H} \frac{\partial \eta}{\partial \alpha} \frac{\partial \left( \frac{\partial}{\partial x} \right)}{\partial \sigma} - \frac{\sigma}{H} \frac{\partial H}{\partial \alpha} \frac{\partial \left( \frac{\partial}{\partial x} \right)}{\partial \sigma} \\ &\cdot \frac{\partial \left( \frac{\partial}{\partial x} \right)}{\partial \sigma} = \frac{\partial}{\partial \alpha} \left( \frac{\partial}{\partial \alpha} + \frac{1}{H} \frac{\partial \eta}{\partial \alpha} \frac{\partial}{\partial \sigma} - \right. \\ &\quad \left. \frac{\sigma}{H} \frac{\partial H}{\partial \alpha} \frac{\partial}{\partial \sigma} \right) + \frac{1}{H} \frac{\partial \eta}{\partial \alpha} \frac{\partial}{\partial \sigma} \left( \frac{\partial}{\partial \alpha} + \frac{1}{H} \frac{\partial \eta}{\partial \alpha} \frac{\partial}{\partial \sigma} - \right. \\ &\quad \left. \frac{\sigma}{H} \frac{\partial H}{\partial \alpha} \frac{\partial}{\partial \sigma} \right) - \frac{\sigma}{H} \frac{\partial H}{\partial \alpha} \frac{\partial}{\partial \sigma} \left( \frac{\partial}{\partial \alpha} + \frac{1}{H} \frac{\partial \eta}{\partial \alpha} \frac{\partial}{\partial \sigma} - \right. \\ &\quad \left. \frac{\sigma}{H} \frac{\partial H}{\partial \alpha} \frac{\partial}{\partial \sigma} \right) \quad (D-20) \end{aligned}$$

then, after performing the partial differentiation and combining terms (noting  $\frac{\partial \eta}{\partial \sigma} = \frac{\partial H}{\partial \sigma} = \frac{\partial \sigma}{\partial \alpha} = 0$ ) one obtains:

$$\begin{aligned} \frac{\partial^2}{\partial x^2} &= \frac{\partial^2}{\partial \alpha^2} - \frac{2}{H^2} \frac{\partial \eta}{\partial \alpha} \frac{\partial H}{\partial \alpha} \frac{\partial}{\partial \sigma} + \frac{2}{H} \frac{\partial \eta}{\partial \alpha} \\ &\cdot \frac{\partial^2}{\partial \sigma \partial \alpha} + \frac{2\sigma}{H^2} \left( \frac{\partial H^2}{\partial \alpha} \right) \frac{\partial}{\partial \sigma} - \frac{2\sigma}{H} \frac{\partial H}{\partial \alpha} \frac{\partial^2}{\partial \alpha \partial \sigma} \\ &- \frac{2\sigma}{H^2} \frac{\partial \eta}{\partial \alpha} \frac{\partial H}{\partial \alpha} \frac{\partial^2}{\partial \sigma^2} + \frac{1}{H} \frac{\partial^2 \eta}{\partial \alpha^2} \frac{\partial}{\partial \sigma} \end{aligned}$$

$$\begin{aligned}
& - \frac{\sigma}{H} \frac{\partial^2 H}{\partial \alpha^2} \frac{\partial}{\partial \sigma} + \frac{1}{H^2} \left( \frac{\partial \eta}{\partial \alpha} \right)^2 \frac{\partial^2}{\partial \sigma^2} + \frac{\sigma^2}{H^2} \\
& \bullet \left( \frac{\partial H^2}{\partial \alpha} \right) \frac{\partial^2}{\partial \sigma^2} \qquad \qquad \qquad (D-21)
\end{aligned}$$

Now since in the model of South Biscayne Bay  $\Delta\alpha=1.6$  km, and, coupled to the fact that the bay is shallow and surface heights vary quite slowly with respect to the integration time step  $\Delta t$  ( $\ll$  period of tidal cycle), we can neglect "squared"  $\frac{\partial H}{\partial \alpha}$  and  $\frac{\partial \eta}{\partial \alpha}$  terms, and products of these terms to a first order approximation.

Therefore, equation (D-21) reduces to:

$$\begin{aligned}
\frac{\partial^2}{\partial x^2} & \approx \frac{\partial^2}{\partial \alpha^2} + \frac{2}{H} \frac{\partial \eta}{\partial \alpha} \frac{\partial^2}{\partial \sigma \partial \alpha} - \frac{2\sigma}{H} \frac{\partial H}{\partial \alpha} \\
& \bullet \frac{\partial^2}{\partial \sigma \partial \alpha} + \frac{1}{H} \frac{\partial^2 \eta}{\partial \alpha^2} \frac{\partial}{\partial \sigma} - \frac{\sigma}{H} \frac{\partial^2 H}{\partial \alpha^2} \frac{\partial}{\partial \sigma} \qquad \qquad \qquad (D-22)
\end{aligned}$$

But we already know that,

$$\frac{\partial \sigma}{\partial x} = \frac{1}{H} \frac{\partial \eta}{\partial \alpha} - \frac{\sigma}{H} \frac{\partial H}{\partial \alpha} \qquad \qquad \qquad (D-23)$$

(Since  $\sigma = \frac{Z}{H} = \frac{z+\eta}{H}$ )

Thus, equation (D-22) reduces to:

$$\frac{\partial^2}{\partial x^2} \approx \frac{\partial^2}{\partial \alpha^2} + 2 \left( \frac{\partial \sigma}{\partial x} \right) \frac{\partial^2}{\partial \alpha \partial \sigma} + \frac{1}{H} \frac{\partial H}{\partial \alpha} \frac{\partial \sigma}{\partial x} \frac{\partial}{\partial \sigma} \qquad \qquad \qquad (D-24)$$

Now, for a shallow, well-mixed bay,

$$\frac{\partial^2 ( )}{\partial \alpha \partial \sigma} \approx 0$$

and  $\frac{\partial \sigma}{\partial x} \frac{\partial}{\partial \sigma} = \frac{\partial}{\partial x}$  is always true,

Hence,

$$\frac{\partial^2}{\partial x^2} \cong \frac{\partial^2}{\partial \alpha^2} + \frac{1}{H} \frac{\partial H}{\partial \alpha} \frac{\partial}{\partial x} \quad (D-25)$$

and, since  $\frac{\partial}{\partial x} = \frac{\partial \alpha}{\partial x} \frac{\partial}{\partial \alpha}$  and  $\frac{\partial \alpha}{\partial x} = 1$  we finally obtain:

$$\frac{\partial^2}{\partial x^2} \cong \frac{\partial^2}{\partial \alpha^2} + \frac{1}{H} \frac{\partial H}{\partial \alpha} \frac{\partial}{\partial \alpha} \quad (D-26)$$

or,

$$\boxed{\frac{\partial^2}{\partial x^2} = \frac{1}{H} \frac{\partial}{\partial \alpha} \left( H \frac{\partial}{\partial \alpha} \right)} \quad (D-27)$$

In Summary, equation (D-27) has been derived by the following approximations :

$$\boxed{\begin{aligned} \left( \frac{\partial H}{\partial \alpha} \right)^2 &\cong 0 \\ \left( \frac{\partial \eta}{\partial \alpha} \right)^2 &\cong 0 \\ \left( \frac{\partial H}{\partial \alpha} \cdot \frac{\partial \eta}{\partial \alpha} \right) &\cong 0 \\ \frac{\partial^2 ( \quad )}{\partial \alpha \partial \sigma} &\cong 0 \end{aligned}}$$

However, for the South Biscayne Bay the horizontal diffusion terms are much less than vertical diffusion term and advective terms, and, therefore the above approximations are really quite justifiable in a rigorous mathematical sense.

APPENDIX E  
VELOCITY CALIBRATION

The model was calibrated by utilizing a recent current data base acquired by Wang (1977) for the South Biscayne Bay. Values of the vertical eddy kinematic viscosity,  $K_v$  were adjusted until good agreement was obtained between the measured values of surface current and the model predicted values. A close study of comparing these values of surface current led to a value of  $K_v=20 \text{ cm}^2/\text{sec}$ .

The following Table E-2 indicates the current data base used for the model calibration, but first Table E-1 presents the times of high tide for the six days that Wang acquired current measurements. This information of course was necessary in order to compare with the model current predictions which are based upon a "statistical" 24 hour simulation run using meteorological data for April 15, 1975, and tide data from Schneider (1969). Model high tide occurred at 10:00 A.M.

TABLE E-1

DATA	HIGH TIDE
Sept. 14, 1977	8:29 A.M.
Sept. 15, 1977	9:12 A.M.
Sept. 19, 1977	12:46 P.M.
Sept. 22, 1977	3:24 A.M.
Sept. 23, 1977	4:30 A.M.
Sept. 27, 1977	7:55 A.M.

Table E-2 now presents the locations of current measurements, time and date, hi water, and time with respect to the model (hi water at 10:00 A.M.).

TABLE E-2

Date	Hi Water	Time	Time Wrs Model	Station No.	Grid Pt.	Calibration No.
9/15/77	9:12 AM	11:05 AM	11:53 AM	1	(4,9)	1
9/15/77	9:12 AM	12:05 PM	12:53 PM	1	(4,9)	2
9/15/77	9:12 AM	13:05	13:53	1	(4,9)	3
9/15/77	9:12 AM	14:05	14:53	1	(4,9)	4
9/15/77	9:12 AM	15:05	15:53	1	(4,9)	5
9/19/77	12:46 PM	10:10 AM	19:24	2	(6,8)	6
9/19/77	12:46 PM	11:10 AM	20:24	2	(6,8)	7
9/19/77	12:46 PM	12:10 PM	21:24	2	(6,8)	8
9/19/77	12:46 PM	13:10	22:24	2	(6,8)	9
9/14/77	8:29 AM	11:15 AM	12:46 PM	3	(12,9)	10
9/14/77	8:29 AM	12:15 PM	13:46	3	(12,9)	11
9/14/77	8:29 AM	13:15	14:46	3	(12,9)	12
9/14/77	8:29 AM	14:15	15:46	3	(12,9)	13
9/23/77	4:30 AM	11:15 AM	16:45	4	(22,7)	14
9/23/77	4:30 AM	12:15 PM	17:45	4	(22,7)	15
9/23/77	4:30 AM	13:15	18:45	4	(22,7)	16
9/23/77	4:30 AM	14:15	19:45	4	(22,7)	17
9/22/77	3:24 AM	10:15 AM	16:51	5	(23,4)	18
9/22/77	3:24 AM	11:15 AM	17:51	5	(23,4)	19
9/22/77	3:24 AM	12:15 PM	18:51	5	(23,4)	20
9/22/77	3:24 AM	13:15	19:51	5	(23,4)	21
9/27/77	7:55 AM	11:00 AM	13:05	6	(8,7)	22
9/27/77	7:55 AM	12:00 Nn	14:05	6	(8,7)	23

Now Table E-3 shows the comparison between Wang's data base and the model predictions for  $K_v=20 \text{ cm}^2/\text{sec}$ . Generally, the comparison is quite good, and, therefore, the model is considered calibrated with respect to surface current measurements for  $K_v=20 \text{ cm}^2/\text{sec}$ .

TABLE E-3

Cali- bration No.	(Model) Time	(Model) Grid Pt.	Measured Current	Model Current For $K_v=20$	
				First Cycle	Second Cycle
1	1200	(4,9)	13.2cm/s/210°	7.5cm/s/140°	5.3 cm/s/205°
2	1300	(4,9)	13.8/210°	14.0/170°	11.2/190°
3	1400	(4,9)	15.6/270°	16.3/167°	13.5/200°
4	1500	(4,9)	19.7/360°	14.6/164°	15.4/183°
5	1600	(4,9)	17.5/360°	12.0/158°	11.8/145°
6	1950	(6,8)	19.0/360°	17.3/10°	17.2/355°
7	2050	(6,8)	17.9/270°	24.5/9°	20.1/2°
8	2150	(6,8)	12.9/230°	22.7/12°	21.6/13°
9	2250	(6,8)	16.7/230°	11.3/268°	17.5/10°
10	1300	(12,9)	15.6/193°	43.9/83°	20.2/148°
11	1400	(12,9)	15.5/110°	49.5/81°	24.5/102°
12	1500	(12,9)	16.5/63°	38.7/67°	22.1/71°
13	1600	(12,9)	19.9/44°	34.7/62°	20.1/58°
14	1700	(22,7)	12.7/50°	20.0/31°	12.5/12°
15	1800	(22,7)	14.2/16.60°	15.3/21°	12.0/13°
16	1900	(22,7)	11.6/25°	11.5/26°	8.0/8°
17	2000	(22,7)	15.2/5°	5.3/30°	2.0/250°
18	1700	(23,4)	14.9/345°	12.3/37°	6.5/19°
19	1800	(23,4)	14.9/360°	9.0/25°	6.1/8°
20	1900	(23,4)	9.9/12°	6.5/17°	5.2/8°
21	2000	(23,4)	7.3/60°	5.1/20°	1.0/290°
22	1300	(8,7)	14.8/200°	16.3/130°	19.0/162°
23	1400	(8,7)	10.3/107°	17.1/107°	10.7/111°



